Master's Thesis

Study on Natural Circulation Heat Transfer and Flow Characteristics of High-Pr Oil Simulant of Molten Salts

Yukyung Shin

Department of Nuclear Engineering

Graduate School of UNIST

2017

Study on Natural Circulation Heat Transfer and Flow Characteristics of High-Pr Oil Simulant of Molten Salts

Yukyung Shin

Department of Nuclear Engineering

Graduate School of UNIST

Study on Natural Circulation Heat Transfer and Flow Characteristics of High-Pr Oil Simulant of Molten Salts

A thesis/dissertation
submitted to the Graduate School of UNIST
in partial fulfillment of the
requirements for the degree of
Master of Science

Yukyung Shin

1. 16. 2017

Approved by

Bang, In Cheol

Advisor

In Cheol Bang

Study on Natural Circulation Heat Transfer and Flow Characteristics of High-Pr Oil Simulant of Molten Salts

Yukyung Shin

This certifies that the thesis/dissertation of Yukyung Shin is approved.

1. 16. 2017

Bang, In Cheol

Advisor: In Cheol Bang

Chunsang Yoo

Chun Sang Yoo: Thesis Committee Member #1

Sungyeol Choi: Thesis Committee Member #2

Abstract

After the Fukushima accident, the application of the passive safety system was emphasized to prevent the expanded or secondary disaster of the accidents. This trend brought the spotlight back onto the molten salt application in nuclear system which had inherent safety. Among the concepts of the six advanced reactors, molten salt reactor which uses molten salt as fuels and/or coolants was not a good choice due to the problem of the nuclear proliferation and corrosion. However, with the new concept of the reactors such as FHR or MCR, molten salt became to have advantages without the problems.

The strengths of molten salts in nuclear systems come from the thermo-physical properties they hold. Molten salts have high boiling point and operating temperature compared to water. And it is already in liquid phase so that it gives the superiority of core safety. Especially, molten salts have high Prandtl number (Pr) and high volumetric heat capacity compared to other coolants such as He and sodium. Therefore, it can perform the passive heat transfer through the natural convection well without electric power. According to the strong point, passive safety systems of high-Pr molten salts are applied to the various nuclear systems.

For the application of molten salts, the study on the understanding of heat transfer capability and characteristics of high-Pr molten salts based on the natural convection is important. However, lab-scale molten salt heat transfer experiment possesses some difficulties due to its characteristics including high operating temperature and high temperature corrosion and toxicity with materials. Fortunately, the similarity techniques can be used to simulate specific thermal-hydraulic phenomena. Using simulant materials for the experiment enables the research to reproduce the thermal behavior and fluid dynamics of molten salt at reduced temperature, pressure, dimension, and power scale. However, the actual application of the similarity technique is not enough for molten salts. Also, the limitation of the similarity was not proved exactly.

Thus, in this paper, similarity study on high-Pr molten salt heat transfer using a new simulant fluid, DOWTHERM RP, was performed on the natural circulation loops. Through the performance, the feasibility of a new simulant fluid was evaluated based on the similarity technique using scaling laws. In addition, the quantitative and qualitative analysis of DOWTHERM RP natural circulation was conducted in experiment and code simulation using MARS code and CFX code.

From the experiment, heat transfer correlation of single-phase natural circulation on the high-Pr range was developed. In MARS code application, heat transfer simulation and sensitivity study on the thermo-physical properties on natural circulation were conducted. Using CFX code, flow characteristics of

high-Pr natural circulation were observed. By visualization of the natural circulation in experiment and CFX simulation, flow patterns and boundary layers were analyzed following different Pr range using temperature and velocity distribution. This study on the natural circulation of high-Pr simulant fluid, DOWTHERM RP, will contribute to the evaluation of the similarity and its limitation in terms of both quantitative and qualitative similarity.

Contents

List of figures

List of table

Nomenclature

C_p	specific heat	[J/kg-K]
k	thermal conductivity	[W/m-K]
L	characteristic length scale	[m]
$\dot{V}$	volumetric flow rate	[m^3/s]
Q	heating power	[W]
T	temperature	[K]
U_b	buoyant velocity	[m/s]
h	heat transfer coefficient	[W/m^2-K]

Greek symbols

v	kinematic viscosity	[m^2/s]
α	thermal diffusivity	[m^2/s]
μ	dynamic viscosity	[kg/m/s]
β	thermal expansion coefficient	[1/K]
ρ	density	[kg/m^3]

Subscripts

m	model
p	prototype

Abbreviations

Pr	Prandtl number
Gr	Grashof number
Nu	Nusselt number
PIV	Particle Image Velocimetry
CFD	Computational Fluid Dynamics
FHR	Fluoride salt-cooled High-temperature Reactor
MCR	Molten Chloride (Fast) Reactor
MSR	Molten Salt Reactor

DRACS	Direct Reactor Auxiliary Cooling System
IETs	Integral Effects Tests
SETs	Separate Effects Tests
PB-FHR	Pebble-bed FHR
KALIMER	Korea Advanced Liquid Metal Reactor
DHX	Decay Heat Exchanger
EBR-II	Experimental Breeder Reactor-II

I. Introduction

1.1 Background

On the chemical industry, various liquid salts have been used in the heat transport and heat storage systems with low temperature conditions. Differently from that, molten salts were applied to the nuclear industry in 1960s from the Molten-Salt Reactor Experiment (MSRE) at the Oak Ridge National Laboratory (ORNL) with higher temperature conditions. Molten salts, which are liquid salts were used as solvents for liquid fuels in the Aircraft Nuclear Propulsion Program and the Molten Salt Breeder Reactor Program were studied for the developments of the partial systems[1]. A variety of test loops using salts were utilized and the thermophysical properties of the various liquid salts were measured and studied with the nuclear materials. However, the studies on the nuclear systems using molten salts were stopped due to the problems of proliferation, corrosion, and so on. The existing material in the age of 1960s could not handle the corrosive problems of molten salts for sustainability and the reactor concept enabled Pu to be separated from the nuclear fuel which can be used as the nuclear weapons.

According to the emphasis of the safety over the Design Basis Accidents (DBAs) which can prevent extended disasters after a series of severe accidents of NPPs (nuclear power plants) such as TMI (Three Mile Island) accident, Chernobyl accident, and Fukushima accident, however, molten salt systems in nuclear area started to receive attention again. It is because of the excellent inherent and passive safety of the molten salts. Molten salts, especially for the fluoride-based molten salts, have lots of advantages as the major fluid in nuclear reactor systems. Molten salts are normally used as fuels or coolants in the systems. In terms of the inherent safety induced by the physical and chemical properties in the systems, they have the low operating pressure near atmospheric condition and stable state with the radioactive material including Cesium (Cs) and Strontium (Sr) by forming stable fluorides. Properties of the high negative temperature and void coefficients of them also contribute to the safety with the automatic load instantly[2]. In case of the Molten Salt Reactor (MSR) concepts which are the representative reactors using molten salts, fuel clean-up is processed during the operation. It enables the elimination of most fission products which induce the parasitic neutron capturing and make nuclear chain reaction slowing down[3]. In addition to the strength of the inherent safety, molten salts have superiority in the passive safety thanks to their great thermophysical properties with high Prandtl number (Pr). Together with the inherent safety, the passive safety systems are highly important because it fulfills the heat removal for a long time without any external power or electric sources. In aspect of the advanced design of the nuclear reactor, the natural circulation can satisfy the higher safety and economics among the various goals for the GEN-IV nuclear systems. Using natural circulation systems enables the simplicity of the systems including the elimination of pumps so that the cost can be reduced. In addition, major

advantages such as the possibility of the improved core flow distribution, larger thermal inertia, and better characteristics of two-phase flow in terms of power are also followed[4].

Among the various types of the passive safety systems, a large proportion of them are depend on the natural circulation as the main principle. Natural circulation in closed systems occurred by local density difference without any other directly external force. It is induced by the change of properties of the main fluid that results in the occurrence of the buoyancy force. Thus, the thermophysical properties and the geometry of the natural circulation system which give the considerable effect to the force are important, especially for the natural circulation heat transfer capability. Considering the difference of the thermophysical properties of fluoride molten salts from other coolants, natural circulation in molten salt systems is supposed to have difference in heat transfer capability due to the different Pr range. For this reason, enough studies on each natural circulation of molten salts are required. Thus, in this paper, the study on molten salt natural convection is conducted, particular to the fluoride salt. Especially, this study concentrated to the 'natural circulation heat transfer' and 'high-Pr' fluid. To increase and develop the accessibility of the molten salt heat transfer, the similarity technique with scaling laws was applied and new simulant fluid for molten salt natural circulation system was developed.

1.2 Literature Review

1.1.1 High Prandtl number (Pr) Molten Salt

Fundamentally, molten salts have many of characteristics such as very low volatility at high operating temperature, low chemical reactivity with air and water, and high retention of fission products which can contribute to the excellent role of a coolant[5]. Those characteristics assure the possibility of excellent coolants, but they have each different property following the types of combination. The large classification of the using molten salt-base is divided into two parts, fluoride base and chloride base. Among the various molten salts applied to the nuclear reactors as coolants or fuels, the major fluoride salts in forms of mixtures have enough possibility of coolants because they have both high heat transfer capacity of convection and conduction on the operating condition. The outstanding heat transfer is induced by their thermophysical properties. Compared to the other existing coolants such as air, He or sodium, fluoride molten salts have high values of the major properties relating to the heat transfer in general. Especially, the high volumetric heat capacity enables the heat transfer more effectively in natural circulation. It results from the high Prandtl number (Pr) on the operating condition differently from the other coolants as seen in Table 1-1.

Prandtl number (Pr) is the dimensionless number which consists of the thermophysical properties only and it represents the ratio of the momentum diffusivity to thermal diffusivity[7] as seen in equation (1).

By the definition of Pr, it gives the information of both thermal and velocity boundary layer development that affects the heat transfer mode. Theoretically, as the Pr increases, the velocity boundary layer becomes thicker and the thermal boundary layer becomes thinner. The comparative criterion of the heat transfer mode is 1 of Pr. When a fluid has the value of Pr over 1, the thickness of the velocity boundary layer get to be thicker than the thermal boundary layer as shown in Figure 1-1 and the convective heat transfer mode becomes more active. In inverse case, the conductive heat transfer mode becomes more active. Because the fluoride molten salts have high Pr over 1 and other coolants have low Pr less than 1, the heat transfer of the fluoride molten salts is expected to be remarkable in terms of the convective heat transfer[8]. The unusual property, high-Pr, gives the great ability of natural circulation without thermal shock. Thus, based on the high-Pr, fluoride molten salts have strong points as coolants for passive cooling, especially when using natural convective heat transfer. It gives the important meaning of the study on the natural circulation heat transfer of the molten salts. Furthermore, the flow characteristics of the fluoride molten salt related to Pr can have special value in terms of the high-Pr natural circulation.

$$\mathrm{Pr} = \frac{\mu C_p}{k} = \frac{\nu}{\alpha} \tag{1}$$

1.1.2 Molten Salts Application in Nuclear Reactors

Though the spotlight has been brought back to the nuclear reactor concepts using the molten salts with the interesting advantage of the high-Pr properties, more diverse concepts of MSRs were developed for the actual commercialization. In general, the recently developing Molten Salt Reactors (MSRs) are divided into three categories with each two concepts largely. The first is the geometric types of heat removing that are divided into pool type and loop type. Basically, loop type has the primary coolant system outside the reactor vessel by connecting with the circulation loop and the pool type submerges the primary coolant system in the pool-type reactor vessel. The pool type can integrate the overall design and minimize the risk of a loss of coolant accident (LOCA) by including heat exchangers within the reactor vessel. The second is the fuel types which are separated into the solid fuel and the liquid salt fuel. The former is the salt-cooled reactors in which molten salts are used as coolants and the latter is the salt-fueled reactors in which molten salts are used as both fuels and coolants. The last category of the MSRs can be separated into two concepts according to the types of molten salts as Fluoride-salt-cooled High-temperature Reactor (FHR) and Molten Chloride salt-cooled Fast Reactor (MCFR). FHR is the concept of “fluoride- salt-cooled” with the combination of the advantages of the advanced reactors.

It uses Nickel-based structural materials, coated particle fuels which is solid fuels, and the liquid fluoride salt coolants[9]. Fluoride salts are basically used in the thermal neutron spectrum which chooses the reactor type as a thermal reactor. The used fluoride salts are limited to lithium and beryllium based fluorides because of keeping the not high operating temperature. The different concept of MSR, MCFR, utilizes chloride salts instead of fluoride salts. Differently from the fluoride salts, the used chloride salts are used in the fast neutron spectrum which chooses the reactor type as a fast reactor. It is due to the higher parasitic neutron-capture cross-section of the chlorine atom compared to the fluoride salts. Besides the major MSR concepts, molten salts are also utilized in the Advanced High-Temperature Reactor (AHTR) concepts as coolants including the small and medium nuclear reactors. It is because the properties of the molten salts can follow the trend of the advanced reactors heading for the various applications in diverse conditions.

With the different characteristics of each molten salts and the different purpose of use, a variety of reactor concepts using molten salts are being developed by receiving funding. For the development of the FHR, the active research has been conducted from several main projects. Especially, the Integrated Research Project (IRP) supported by the U.S. Department of Energy is one of the massive project to develop the design basis, development, and licensing of FHR commercially with economic performance[10]. Through the project, major research institutes of U.S., including University of California at Berkeley (UCB), Massachusetts Institute of Technology (MIT), Oak Ridge National Laboratory (ORNL), University of New Mexico (UNM), and University of Wisconsin Madison (UW), have played a leading part at the foundation of the FHR design. The concept of MCFR is also developed by several projects including the major projects such as Safety Assessment of Molten Salt Fast Reactor (SAMOFAR). The project of SAMOFAR targets to develop the innovative safety design and assessment of the Molten Salt Fast Reactor (MSFR). Through the experimental and the numerical studies, the project aims to achieve the robust safety of MSFR which has the characteristics of strong coupling of neutronics and thermal-hydraulics thanks to the single fluid concepts between fuel and coolant[11]. Together with the MSR development leading from the FHR and MCFR, several concepts of the advanced reactors based on the combination of molten salt are also evolved. They are explained in the next section 1.1.3.

1.1.3 Molten Salts Natural Circulation in Passive Safety System

The main reasons of the molten salt use in nuclear reactors are the outstanding safety and efficiency from the sustainable point of view. The reactor types using molten salts can reduce the scale and pumping power with simplification of the systems which satisfy both strengths so that they are appropriate to the scale-down reactors, too. In addition, they are particularly good for the preparation

of the severe accidents in safety aspect. Basically, the major safety concepts in engineering systems consist of the four elements, inherent safety, passive safety system, active safety system and control (operating procedure). Among them, molten salt systems have superiority in the two concepts, inherent safety and the passive safety system which are the most important factors in the nuclear systems in case of the blackout accident. It is because of the characteristics that they have the advantages in safety including the excellent neutronic properties and heat transfer efficiency by their thermophysical properties. Thus, for the optimization and commercialization of the molten salt systems in nuclear reactors, the study on the safety principles of molten salts using their inherent properties is important.

In thermal-hydraulic field, the investigation of the thermophysical properties and the evaluation of the heat transfer ability according to them can contribute to the safety in terms of the passive safety systems. In actual, the design and evaluation of the passive safety systems are one of the major interest in the MSR development. The various passive safety systems using various molten salts fluids were applied to the auxiliary safety system for sustainable nuclear energy which can also be utilized in the varied improved or the advanced reactor concepts. The passive safety systems are utilized with diverse purposes and forms such as Direct Reactor Auxiliary Cooling System (DRACS) systems or fuel draining in the developing advanced reactor concepts. Table 1-2 shows the several passive safety systems with the applied molten salts in a variety of the reactors. Pebble Bed Advanced High Temperature Reactor (PB-AHTR), the original concept of the FHR in University of California at Berkeley (UCB) uses liquid salt as coolants. It uses FLiBe as a primary coolant in a close loop and NaF-$NaBF_4$ as a separate buffer salt in a pool which reduces the risk of the exposure to peak temperature during a Loss of Forced Cooling (LOFC) accident[12]. The buffer salt provides the heat removal of the core by receiving heat from Pool Reactor Auxiliary Cooling Heat Exchanger (PHX) and rejecting the heat to the outside using a natural circulation of the DRACS. A Fluoride-Salt-Cooled Small Modular Advanced High-Temperature Reactor (SmAHTR) is the integral primary system FHR concept with 125 MWt[13]. The reactor uses the philosophy of “two-out-of-three system” in decay heat removal systems by operation or shutdown. Three Direct Reactor Auxiliary Cooling System (DRACS) cooling loops are employed though only two loops are needed for the safe operation. Also, it has special concept, salt vault, which is a thermal energy storage tank. It is used to serve as a thermal energy reservoir for the process heat or power production customer. The Liquid Fluoride Thorium Reactor (LFTR) is two fluid breeder reactor type with 2 MWt. It is equipped with drain fuel acts as the passive safety system in accidents. When the reactor overheats, a frozen plug at the bottom of the core melts and the fuel drains into the tanks quickly where nuclear reaction is physically impossible. Fuel draining is triggered by power outage, seismic alert, chemical or temperature sensors, or operator control. ThorCON is a thorium converter reactor with single fluid. Its originality is from the Molten Salt Reactor of ORNL and it also applied fuel draining as the passive safety system. Stable Salt Reactor (SSR) is the UK design

which is a fast spectrum reactor with pool type[14]. The fuel salt of SSR is provided from the spent nuclear fuel of a sodium chloride solution in tubes which are in a coolant salt pool. – Seaborg Waste Burner (SWaB) is a single fluid reactor within the thermal-epithermal spectrum with 50 MWt. SWaB uses an overflow system (OS) and a salt plug system as the passive safety systems. In situation of overheating or loss of the operational power, OS directly overflows to the subcritical and cooled dump tank passively[15]. Integral Molten Salt Reactor (IMSR) is also driven from the MSR Experiment of ORNL with modifications. In IMSR, decay heat removal in situ without dump tanks is performed. Also, it uses buffer salt which has higher melting point than coolant salt as the decay heat removal system using natural circulation. Transatomic Power Reactor (TAP) is a demonstration reactor with 20 MWt. It is similar concept of MSR Experiment but it uses zirconium hydride as a moderator and LiF-based salt. It also uses fuel draining principle which can be applied to fuel salt.

Among the passive safety systems using molten salt fuel or coolant in various molten salt reactor concepts, the outstanding point is that most systems use the principle of the natural convection or natural circulation of the fluoride molten salts. The natural circulation is the heat transport mode in fluid occurred by the buoyancy driving force due to the density difference induced by the local temperature difference. Thus, it is the natural result that the natural circulation is used as passive systems. In practice, the principle is widely used for other reactor core cooling, cooling containment, ventilation, and so on in general nuclear reactor types, such as PWR, PHWR, or VVER[16]. However, the meaning of the passive safety with the natural circulation can be maximized in case of MSR. It is because the molten salts systems in most of the nuclear reactors use the high-Pr natural circulation in a pipe with the fluoride molten salts in accidents applied to the primary or secondary loops. Generally, the natural circulation in a flat plate or in a pipe with enough developing length shows the laminarization near the wall is large which affect the buoyancy force. They are induced by the reason that the excellent natural circulation can occur when turbulence and friction are reduced which can lead the large head loss[11]. When translating the natural circulation in terms of the high-Pr molten salts, the laminarization and active development of convective boundary layers near the wall are more effective thanks to the thermophysical properties of the fluoride molten salts as explained in section 1.1.1.

In actual, because the molten salt systems have an important roles as passive safety, the high-Pr natural circulation in which the heat transfer occurs constantly with lower flow rate are required to be studied enough for verification and validation (V&V) of MSRs. According to the trend, several research institutes have participated in the studies of molten salt natural circulation with diverse regions in nuclear industry these days. In the thermal-hydraulic field, most research is underway for the design and development of the specific passive safety systems of each MSR concepts as seen in the upper part. In addition to the research, theoretical studies on the molten salt natural circulation are also conducted actively. The representative case is the study of Politecnico di Milano in Italy. They study on the natural

circulation as a type of intrinsic safety for GEN-IV reactors with the theoretical analysis in HORIZON 2020 program. Adding to the normal natural circulation by the locally-external heat source, the natural circulation by the internal heat source is also considered in this research institute. The reflection of the effect of internal heat source can be applied in terms of the molten salt fuel in nuclear systems. They performed the prediction of the stability of natural circulation with internal heat generation using linear and nonlinear analysis methods. The optimization of the configuration of natural circulation loops through the evaluation of the effect of parameters on the geometric and thermal characteristics is also studied[17]. According to the appearance of the noble concepts of molten salt reactors which can solve the proliferation problem with consideration of the adequate materials, the study is also adopted to the design and V&V of the safety systems of each reactor. Though the study on the heat transfer ability and the flow characteristics of the high-Pr heat transfer, especially for the natural circulation, is identified as valuable in the previous parts, the accessibility of the molten salt study with the actual experiment is still high due to the characteristics of molten salts. Thus, in this paper, the molten salt natural circulation study was conducted to contribute to the molten salt study using the similarity technique.

1.1.4 Similarity Technique for Molten Salt Heat Transfer

Studies on the molten salt heat transfer phenomena in a real system-scale is limited due to the difficulties of the experimental conditions such as high operating temperature, large-scaled facility, high temperature corrosion and toxicity, and so on. To overcome the limitation, previous studies applied the similarity technique to the molten salt studies. Similarity experiment of molten salt heat transfer system can make the experiment more easily. Real-scale molten salt heat transfer system has high-temperature and complex structure with high cost operating condition. Also, erodibility of materials has to be considered due to the chemical properties of molten salts as explained in Table 1-3. Compared to molten salt system, similarity experiment condition has low-temperature and simple structure which has specific observation points with small scale. Additionally, proper simulant can remove the erodibility problem which gives a chance of selecting materials more widely.

To replicate the heat transfer phenomena of the molten salt systems, simulant fluids which can simulate the target molten salt in the experimental conditions at reduced temperature, length scale, and etc. are used with scaling laws. For the convective heat transfer system, several dimensionless numbers such as Prantl (Pr), Reynolds (Re), Grashof (Gr) are used in scaling laws. Three non-dimensional numbers, Pr, Re, and Gr are induced from the conservation equations of mass, momentum, and energy by non-dimensionalization[18]. Based on the Prandtl number (Pr) which is one of the criteria of the heat transfer phenomena by consisting of only the fluid properties, the simulant was selected and the operating range of the similarity experiment was set. After selecting of the simulant, the experimental conditions are set

according to the scaling with dimensionless numbers. Reynolds number (Re) and Grashof number (Gr) are used in forced and natural convection heat transfer each. Re indicates the ratio of inertial to viscous forces which is important parameters in forced convection. Gr indicates the ratio of buoyancy to viscous forces which is important in natural convection. Both numbers are used to predict the heat transfer ability satisfying the similarity conditions. Thus, matching Pr and Re for the forced convection, or Pr and Gr for the natural convection, assure the heat transfer phenomena between the target molten salt system and the scale-down experimental system identically.

$$\mathrm{Re} = \frac{\rho v^2/L}{\mu v/L^2} = \frac{\rho v L}{\mu} = \frac{vL}{\nu} = \frac{Inertial\ forces}{Viscous\ forces} \tag{2}$$

$$Gr = \frac{g\beta(T_S - T_\infty)L_c^3}{\nu^2} = \frac{Buoyancy\ force}{Viscous\ force} \tag{3}$$

$$\mathrm{Pr} = \frac{c_p \mu}{k} = \frac{\nu}{\alpha} = \frac{Viscous\ diffusion\ rate}{Thermal\ diffusion\ rate} \tag{4}$$

In nuclear field, scale-down experiments for design of the FHR concepts were performed in several leading research institutes such as UC Berkeley, Oak Ridge National Laboratory, and Chinese Academy of Sciences (CAS). Especially, UC Berkeley used simulant fluid for duplication of the thermodynamic phenomena for molten salts. Simulant fluid, DOWTHERM A heat transfer oil, was used for validation & verification (V&V) of heat transfer phenomena instead of FLiBe and FLiNaK molten salts in Pebble-Bed FHR (PB-FHR)[19]. Using the simulant oil, several experiments at steady state and transient conditions in FHR system were investigated using Compact Integral Effects Test (CIET) facilities. CIETs were the test facilities to reproduce fluid dynamic behavior or heat transfer of the passive safety system of Mk1 PB-FHR which was design as pre-conceptual modular type with 236 MWt. In addition, simplified natural circulation was performed on the CIET Test Bay which was experimental loop designed to collect experimental data using the simulant, DOWTHERM A, before the CIET tests[20]. UCB obtained experimental data in various cases such as loss of forced coolant (LOFC), Loss of heat sink transient, or buoyant shutdown rod operation during transients using the IET facilities. In this study, for the development of the similarity technique in molten salt heat transfer systems, new high-Pr heat transfer oil was adopted as a simulant of the fluoride salt and the feasibility was identified by the similarity experiment with the theoretical similarity.

Table 1-1. Comparison of thermophysical properties of each coolant on the operating condition[6].

Coolant		Temperature (°C)	Volumetric heat capacity *Cp* (kJ/m^3-K)	Viscosity *v* ($m^2/s*10^6$)	Thermal conductivity *k* (W/m-K)	Pr (Prandtl number)
Water (7.5 MPa, saturated)		300	4130	0.13	0.54	0.97
Na (atm)		550	1040	0.28	62.0	0.004
He (7.5 MPa)		700	19	12.4	0.36	0.66
Molten salts	$2LiF\text{-}BeF_2$	700	4690	2.9	1	13.5
	LiF-NaF-KF	700	3810	1.4	0.92	5.9
	$NaF\text{-}NaBF_4$	700	2640	0.5	0.40	3.3

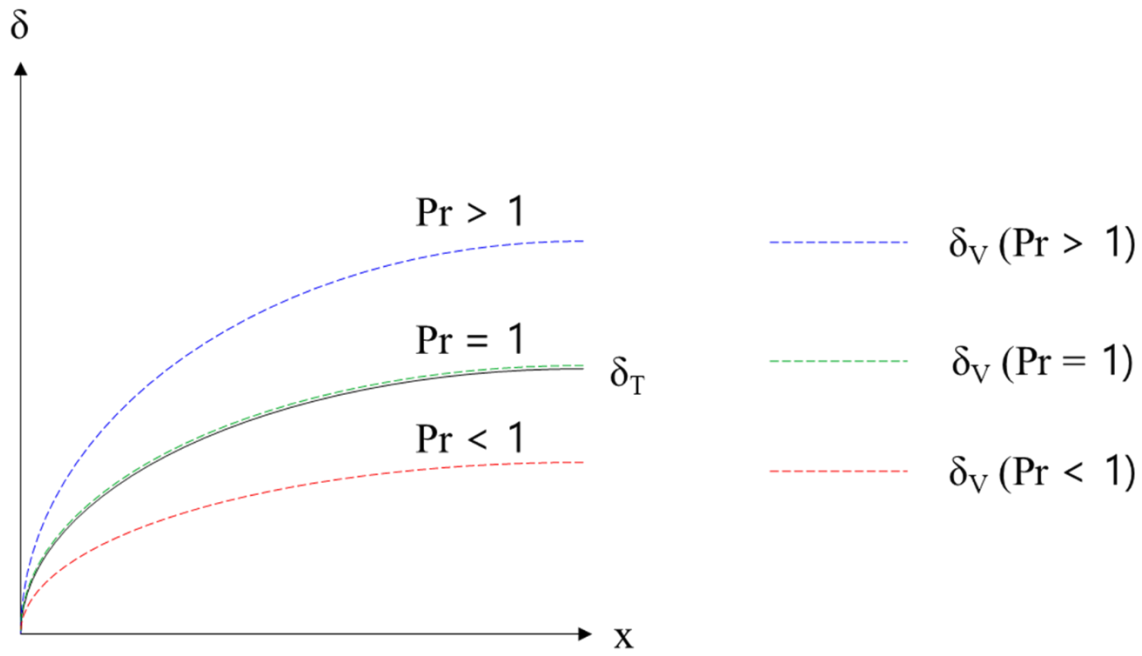

Fig. 1-1. Boundary layer thickness near the vertical heating surface.

Table 1-2. Passive safety systems in Molten Salt Reactors[12,14].

Research Institute	MSR concept	Fuel salt	Coolant salt	Passive safety system Using molten salts
UC Berkeley	PB-AHTR	Solid fuel	LiF-BeF_2, NaF-$NaBF_4$ (buffer salt)	DRACS Buffer salt
ORNL	SmAHTR	Solid fuel	LiF-BeF_2, LiF-NaF-KF	Three DRACS Salt vault
Flibe	LFTR	U&Th in FLiBe -$(Th/U)F_4$	$NaBF_4$-NaF	Fuel draining
Martingale Inc.	ThorCON	U&Th in NaF-BeF_2 -$(Th/U)F_4$	NaF-BeF_2	Fuel draining, Sealed primary loop
Moltex Energy	SSR	SNF in NaCl -(U/Pu/La)Cl	ZrF-KF-NaF	Sealed unit, Poison pill
Seaborg Technologies	SWaB	Th&SNF in LiF -$(Th/Pu/MA)F_4$	LiF-NaF-KF	Overflow system (OS), Fuel draining, Fuel coolant
Terrestrial Energy	IMSR	U in NaF-RbF-UF_4 (or LiF-BeF_2-UF_4)	KF-ZrF	Buffer salt, Sealed unit, Poison pill
Transatomic Power Reactor	Therml-epithermal	U in LiF-$(U/Pu/La)F_4$, SNF in later editions	LiF-KF-NaF	Fuel draining

Table 1-3. Comparison of the experimental conditions between molten salts and simulant fluids.

Molten slat	Simulant fluid
High-temperature	Low-temperature
Erodibility O	Erodibility X
Large-scale	Small scale
Complex condition	Simple condition
High-cost	Low-cost

II. Theoretical Similarity of Molten Salt Natural Circulation with High-Pr Heat Transfer Oil

2.1 Introduction

Though molten salts have been used as heat transfer or heat storage fluid in diverse fields including solar power, each application uses different types of molten salts with different operating conditions and properties. Also, the use of the similarity technique is not developed enough in molten salts heat transfer area. Accordingly, the introduction of new simulants for molten salt similarity can increase the accessibility for the study on molten salt heat transfer and the efficient use of similarity technique with the confirmed simulants. In the previous work of UC Berkeley, the generalized heat transfer oil in research area, DOWTHERM A which is a eutectic mixture of biphenyl ($C_{12}H_{10}$) and diphenyl oxide ($C_{12}H_{10}O$), was adopted as a simulant of FLiBe ($2LiF\text{-}BeF_2$) molten salts. With the simulant, theoretical similarity technique with scaling laws was applied to the heat transfer system with molten salts and helium which were used as coolants in the Advanced High Temperature Reactor (AHTR)[21]. Also, based on the theory, the similarity experiment was utilized to obtain enough database of both natural and forced convection for FLiBe molten salts in the coolant systems of FHR design. As an extension of the previous work, new heat transfer oil with high-Pr was introduced and the theoretical similarity was evaluated in this section. As shown in the previous section 1.1.2, the main application of the passive safety systems for molten salt-used reactors applies the natural circulation of the fluoride molten salts. Therefore, for the selection of a simulant and the heat transfer system, the auxiliary coolant system of fluoride molten salt using natural circulation was considered as the prototype of the similarity.

2.2 Application of Similarity to Molten Salt and Natural Circulation System

2.2.1 Selection of Molten Salt and Natural Circulation System

In nuclear reactor systems, various molten salts are used as fuels or coolants. Among them, fluoride-base molten salts have higher Pr range compared to the chloride-base molten salts. In addition, they have been applied more times in nuclear reactor systems. Especially, $LiF\text{-}BeF_2$ (FLiBe) which is the mixture of lithium fluoride (LiF) and beryllium fluoride (BeF_2) is recommended as one of the most promising coolants. In real, FLiBe was selected as the primary coolant in various concepts of MSR, particularly to FHRs which are developed actively these days. Accordingly, FLiBe was selected as the target molten salt in this study. Addition to the selection, the choice of the prototype system is required for the reproduction of the natural circulation of FLiBe molten salt in similarity experiment. Considering the contribution to the passive safety system of molten salts, DRACS system of FHR,

which is one of the passive safety system using FLiBe natural circulation was selected as a prototype system. DRACS is a concept of the passive heat removal system developed from the Experimental Breeder Reactor-II (EBR-II) resulting in the improvement in the subsequent design of fast reactor[22]. As the real-scale of FHRs have very large dimensions, the modular reactor types were considered to satisfy the scaling of the experimental conditions. In addition, there is no actual prototypic DRACS systems for FHRs built or test yet. Therefore, DRACS system in FHR concept of Ohio State University (OSU) as seen in Figure 2-1 was selected as a prototype of natural circulation system taking account of the limitation of the experimental conditions. The prototypic power was calculated as the capacity of decay heat removal. The FHR of OSU is a 20 MW modular loop-type test-scale FHR. From the heat generation capacity, the heat removal capacity of the DRACS was set as 1 % of the nominal core power, 200 kW[22].

2.2.2 Selection of Simulant Fluid and Experimental Apparatus

According to the selection of the target molten salt, FLiBe, and its natural circulation system, simulant fluid and the experimental facilities were considered. The operating temperature range of FLiBe in the primary system of the target FHR from 700 °C to 750 °C by reflecting the inlet and outlet temperatures. Taking account of the use of FLiBe in various coolant systems, the operating temperature range was applied widely from 500 °C to 800 °C. The selection of a simulant was based on matching of Prandtl number (Pr) with FLiBe on the operating range. Candidates of a simulant were considered from several heat transfer oils which can simulate the molten salt heat transfer on the lower temperature range. On the operating temperature of FLiBe, Pr has the range of $10 < Pr < 50$. Reflecting the Pr range and the suitability of the experimental condition, major heat transfer oils, DOWTHERM A and DOWTHERM RP, were considered as adequate simulants for the molten salt as shown in Figure 2-2 and Table 2-2. Both DOWTHERM RP and DOWTHERM A match the Pr range for the main molten salts in nuclear field such as FLiNaK or LiCl-KCl. That shows the possibility of them as useful simulants for molten salt heat transfer. For FLiBe molten salt, DOWTHERM A, which was used in the previous similarity experiment of UC Berkeley, can cover the Pr range on the temperature range of 45°C to 105°C.

For the introduction of new simulant in molten salt similarity technique, DOWTHERM RP heat transfer oil was selected as a simulant for FLiBe molten salt for both the current and the on-going studies. It is the most stable heat transfer fluid thermally in low-pressure today[23]. It has excellent performance in liquid phase heat transfer systems within operating temperature. The Pr range is also well matched with FLiBe molten salt over the whole range of the operating temperature assuring the similarity of the heat transfer cases as seen in Figure 2-3. The reasons why we used DOWTHERM RP instead of DOWTHERM A are as follows. First of all, the feasibility of DOWTHERM A as a simulant oil for molten salt was already proven in the previous study of Berkeley and Idaho National Laboratory[26,27],

while that of DOWTHERM RP was not proven yet. Therefore, finding another simulant could be also one of our objectives for various applications of molten salts and simulant fluids. Secondly, the study with DOWTHERM RP in addition to DOWTHERM A can give pertinence and reliability of scaling law, which use simulant fluid. For further utilization, DOWTHERM RP also has advantages in higher boiling point, wider temperature, and wider Pr range, which can cover more various target fluids, as seen in Figure 2-2. In addition, the experiment with DOWTHERM RP enables to experience the high-temperature experiment because of the higher operating temperature than DOWTHERM A. Finally, DOWTHERM RP has lower toxicity compared with DOWTHERM A, which should be considered as the important factor in experiment.

For the similarity experiment of molten salts, single phase natural circulation loops were designed and manufactured for DOWTHERM RP natural circulation in UNIST thermal-hydraulics and reactor safety laboratory. The two types of natural circulation loops were used with different height difference (ΔH) between heating section and cooling section ($\Delta H1$=1.415 m, $\Delta H2$=0.415 m). The detailed design of the natural circulation loops is shown in Figure 2-4 and Table 2-3. The UNIST natural circulation molten salt simulant loop consists of one vertical heating section, three cooling sections, and other remaining pipe line with insulation. Most sections of the loop, except the cooling section, are contained within a furnace that maintains the interior temperature and heat balance. Dimensions of the experimental facilities are listed in Table 2-3. The vertical and horizontal lengths of the loop are 0.8 m and 1.54 m, respectively. The inner and outer diameters of the pipe are 0.023 m and 0.025 m, respectively, and are constant over the entire length. All piping in the loop was constructed using SS304. Heating section is located at the lower part of the left side in the loops. The exterior of the vertical heating section is equipped with a coil heater with a length of 0.22 m. Heat source was provided by indirect heating using the coil heater. The power supply was designed to supply input heat up to 5 kW. The cooling sections are coaxial heat exchangers with water flowing through the annular sections. Three water-cooling sections are connected by rubber tubes, and chilled water is supplied in reverse direction of the main flow with the constant inlet temperature and mass flow rate. A furnace was designed to minimize heat loss in the natural circulation loops which maintains an indoor temperature constantly except cooling sections. For temperature data acquisition, 10 of K-type thermocouples and two pressure transducers on the bottom level and the upper surface were installed.

2.3 Results and Discussion

Heat transfer fluids and the natural circulation systems for target molten salt and its simulant were determined in the previous section 2.2. Normally, the dimensions of the scale-down test facility are determined by the theoretical calculation of the scaling law. It is because the scaling analysis for the

scale-down facilities gives the suitable dimensions to reproduce key phenomena of the target heat transfer systems. However, this study has two objectives which are the verification of the simulant feasibility and the evaluation of the high-Pr fluid natural circulation for the fundamental and wide applications. Thus, the theoretical scaling law was applied to the determined fluid and system conditions which can be utilized in the on-going studies. By utilizing DOWTHERM RP, which was used as a working fluid in this experiment, the scaling law was also applied to geometric and other parameters.

$$Gr \equiv gL^3\beta\Delta T/\nu^2 \tag{5}$$

$$(\beta\Delta T)_m = (\beta\Delta T)_p \rightarrow \beta_m/\beta_p = \Delta T_p/\Delta T_m \tag{6}$$

$$\left(\frac{gL^3}{\nu^2}\right)_m = \left(\frac{gL^3}{\nu^2}\right)_p \rightarrow \left(\frac{L_m}{L_p}\right)^{\frac{3}{2}} = \frac{\nu_m}{\nu_p} \tag{7}$$

$$Q_m = \rho C_p \Delta T \dot{V} = \rho C_p \Delta T U_b L^2 \tag{8}$$

$$U_b \equiv (gL\beta\Delta T)^{1/2} \tag{9}$$

For the similarity of the natural circulation, matching of Gr was applied with the decoupled equations (6) and (7)[21]. Matching these two dimensionless groups for the prototype and the model enables the scaled experiment to simulate the natural circulation system adequately. For the calculation, the thermophysical properties of FLiBe and DOWTHERM RP, geometric parameters, and power with operating temperature condition of FLiBe were used. The scaling parameters of the two types of reactors are presented in Table 2-4. The inner diameter of the primary loop was used as the characteristic fluid length scale, L. The temperature difference, ΔT (the difference between the maximum and minimum temperatures in the test loop), and the length scale were determined. The temperature difference of the model, ΔT_m, was calculated to be 29.53 K. For the calculation of power range, the input power range was set based on the heat removal capacity of the DRACS at OSU. The 1% of the nominal core power of the DRACS capacity following the decay heat level, 200 kW, was used as the prototype heating power (Q_p)[22]. Then, the model heating power (Q_m) was calculated using Equation (8)[21]. $\dot{V}$ is the volumetric flow rate, and U_b is the buoyant velocity scale, $U_b = (gL\beta\Delta T)^{1/2}$. From the power scaling analysis, the heater power (Q_m) for FHR was determined to be 6.94 kW.

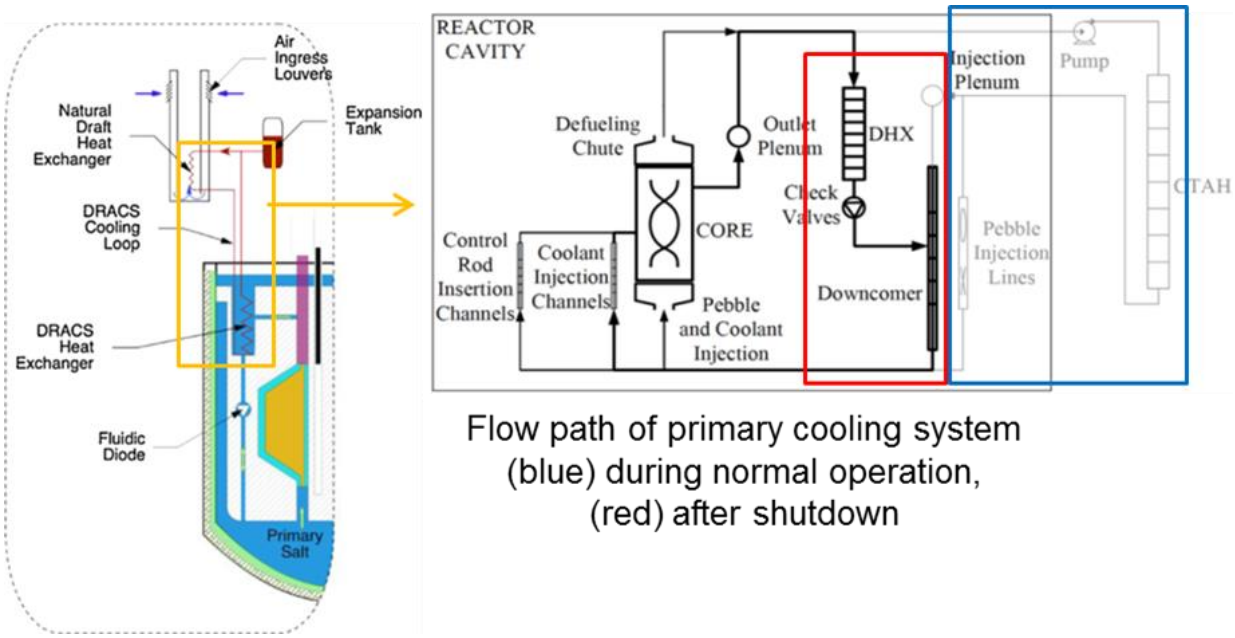

Fig. 2-1. DRACS system in FHR and prototypic design at OSU[22].

Table 2-1. Dimensions and design conditions of the prototypic DRACS at OSU[22].

	Primary salt (FLiBe)	Secondary salt (FLiNaK)	Air
T_{hot} (°C)	750	680	100
T_{cold} (°C)	705	630	40
ΔT (°C)	45	50	60
Mass flow rate (kg/s)	1.84	2.12	3.31
Loop height (m)	2.28	2.3	10.43
Pipe I.D. (cm)	15	15	282

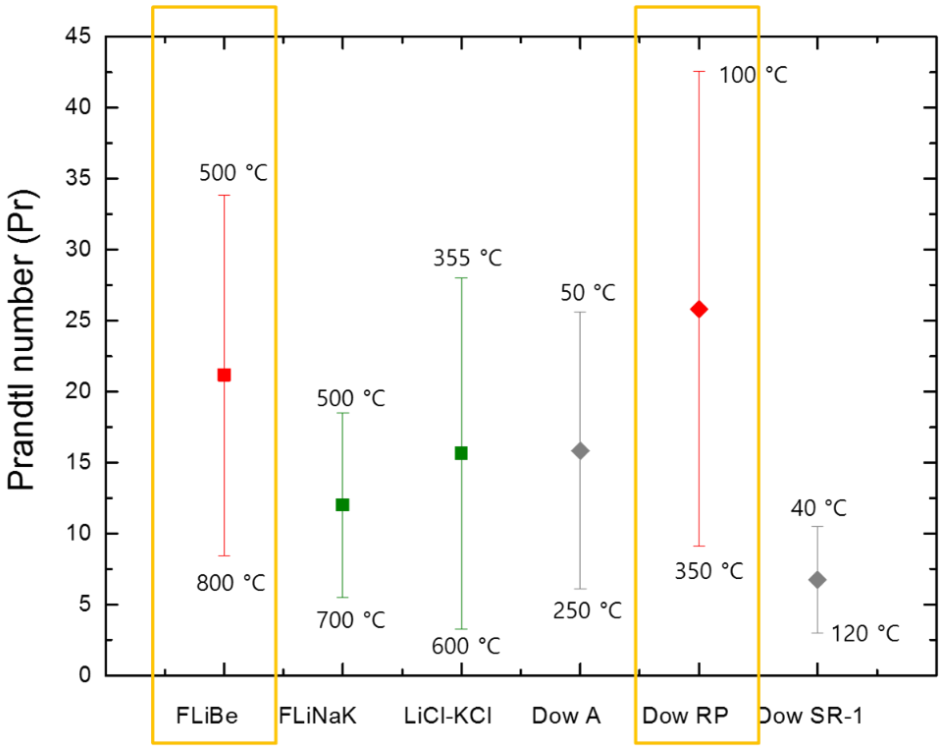

Fig. 2-2. Comparison of the Pr range between molten salts and simulant fluids[6,23,24,25,].

Table 2-2. Candidates of a simulant for the simulation of heat transfer system with FLiBe[6,23,24].

	T (K)	ρ (kg/m^3)	ν (m^2/s *10^6)	C_p (kJ/kg·K)	k (W/m·K)	Pr
$LiF\text{-}BeF_2$ (FLiBe)	773.15	2035.7	7.3283	2.386	1.1	32.36
	1073.15	1889.3	2.0313	2.398	1.1	8.36
DOWTHERM RP	373.15	973.0	2.8469	1.858	0.1210	42.53
	423.15	937.3	1.4083	2.007	0.1145	23.14
	473.15	901.0	0.8879	2.156	0.1080	15.9
	623.15	768.1	0.3979	2.602	0.0886	8.97
DOWTHERM A	323.15	1035.8	1.9985	1.658	0.1339	25.63
	373.15	994.9	0.9750	1.800	0.1259	13.87
	423.15	952.2	0.6091	1.940	0.1179	9.54
	523.15	859.0	0.3260	2.218	0.1019	6.09

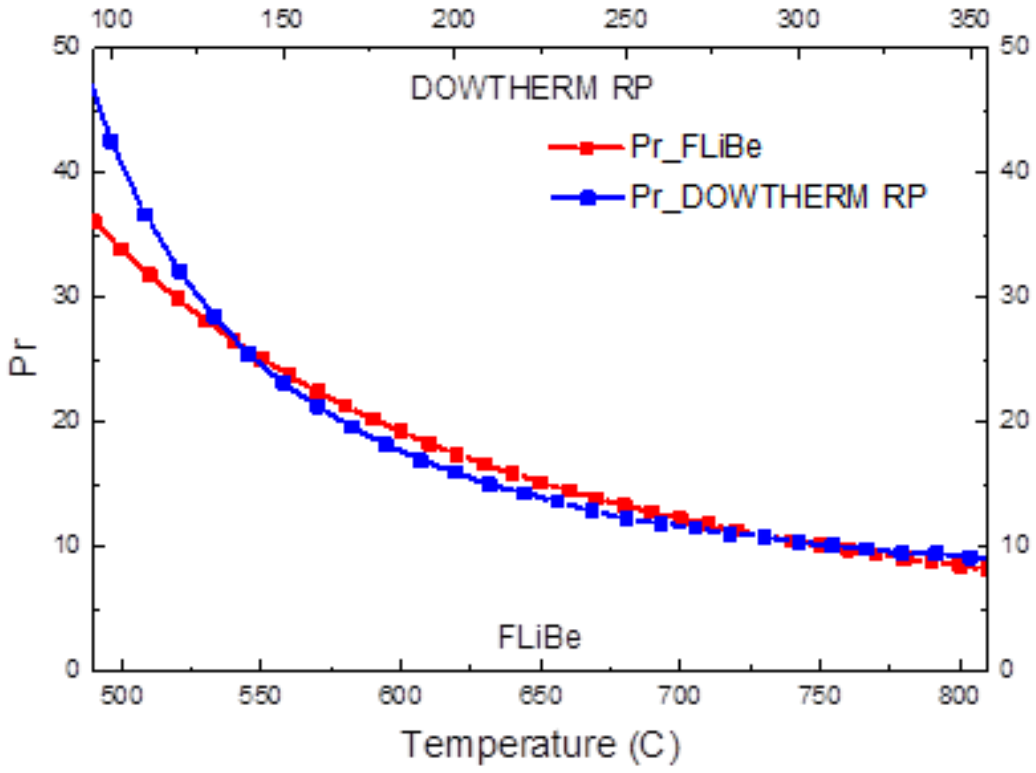

Fig. 2-3. Matching of Prandtl number (Pr) between LiF-BeF_2 (FLiBe) and DOWTHERM RP within operating temperature range[6,23,24].

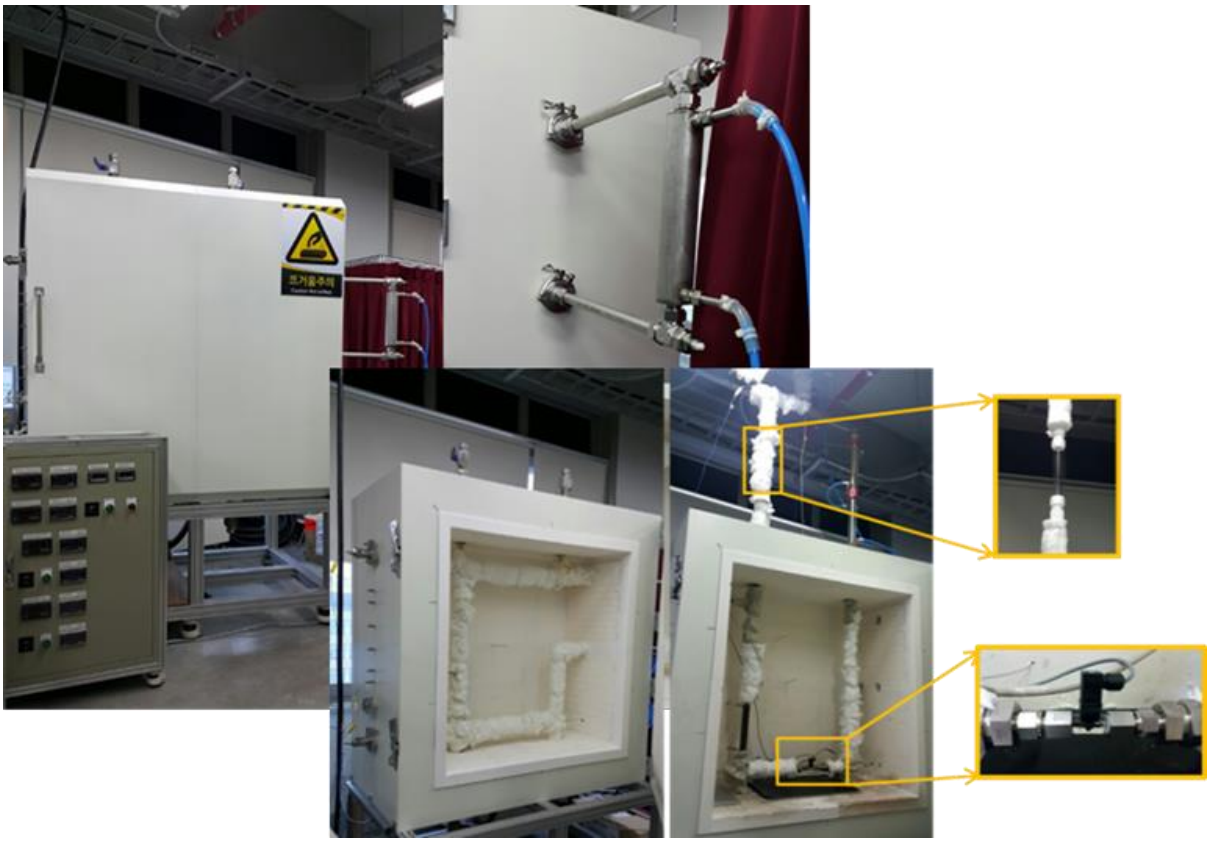

Fig. 2-4. Single-phase natural circulation loop
(a) ΔH=1.415 m, (b) ΔH=0.415 m.

Table 2-3. Dimensions of the natural circulation loops.

(a)	(m)	(b)
2.04	Loop height	0.80
0.60	Loop width	1.54
0.023/0.0254	Inner/Outer diameter	0.023/0.0254
0.22	Heating section length	0.22
1.14	Cooling section length	1.14
1.415	Height difference between heating and cooling sections	0.415

Table 2-4. Comparison of the scaling parameters between prototypic and simulating condition.

	FLiBe (973.15 K)	
DOWTHERM RP (503.15 K)	Gr_m/Gr_p	1
	L_m/L_p	0.0767
	v_m/v_p	0.2472
	$\Delta T_m/\Delta T_p$	0.7971
	Qh_m/Qh_p	0.00021

III. Performance for Heat Transfer Capability of High-Pr Natural Circulation

3.1 Introduction

From the theoretical calculation of the similarity, the adequacy in terms of the geometric parameters and the experimental condition was identified. To use the simulant in the heat transfer similarity of molten salts, the validation of the heat transfer capability which can simulate that of molten salts is required. Thus, the direct heat transfer experiment for the natural circulation of the simulant, DOWTHERM RP, was performed in this part. The evaluation of the heat transfer capability in natural circulation was conducted by developing the experimental heat transfer correlation which was composed of the dimensionless numbers. As seen in Table 3-1, several convective heat transfer correlations were developed from the experiments. However, the application range and conditions are included in the forced convection. And the range is broad so the adequacy is not high. Thus, the development of the experimental correlation for the natural circulation can have the meaning. In addition to the experiment, computational numerical analysis using the thermal-hydraulic analysis code was also performed to validate the experimental data and extend the similarity application to the code simulation. Additional sensitivity study on the process of the code simulation was conducted, too. It is because the molten salts have considerable error in measurement of thermophysical properties that the effect of each property need to be identified. Through the experimental and the computational numerical study, the heat transfer capability of the high-Pr simulant, DOWTHERM RP, was evaluated.

3.2 DOWTHERM RP Natural Circulation Experiment

The natural circulation experiment with the simulation of FLiBe molten salt, DOWTHERM RP, was performed with the natural circulation loop of UNIST thermal-hydraulics and reactor safety laboratory. To obtain enough data, two types of the experimental loops with different height difference between heating section and cooling sections were used as shown in Figure 3-1. With two different types of the experimental loops by changing the location of the cooling sections, the comparison of the effect of the height difference to the mass flow rate and temperature distribution was conducted. Power range of this experiment was set from the similarity condition and the fluid property. Considering the similarity with FLiBe, the operating temperature of DOWTHERM RP where Pr of FLiBe and DOWTHERM RP are matched is from 100 °C to 350 °C as shown in Figure 2-3. Also, the temperature range under the liquid-phase condition of DOWTHERM RP is lower than 353 °C which is the boiling point of the fluid. Reflecting those conditions and through the preliminary experiment, the power levels were ranged from 60 to 600 W. Three heat exchangers cool locally with constant inlet temperature (10 °C) and mass flow

rate (2.42 kg/s) in reverse direction. In the natural circulation experiment of DOWTHERM RP, temperature, pressure, and the mass flow rate data were obtained in each power step.

3.3 Modeling of DOWTHERM RP Natural Circulation in MARS Code

In the previous section, high-Pr DOWTHERM RP natural circulation experiment was conducted. For the verification and validation (V&V) of the experimental results, proper thermal hydraulic models were developed. Multi-dimensional Analysis of Reactor Safety (MARS) code which was the multi-dimensional thermal-hydraulic system analysis code for Light Water Reactor (LWR) was utilized in this study. MARS code is based on the RELAP5/MOD3.2.1.2 and the COBRA-TF codes of USNRC[32]. From MARS code, MARS-LMR code was developed for liquid metal application including Sodium (Na), Lead (Pb), and Lead-Bismuth Eutectic (LBE) in the advanced reactors. However, the code was not extended to the molten salts application. Also, the heat transfer oil, DOWTHERM RP, used as a simulant was not utilized. Thus, it is necessary to apply both molten salts and the simulant to the analytic code for constant use. In the previous study of UNIST thermal-hydraulics and reactor safety laboratory, thermophysical properties of FLiBe were implemented using the soft-sphere model with Monte Carlo calculations based on the MARS-LMR code for molten salt application[33]. For the simulant, additional implementation was conducted. In addition to DOWTHERM RP, DOWTHERM A which was used as a simulant of molten salts in UCB was also implemented because it can be utilized to the parameter study or to the further study of molten salts. The implementation was based on the property tables of DOWTHERM oils from DOW Chemical Company and the previous study of Idaho National Laboratory (INL) relating to the implementation of DOWTHERM A into RELAP code. For the implementation, proper correlations of each properties are required which can change adequately following temperature and pressure change. In case of DOWTHERM A, correlations of the saturated property values for liquid phase and vapor phase used in INL reference were utilized which were based on Moore[27]. The property implementation was performed for the thermophysical properties and the transport properties. For most thermophysical properties, the regression analyses with Mathcad was used and 5th degree polynomial was fitted to data normally. Properties of liquid phase were fitted by the temperature-dependent equation adding the pressure term as shown in Equation (10). The equation was applied for density (kg/m^3), enthalpy (J/kg), and specific heat (J/kg-K). Other properties which are specific volume (m^3/kg), internal energy (J/kg), thermal expansion coefficient (1/K), isothermal compressibility (1/T), and entropy (J/kg-K) were implemented by the following equations (12) - (15).

$$Property = (a + bT + cT^2 + dT^3 + eT^4 + fT^5)(P \cdot dd)^{dd} \quad (10)$$

$$v_f = \frac{1}{\rho_f} \tag{11}$$

$$u_f = h_f - pv_f \tag{12}$$

$$\beta_f = \frac{1}{v_f}\left(\frac{\partial v_f}{\partial \mathrm{T}}\right)_p \tag{13}$$

$$\kappa_f = -\frac{1}{v_f}\left(\frac{\partial v_f}{\partial P}\right)_T \tag{14}$$

$$s_f = \frac{u_f + pv_f}{T} \tag{15}$$

Similar to the liquid phase, vapor properties were fitted to implement on MARS code properties. The pressure-dependent equation with adding of the temperature term was used for major properties as seen in Equation (16). The equation was applied for density, enthalpy, and specific heat of the vapor phase with proper fitting. Other properties used the following equations (17) – (20) to implement each property as same with the liquid phase. In case of the thermal expansion for vapor phase, exponential fitting was used for more accuracy. The results of the fitting and calculation were compared with the original experimental data as seen in Figure 3-2 and 3-3.

$$Property = (a + bP + cP^2 + dP^3 + eP^4 + fP^5)\frac{283.15}{T} \tag{16}$$

$$v_g = \frac{1}{\rho_g} \tag{17}$$

$$u_g = h_g - pv_g \tag{18}$$

$$\kappa_g = -\frac{1}{v_g}\left(\frac{\partial v_g}{\partial P}\right)_T \tag{19}$$

$$s_g = \frac{u_g + pv_g}{T} \tag{20}$$

The transport properties, viscosity (Pa-s), thermal conductivity (W/m-K), and surface tension (N/m), were implemented for the generation of the execution file. Viscosity and thermal conductivity were fitted using the equations (10) and (16) which were used for other properties in the upper paragraph. Viscosity used additional 3 terms (g,h,i) for fitting. Table 3-2 and 3-3 shows the coefficients of the equations for each property. Surface tension was applied as a form of a correlation which was developed from three point values of the experimental data as seen in Equation (21).

$$Surface\ \ Tension = 0.07225 - (1.1^{-4}) \cdot T \tag{21}$$

Using the implemented thermophysical properties of DOWTHERM RP, the simulation of natural circulation was conducted based on the experimental condition and results. The conditions of the geometry and dimensions of the natural circulation loops are the same with the experiment as explained in section 3.2. Nodalization of the natural circulation loops developed in MARS code is shown in Figure 3-3. In the simulation models, heat structures are applied to the heater section and three heat exchangers with SS304 material properties. Heat source is provided to the outer surface of the heat structure of the heater. It was injected to each node as a form of heat flux equally. Cooling condition was set to maintain constant temperature of the outer surface of the three heat exchangers, 10 °C. Because the natural circulation is affected largely by pressure drop, the additional condition of pressure loss coefficients was inserted. Friction factor was calculated based on the Moody chart[17]. Because the experimental condition of the natural circulation was assumed to be in laminar flow region, the friction factor was calculated using the Hagen-Poiseuille correlation as seen in Equation (22)[34].

$$f = \frac{64}{Re} \qquad (0 \leq \mathrm{Re} \leq 2000) \tag{22}$$

Other pressure loss was considered as geometric factors which is named as a form loss. From the reference of the 'K' factor tables, each locally geometric pressure loss coefficient was claculated[35]. The values are calculated for 2 cross, 4 Tee, 1 elbow, and turbine flowmeter. Because the actual experimental loops have the additional two legs below the lower horizontal sections which is for the

drainage, the pressure loss was added through the parameter study.

3.4 Sensitivity Study of Natural Circulation using High-Pr fluids

MARS-LMR code which has each property file of each fluid can also be applied to the parameter study easily due to the convenient change of each property value. In practice, the parameter study is important to the application of the experimental data to develop the proper heat transfer correlation because the thermophysical properties of the working fluids are applied as the calculating parameters. Especially, it is more important to molten salt systems. It is due to that most thermophysical properties of the molten salts which are used in nuclear systems were measured and studied from 1950-60s. Furthermore, the properties of molten salts have sensitive change according to the temperature change. Though the extensive studies for the database were conducted, the major properties, especially for the thermal conductivity, still have the great uncertainties requiring the most challenging of measurement[1]. Also, in case of the liquid fuel salts or salt coolants with fuel materials such as buffer salts in blackout accident, thermophysical properties of the molten salts are changed from the original values. It results in different heat transfer behavior and heat transfer ability in systems including natural circulation. Thus, the parameter studies on the thermophysical properties in the target heat transfer system is meaningful enough.

In the previous study of Massachusetts Institute of Technology (MIT), similar parameter study was conducted. The sensitivity study of thermophysical properties for LiF-BeF_2 (FLiBe) and NaF-ZrF_4 coolants was performed for the Limiting Safety System Settings (LSSS) power uncertainty applied to Fluoride Salt-cooled High Temperature Test Reactor (FHTR) using RELAP5[36]. From the results, it was identified that the sensitivity study was important for the safety margin of the heat transfer systems and more accurate prediction. In this study, the purpose of the parameter study was focused on the sensitivity of each thermohypsical properties of the target molten salt, FLiBe, and its simulants, DOWTHERM RP and DOWTHERM A, in the natural circulation loops. Because mass flow rate of natural circulation which is driven by the density difference due to the temperature gradients is susceptible to the thermophysical properties, the small change of thermophysical properties of the working fluids are more significant in natural circulation compared to other heat transfer systems such as the forced circulation. Thus, the evaluation of the sensitivity of thermophysical properties was conducted for the major parameters, mass flow rate and friction factors. The measurement error of the four major properties including viscosity, thermal conductivity, heat capacity, and density was used as the uncertainty of the thermophysical properties. The information of the thermophysical properties was from the Oak Ridge National Laboratory (ORNL) and Kurchatov Institute data[25]. Each correlation of the properties and its sensitivity by the measurement error is shown in Table 3-5.

3.5 Results and Discussion

3.5.1 DOWTHERM RP Natural Circulation Experiment

In this section, for the heat transfer capability of high-Pr natural circulation, the experimental and computational numerical analysis and the sensitivity study of the thermophysical properties are performed. In the process of the natural circulation experiment, temperature data on major locations and mass flow rate are obtained. Figure 3-5, 3-6 and Table 3-6, 3-7 show the results. As seen in Figure 3-5, the inlet and outlet temperature in the heating and cooling sections have similar values that means the effect of heat loss is not large. Figure 3-6 shows mass flow rates between the calculated values from the temperature data and the measure values from the flowmeter have some difference. Particularly, the values of the mass flow rate in cases of the power lower than 400 W appear clear difference. It can be appeared due to the lower limit of the flowmeter measurement.

Between the two types of the natural circulation loops with different geometry, the mass flow rate was compared in Figure 3-7. Mass flow rates of the first and second experiment with the same condition were converged over 200 W from the several times of the experiment. The overall mass flow rate and its trend was higher in case of dH_2. The results show the different data from the prediction. Due to the large difference of the height between the heating section and cooling section, the case of dH_1 was predicted to form the higher mass flow rate. The reason of the different results could be caused by the heat exchangers. As seen in the Figure 3-1, three heat exchangers were used in both cases, but the direction and location were different. In the case of the second experiment (dH_2), two heat exchangers were horizontal and the height of the location from the bottom was lower than the first experiment (dH_1). Because only the inlet mass flow rate and temperature of the water were constant, the real contact time between the heated, main fluid and the cooled water could be different. Also, power step could be the main reason. Due to the high heat capacity of DOWTHERM RP, the irregular power step with increasing temperature could affect the main results. In real, the experimental data showed that the temperature of cooling part (heating inlet and cooling outlet) was formed higher in case of dH_2 experiment.

The experimental data were compared with the existing convective heat transfer correlations. The two correlations used in the previous studies of single-phase natural circulation in UCB were applied[37]. The first is Scarlat's correlation which is the mass flow correlation using the average thermophysical properties and the loop geometry. The normal correlation is Equation (23) and it is transformed to the Equation (25) in the steady state occasion.

$$\dot{m}^3 = \frac{2\rho_{av}^2 g\beta}{C_{p,av}} \cdot \frac{\Delta Z_{NC} Q_h}{F'} \tag{23}$$

$$F' = \sum_{i=1}^{N} \left(\frac{1}{A_i^2} \cdot \frac{L_i}{D_i} \right) f_i \tag{24}$$

$$m_{NC}^2 = 2\rho_0^2 g\beta \frac{\Delta z_{NC} \Delta T_h}{F'(\mathrm{Re}(m,T(s)))} \tag{25}$$

The second is Vijayan's correlation that is for the steady state mass flow in the fully-developed laminar or turbulent natural circulation loop. Equations (26) – (29) are utilized to calculate the analytic mass flow rate.

$$\mathrm{Re} = C \left[\frac{(Gr_m)_{\Delta z_{NC}}}{N_G} \right]^r \tag{26}$$

$$\mathrm{Re} = \frac{D_r \dot{m}}{A_r \mu_{av}} \tag{27}$$

$$(Gr_m)_{\Delta z_{NC}} = \frac{D_r^3 \rho_{av}^2 \beta_{av} g Q_h \Delta z_{NC}}{A_r \mu_{av}^3 C_{P,av}} \tag{28}$$

$$N_G = \frac{L_t}{D_r} \sum_{i=1}^{N} \left(\frac{l_{eff}}{d^{1+b} a^{2-b}} \right)_i \tag{29}$$

From two correlations, the mass flow rate was calculated and the experimental mass flow rate was compared with this results. Figure 3-8 shows the comparison that the calculated mass flow from the existing two correlations had higher values compared to the experimental mass flow. The difference is analogized due to the lower power and mass flow range. To extend the adequate correlation to the low range of the laminar natural circulation, the experimental correlation was developed in this study.

From 1.1.3 section and 3.2 section, Pr and Gr between the target molten salt system (FLiBe, DRACS system) and the similarity experimental system (DOWTHERM RP, natural circulation loops) were matched. Thus, the heat transfer correlation using Nusselt number (Nu) which is composed of Pr and Gr terms can be developed for both applications from the experimental results. From the experimental and theoretical correlations of heat transfer coefficient, heat transfer correlation was developed based on the experimental data. In single-phase natural circulation, the experimental heat transfer correlation was composed of the Prantl number (Pr) and the Grashot number (Gr) mainly as seen in Equation (33).

Though other parameters can be considered, the first correlation just considered the basic form. To obtain the correlation, theoretical heat transfer coefficient was calculated based on the Equation (34) and the experimental data firstly. The calculated values and the dimensionless numbers were utilized in the experimental equation of the heat transfer coefficient (33). Through the process, Nu correlation was generated for the single-phase natural circulation as seen in Equation (35). The application range of is $4.8\times10^4 < Gr < 5.4\times10^6$ and $7.4\times10^6 < Ra < 1.2\times10^8$. The comparison between the generated correlation and the experimental data was shown in Figure 3-9. It shows the good agreement with the deviation within 7.4 %.

$$Nu = \frac{hD}{k} \tag{30}$$

$$Gr_D = \frac{g\beta(T_w - T_b)D^3}{\nu^2} \tag{31}$$

$$T(r_i) = T(r_o) - \frac{q'''r_o^2}{4k}\left(\left(\frac{r_i}{r_o}\right)^2 - 2\ln\left(\frac{r_i}{r_o}\right) - 1\right) \quad (\ T(r_i) = T_w\ ) \tag{32}$$

$$h = \frac{k}{D}\times Nu = \frac{k}{D}\times a \cdot \mathrm{Gr}^b \cdot \mathrm{Pr}^c \tag{33}$$

$$h = \frac{q}{A\cdot(T_w - T_b)} \tag{34}$$

$$Nu = 0.0014 \cdot Gr^{0.62} \cdot \mathrm{Pr}^{0.4} \tag{35}$$

The correlation of the experiment in terms of the dimensionless numbers was also compared with the molten salt correlations of the natural convection developed in nuclear field. The correlations are obtained from the experimental data of the natural convection from a heated vertical cylinder in salts and simulant oil, DOWTHERM A. Fig. 3-10 shows the comparison with the experimental data. The experimental data of DOWTHERM RP showed similar trend of increase with other experimental data. DOWTHERM RP results had lower Nu on the low range of Ra less than about 10^8 and the trend changed on the higher region. Approximately, the figure shows the feasibility of DOWTHERM RP as a simulant of molten salts but enough experimental data on the higher region is required for more accurate evaluation.

3.5.2 MARS Simulation of DOWTHERM RP Natural Circulation

Figure 3-11 and 3-12 shows the comparison of mass flow rate between the experimental data and the simulation results. The increasing trend according to the power increase matches well so that the reliability of the experiment data can be confirmed. However, the results of the MARS simulation show the higher mass flow rate and lower temperature distribution compared to the experimental data. Basically, the fundamental condition of the MARS simulation includes the wall shear effects only related to the loss terms. Thus, the proper correlations for the pressure drop relating to the geometric effects are required to be inserted. However, the experiment lacks the enough pressure drop data and the effect of the pressure drop can be reflected in MARS simulation by the theoretical values of the loss coefficient as seen in Equation (36)[32]. The loss coefficient is composed of the user-specified constants and the index of Re. Thus, the parameter study on the loss coefficients was conducted to modify each coefficient properly.

$$Loss\ \ coefficient\ \ (K) = A + B\ \ Re^{C} \tag{36}$$

Figure 3-13 shows the results following the change of each coefficient. Initially, the mass flow rate at '1K' case, the theoretical form losses for each junction of 2 cross, 4 Tee, 1 elbow, turbine flowmeter, and two drainage parts are reflected. Because the loss value for the drainages are not fixed accurately, it was also used as one variable in loss term. On the graphs, it was identified that the trends of the increasing mass flow rate changed only according to the changes of K. The effect of the loss coefficient values, B and C showed the decrease or increase of the absolute values with constant trend. Reflecting the effect of each loss term to the mass flow rate, the adequate loss values are fixed.

The results of the MARS simulation showed the similar values of mass flow rate after applying the proper loss terms as seen in Figure 3-14, compared to the original results without and loss. However, the higher mass flow rate was observed under the lower power. The difference between the experimental data and the simulation results is assumed to have heat loss from the power supply in case of the actual experiment, considering the lower values of power. For more accurate prediction using the MARS code simulation, the enough experimental data of pressure drop and the following loss correlations in this simulation are required.

3.5.3 Sensitivity Study of Natural Circulation using High-Pr Fluids

The sensitivity study was based on the uncertainty of each thermophysical property of FLiBe molten salt as seen in Table 3-5. To utilize this study in similarity study, both FLiBe molten salt and its simulant, DOWTHERM RP and DOWTHERM A were used together. The procedure was proceeded with two

parts. The first part evaluates the effect of the sensitivity of each four thermophysical property on the mass flow rate which is the main parameter in natural circulation. For the comparison of FLiBe and two simulants, the same Pr range was applied for each fluid and the sensitivity effects were compared. Pr was calculated from the average temperature data following the increasing power step. Figure 3-15 shows the sensitivity of mass flow rate following the thermophysical properties of each fluid. From the comparison of the change of mass flow rate according to the measured uncertainty of each property, it was identified that viscosity and thermal conductivity had relatively large effect. Especially, the obvious change of viscosity effect can be due to the natural circulation system which is formed affected by the friction parameters largely. The change of mass flow rate appears to be symmetric between the increasing and decreasing values of each property. Compared to the two properties, heat capacity and density showed the less effect which could be negligible. In terms of each fluid, DOWTHERM fluids were observed to be less changed as Pr decreased and power increased. However, FLiBe molten salt showed distinct variation of mass flow rate regardless of the change of Pr and power. From the results, it can be assumed that simulants such as DOWTHERM oils can have some limitation of the prediction and reproduction of molten salt natural circulation due to different sensitivity to the major parameters.

Because FLiBe molten salt showed larger change compared to other fluids, the additional sensitivity study for FLiBe was conducted. For FLiBe molten salt, only two main properties, viscosity and thermal conductivity, were used for detail analysis. Figure 3-16 shows the change ratio of mass flow rate as Pr changes which also reflect the power change influenced by the property uncertainty. From the results, viscosity showed more sensitivity in high Pr range but the difference was not large as Pr changed. On the other hand, thermal conductivity showed more sensitivity in high temperature range with low Pr. The results can be induced from the heat transfer mode following Pr in which convective heat transfer affected by viscosity becomes larger as Pr increases and conductive heat transfer affected by thermal conductivity becomes larger as Pr decreases.

Additional analysis was applied at 1200 W power. It was for the observation of the effect of two properties following the arbitrary scale of the property uncertainty. Differently from the sensitivity in previous section which used the experimental measurement error as an uncertainty, the same random uncertainty was applied in this case. Figure 3-17 shows the results of change of the mass flow rate. The case of thermal conductivity had less effect of the uncertainty scale. The change of mass flow rate was within 1.5 % with any value of uncertainty. Whereas viscosity changed with regular tendency to the property uncertainty scale. As the uncertainty of viscosity increased, the scale of change in mass flow rate also increased. Within the experimental measurement error, the maximum sensitivity was within 12 %.

The effect of the uncertainty combination with the two properties was also evaluated. Figure 3-18 and Table 3-9 shows the results. It also shows that the viscosity effect is absolute and the maximum available

sensitivity within the experimental measurement error is about 12.76 % in natural circulation. From the various analysis of the sensitivity study, the effect of the property uncertainties was identified to affect the natural circulation ability. The change of thermophysical properties must be thought when molten salts are used as forms of eutectics or fuel materials in nuclear application. Thus, the accurate measurement of the thermophysical properties and the effect of them to natural circulation ability should be considered seriously.

The second part is for the friction factor which is induced from the difference of mass flow rate between the experiment and code simulation. In the previous section 3.5.2, the difference between the experimental mass flow rate and the mass flow rate of MARS simulation in DOWTHERM RP natural circulation was identified. The results show the similar tendency of increase following power increase but the higher values in case of MARS simulation. One of the major reason of the difference was considered as the friction factors. It is because the wall friction includes only the wall shear effects omitting other several parameters for geometry effects in basic condition of MARS simulation. In actual, as the mass flow in natural circulation quite depends on the driving head and the pressure losses along the circulation path, the evaluation of the friction factors between the experimental values and MARS simulation can give meaningful analysis.

For the calculation of the friction coefficient, the following theoretical equations were used. Fundamentally, the pressure drop was set as the loop momentum Equation (37) in natural circulation loop. In this equation, the driving head (ΔP_B) and the pressure loss by friction (ΔP_f) have the same values because the pressure drop by pump (ΔP_{pump}) is zero in natural circulation. Also, from the pressure loss by friction, friction factor (f) can be derived. From the equations, the calculation of friction factors was performed.

$$\sum_k L_k \frac{\partial (G_m)_k}{\partial t} = \Delta P_{pump} - \Delta P_f + \Delta P_B \tag{37}$$

$$P_B = \beta \rho_0 \Delta T g \Delta L \tag{38}$$

$$\Delta P_f = f \frac{\rho_l L V^2}{2 D_e} \tag{39}$$

$$f = \frac{2 \Delta P_f D_e}{\rho_l L V^2} \tag{40}$$

Figure 3-19 and Table 3-10 shows the calculated values of the friction coefficients between the

experiment and MARS simulation. From each value in local sections of the natural circulation loop, it was confirmed that the friction coefficient was larger around the heater compared to other sections including the heat exchanger section. In addition, MARS simulation has much lower values in the major sections, heater and heat exchanger, compared to the experiment. Thus, the sensitivity study on the friction coefficient can contribute to the modification of the local friction loss which is for accurate prediction of natural circulation.

For the analysis of the friction coefficients, four main thermophysical properties and each three fluids were used same as the first sensitivity study. It was conducted on the Pr range of 30. As shown in Figure 3-20 and Table 3-11, the effect of the viscosity uncertainty is dominant. In addition, the calculated friction coefficients are the least sensitive to each property uncertainty in case of DOWTHERM RP. It is the similar results with the first study. For the comparison of the effect of friction factor on the mass flow rate, the change of the uncertainty tendency between them was also compared as seen in Figure 3-21. From the results, it was confirmed the value of Pr was not dominant to uncertainty of the mass flow rate and the friction coefficient. The tendency of the decreasing *f* and that of the increasing mass flow rate are proportional.

From the two parts of the sensitivity study, the effect of the uncertainties from the thermophyiscal properties was confirmed. In the process of the study, ambivalent aspects of DOWTHERM oils as simulants was identified. Especially, DOWTHERM RP had the lowest sensitivity to most cases, differently from FLiBe molten salt. The different sensitivity between FLiBe and DOWTHERM RP can give the limitation to DOWTHERM RP as a simulant, however, it can also be used as a more useful simulant if the target fluid can have accurate property values.

Table 3-1. Convective heat transfer correlations including molten salt application[28,29,30,31].

Options	Correlation	Range Condition	
(0.7 ≤ Pr ≤ 160)	$Nu = 0.023\mathrm{Re}^{0.8}\mathrm{Pr}^{n}$ $(n = 0.4\ for\ heating, n = 0.3\ for\ cooling)$	Re ≥ 10,000 L/D ≥ 10	Dittus-Boelter
(0.7 ≤ Pr ≤ 16,700)	$Nu = 0.0242\mathrm{Re}^{0.81}\mathrm{Pr}^{0.333}(\mu_b/\mu_w)^{0.14}$	Re ≥ 10,000 L/D ≥ 10	Sieder-Tate
(molten salts)	$Nu = 0.037(\mathrm{Re}^{0.75} - 180)\mathrm{Pr}^{0.42}(1 + (\boldsymbol{d/l})^{2/3})(\boldsymbol{\mu_b/\mu_w})^{0.14}$	-	Hausen
(molten salts)	$Nu = 0.012(\mathrm{Re}^{0.87} - 280)\mathrm{Pr}^{0.4}(1 + (\boldsymbol{d/l})^{2/3})(\boldsymbol{Pr_b/Pr_w})^{0.11}$	-	Gnielinski
	$Nu = 0.023\mathrm{Re}^{4/5}\mathrm{Pr}^{1/3}$		
(4 < Pr <14)	$Nu = 0.107(\mathrm{Re}^{2/3} - 135)\mathrm{Pr}^{1/3}(\boldsymbol{\mu_b/\mu_w})^{0.14}$ $Nu = 0.0234\mathrm{Re}^{0.8}\mathrm{Pr}^{1/3}(\boldsymbol{\mu_b/\mu_w})^{0.14}$	3500 < Re < 12000 (Turbulent) Re > 12000 (Turbulent)	ORNL FLiBe correlation
(8 < Pr < 36)	$Nu = 0.015(\mathrm{Re}^{0.85} + 138)\mathrm{Pr}^{1/3}(\boldsymbol{\mu_b/\mu_w})^{0.11}$	3400 < Re < 14000 $1.4 < \frac{\mu}{\mu_w} < 3.1$	UCB S-HT[2] (Scaled High Temperature Heat Transfer)
(0.5 < Pr < 2000)	$Nu = [(f/8)\mathrm{RePr}]/[1.07 + 12.7(f/8)^{1/2}(\mathrm{Pr}^{2/3} - 1)]$	10^4 < Re < 5*10^6	Petukhov
(0.5 < Pr < 2000)	$Nu = [(f/8)(\mathrm{Re} - 1000)\mathrm{Pr}]/[1 + 12.7(f/8)^{1/2}(\mathrm{Pr}^{2/3} - 1)]$	3000 < Re < 5*10^6	Modified Petukhov (by Gnielinski)

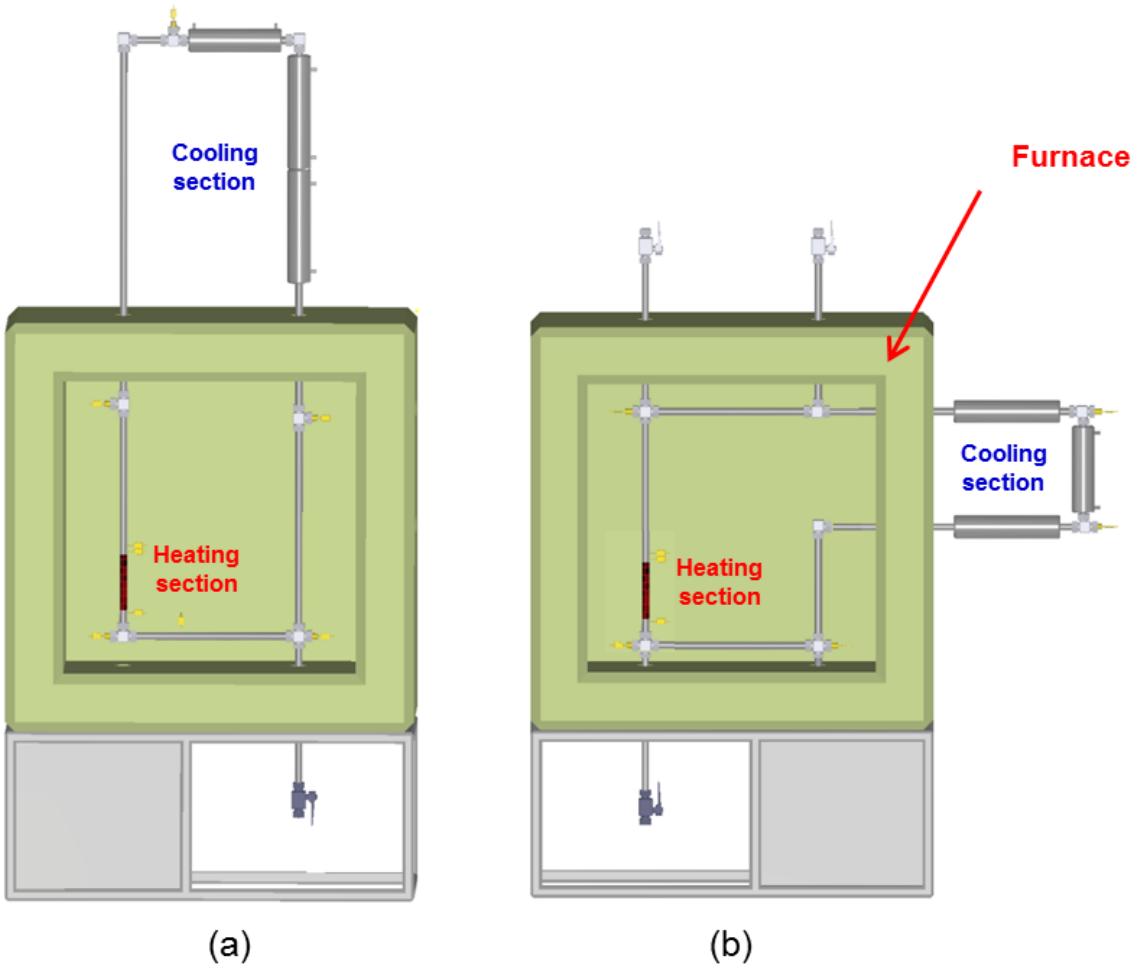

Fig. 3-1. Scheme of the natural circulation loop.

Table 3-2. Experimental condition of DOWTHERM RP natural circulation.

Pipe material	SS 304
Power	60 – 600 W
Pressure	Atmospheric pressure
Heating	Indirect heating (Nichrome coil heater)
Cooling	Tube-in-tube (water, 10 ˚C, 2.42 kg/s)
Fluid	DOWTHERM RP (Diaryl Alkyl)

Table 3-3. Coefficients of the curve fit for liquid thermodynamic properties[27].

Property		a	b	c	d	e	f
Saturated Liquid	Density	1.493.E+03	-3.332.E+00	1.248.E-02	-2.968.E-05	3.444.E-08	-1.622.E-11
	Enthalpy	-6.511.E+05	4.121.E+03	-1.235.E+01	2.771.E-02	-2.777.E-05	1.106.E-08
	Specific Heat	-2.364.E+03	3.946.E+01	-1.703.E-01	3.904.E-04	-4.422.E-07	1.979.E-10
	Thermal conductivity	1.856.E-01	-1.600.E-04	5.913.E-12	-	-	-
	Viscosity	5.135.E+00	-8.395.E-02	5.971.E-04	-2.409.E-06	6.029.E-09	-9.579.E-12

Table 3-4. Coefficients of the curve fit for vapor thermodynamic properties[27].

Property		a	b	c	d	e	f	
Saturated Vapor	Density	4.391.E-05	6.119.E-05	-5.401.E-08	2.245.E-10	-5.422.E-13	5.220.E-16	0<P≤400
		4.144.E-03	4.187.E-05	8.414.E-09	-3.569.E-12	4.893.E-16	-2.110.E-20	400<P≤11000
		9.454.E-02	3.917.E-05	-9.340.E-12	1.696.E-17	-1.010.E-23	2.524.E-30	P>11000
	Enthalpy	4.004.E+05	-1.443.E+03	7.579.E+00	-1.116.E-02	1.103.E-05	-5.134.E-09	-
	Specific Heat	-5.426.E+03	6.248.E+01	-2.532.E-01	5.432.E-04	-5.842.E-07	2.508.E-10	-
	Thermal conductivity	-5.137.E-03	3.016.E-04	4.668.E-08	-	-	-	-
	Viscosity	-5.758.E-06	9.618.E-08	-4.013.E-10	-1.011.E-12	-1.249.E-15	6.114.E-19	-

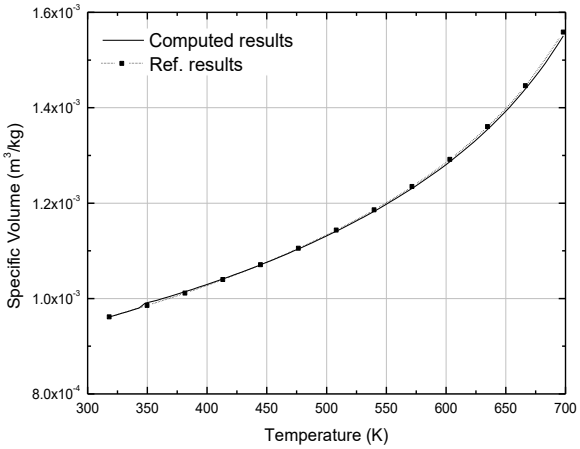

Specific volume

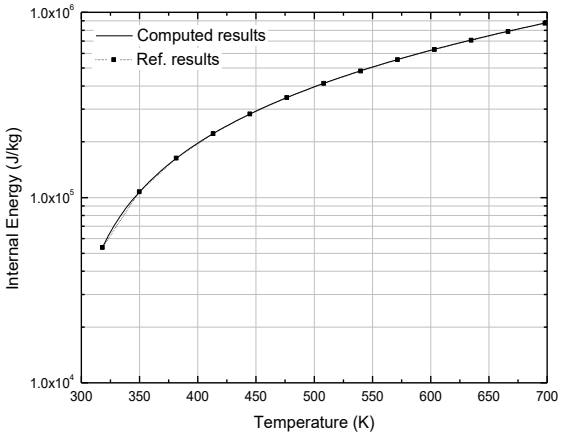

Specific internal energy

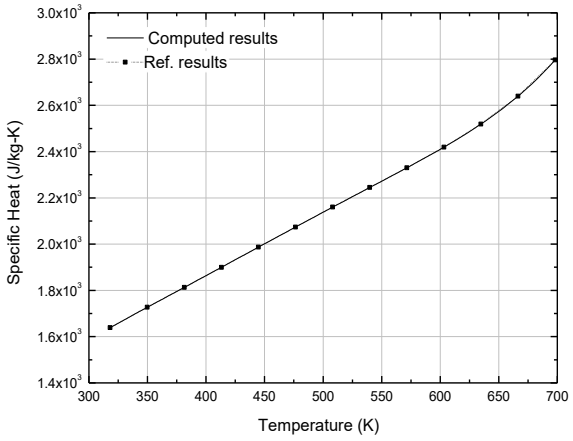

Specific heat

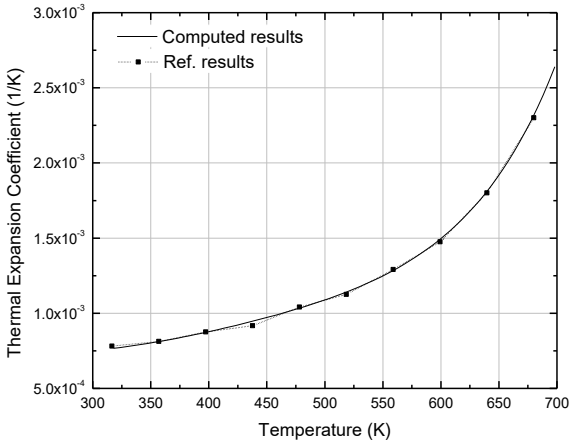

Thermal expansion coefficient

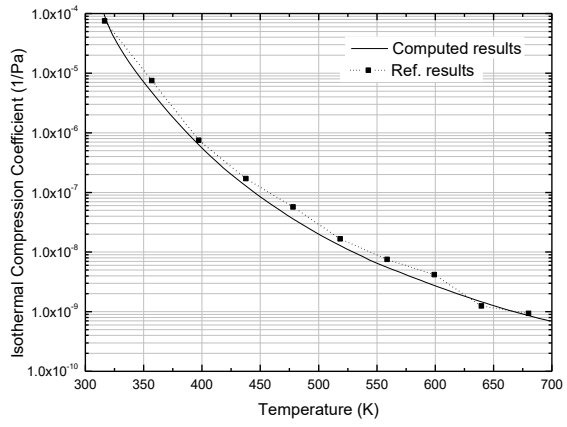

Isothermal compressibility

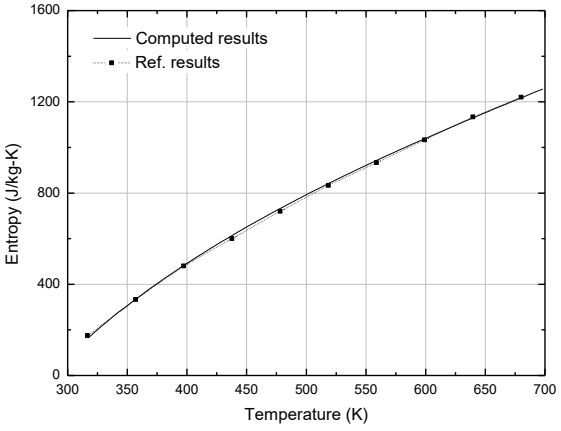

Specific entropy

Fig. 3-2. Thermodynamic properties of liquid phase of DOWTHERM RP.

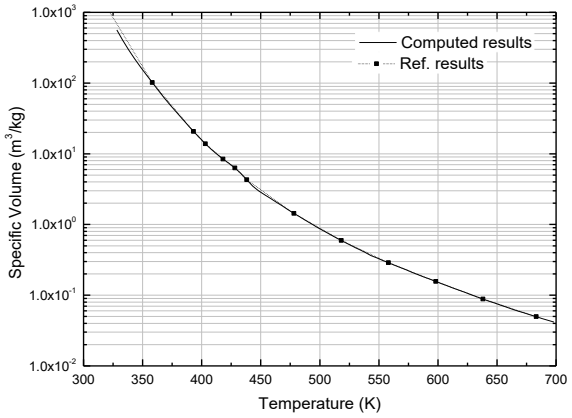

Specific volume

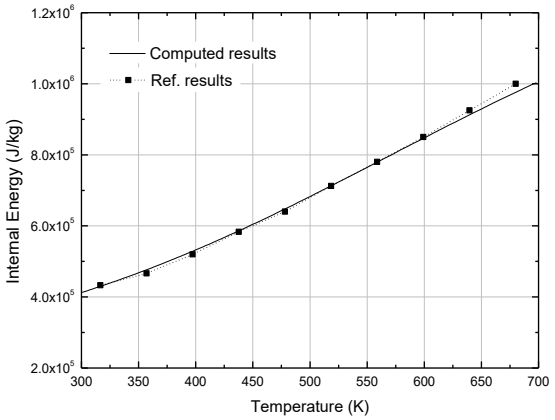

Specific internal energy

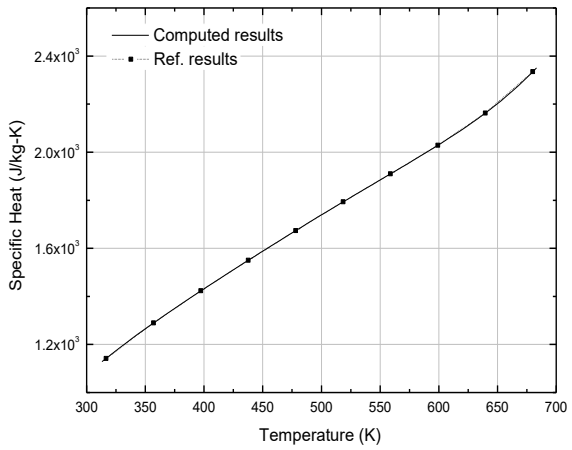

Specific heat

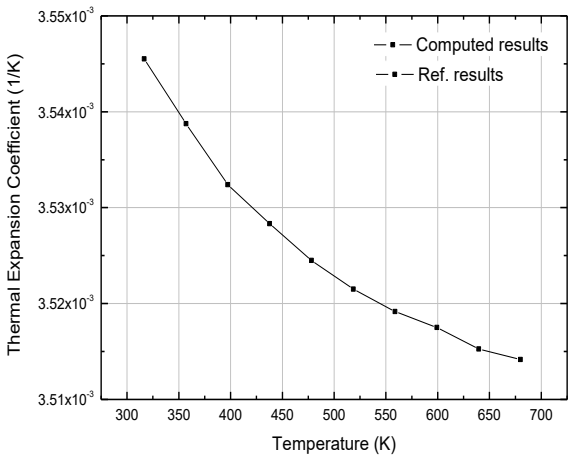

Thermal expansion coefficient

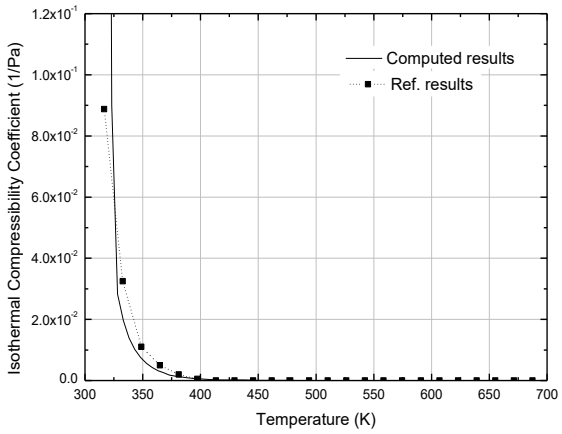

Isothermal compressibility

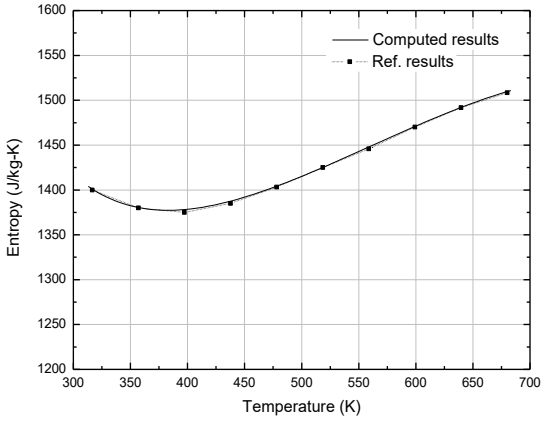

Specific entropy

Fig. 3-3. Thermodynamic properties of vapor phase of DOWTHERM RP.

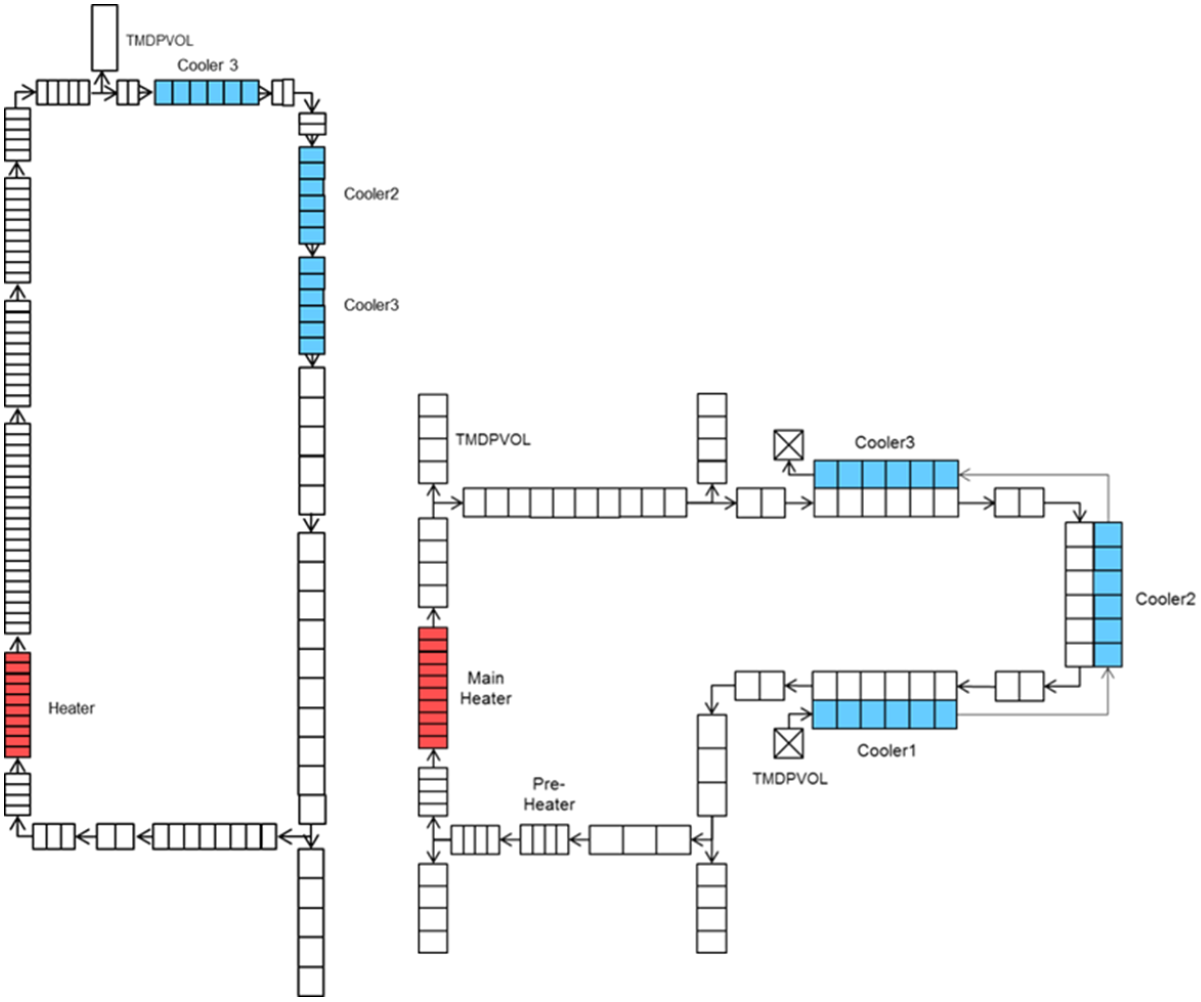

Fig. 3-4. Nodalization of natural circulation loops

(a) ΔH=1.415 m, (b) ΔH=0.415 m.

Table 3-5. Modified thermophysical properties and measurement uncertainties of FLiBe[25].

Properties	Value	Sensitivity
Viscosity (Pa s)	1.16E-4*exp(3755/T)	20 %
Thermal conductivity (W/m K)	0.63+0.0005*T	15 %
Heat capacity (J/kg K)	2416	2 %
Density (kg/m^3)	2413-0.4884*T	0.05 %

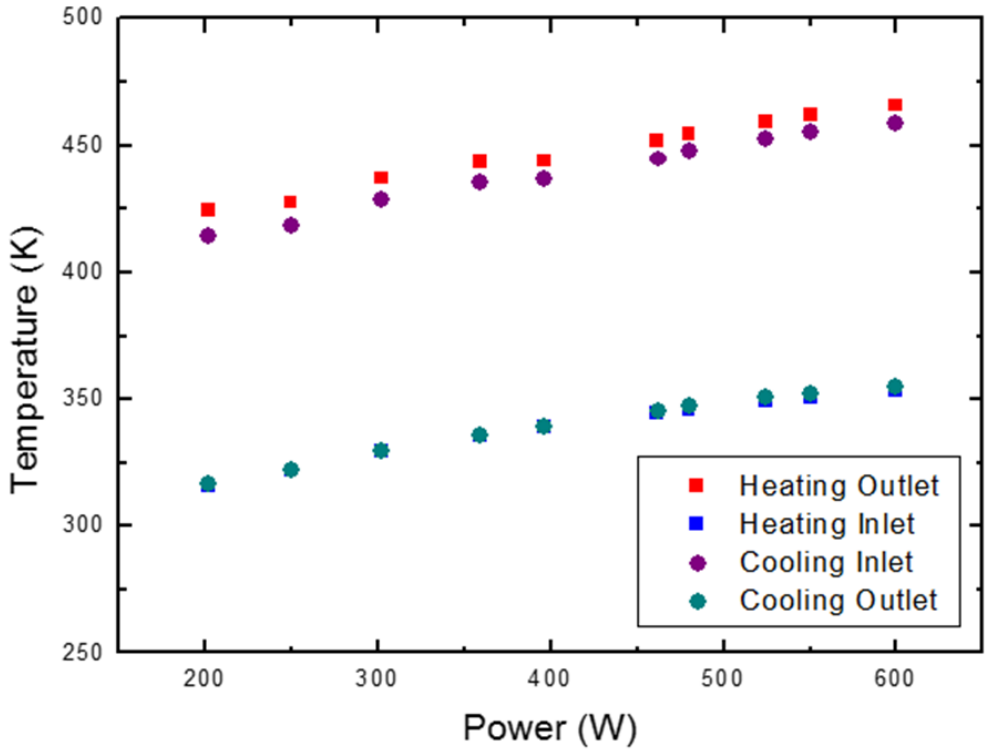

Fig. 3-5. Temperature of the heating and cooling sections in DOWTHERM RP natural circulation (ΔH=1.415 m).

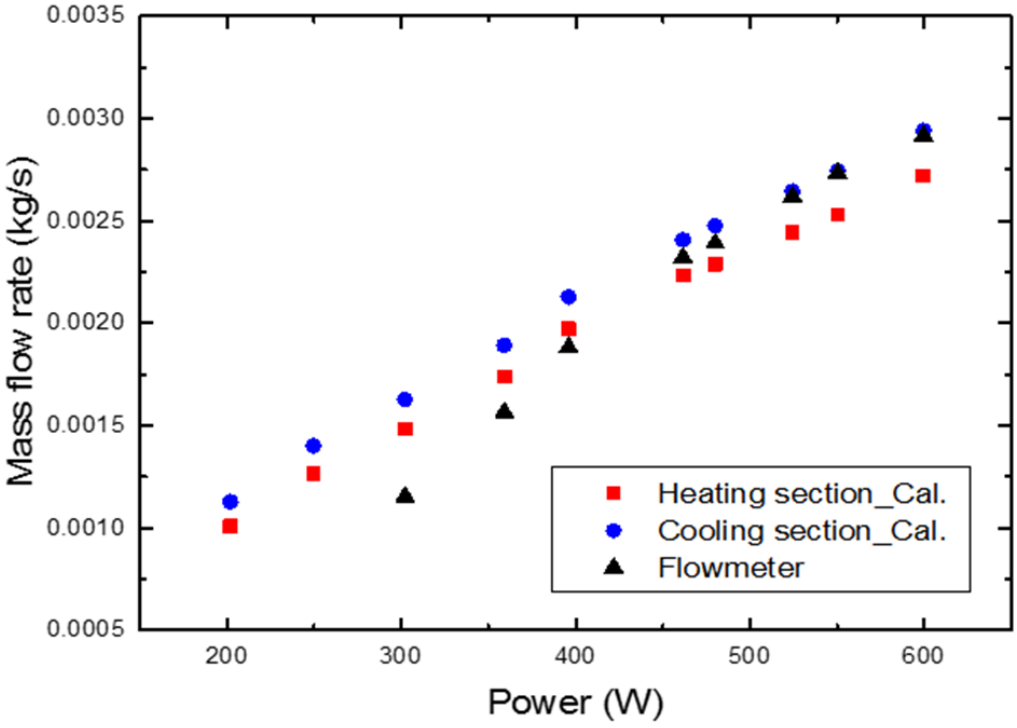

Fig. 3-6. Mass flow rate of DOWTHERM RP natural circulation (ΔH=1.415 m).

Table 3-6. Experimental data of temperature at each power in DOWTHERM RP natural circulation (ΔH=1.415 m).

Power (W)	Heating section outlet (°C)	Heating section inlet (°C)	Heating section ΔT (°C)	Cooling section Inlet (°C)	Cooling section Outlet (°C)	Cooling section ΔT (°C)
202.1	151.19	42.78	108.40	141.48	43.86	97.62
249.6	154.33	48.48	105.85	145.48	49.18	96.30
302.1	163.89	56.24	107.64	155.78	56.85	98.93
359.1	170.58	62.25	108.33	162.74	62.61	100.13
396	170.80	65.89	104.92	164.10	66.35	97.74
461.5	178.42	71.52	106.90	171.73	72.10	99.63
480	181.21	73.05	108.17	174.87	74.56	100.31
524.4	185.98	76.02	109.95	179.63	77.62	102.01
550.25	188.81	77.62	111.19	182.11	79.26	102.85
599.4	192.45	80.42	112.03	185.88	81.85	104.03

Table 3-7. Experimental data of mass flow rate at each power in DOWTHERM RP natural circulation (ΔH=1.415 m).

Power (W)	Mass flow rate (kg/s) (Heating section _calculation)	Mass flow rate (kg/s) (Cooling section _calculation)	Mass flow rate (kg/s) (Flowmeter)	Max. deviation (%)
202.1	0.00101	0.00113	-	-
249.6	0.00127	0.00140	-	-
302.1	0.00149	0.00163	0.00115	40.96
359.1	0.00174	0.00189	0.00157	20.74
396	0.00197	0.00213	0.00188	13.04
461.5	0.00223	0.00241	0.00232	3.79
480	0.00229	0.00248	0.00239	4.33
524.4	0.00244	0.00264	0.00262	6.65
550.25	0.00253	0.00274	0.00274	7.58
599.4	0.00272	0.00294	0.00292	6.74

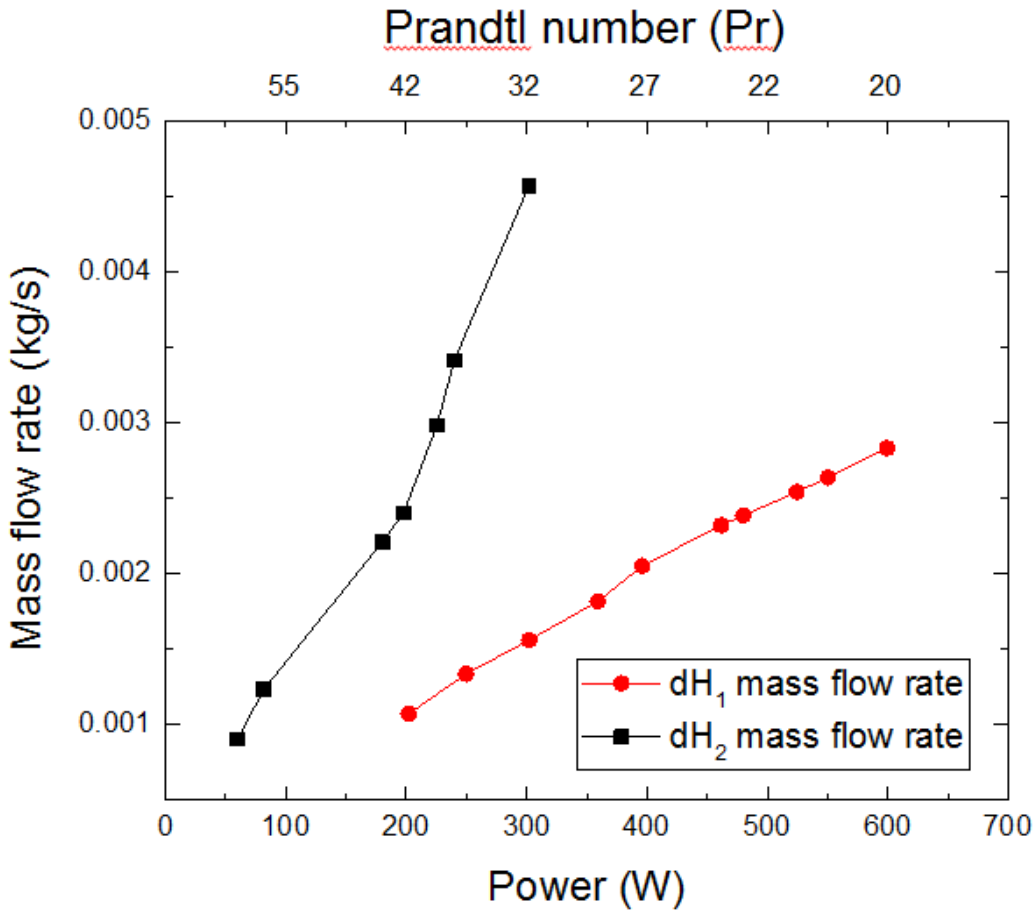

Fig. 3-7. Mass flow of DOWTHERM RP natural circulation

(dH_1: ΔH=1.415 m, dH_2: ΔH=0.415 m).

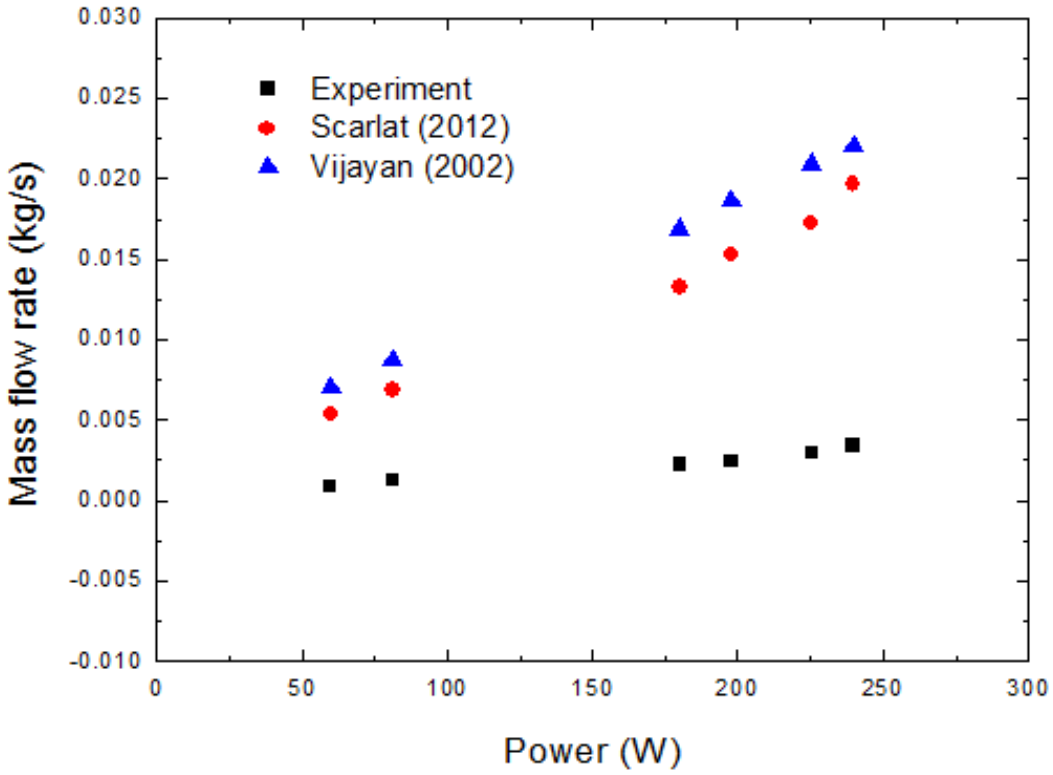

Fig.3-8. Comparison of mass flow rate between the experimental data and the existing heat transfer correlations.

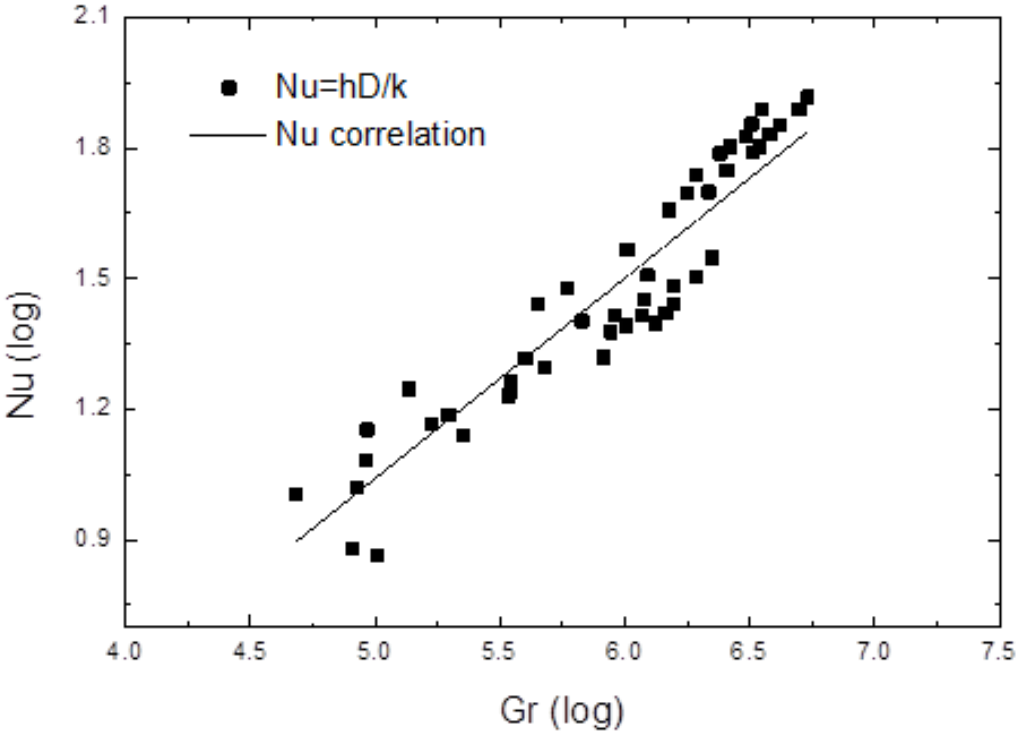

Fig. 3-9. Experimental Nu correlation of single-phase laminar natural convection.

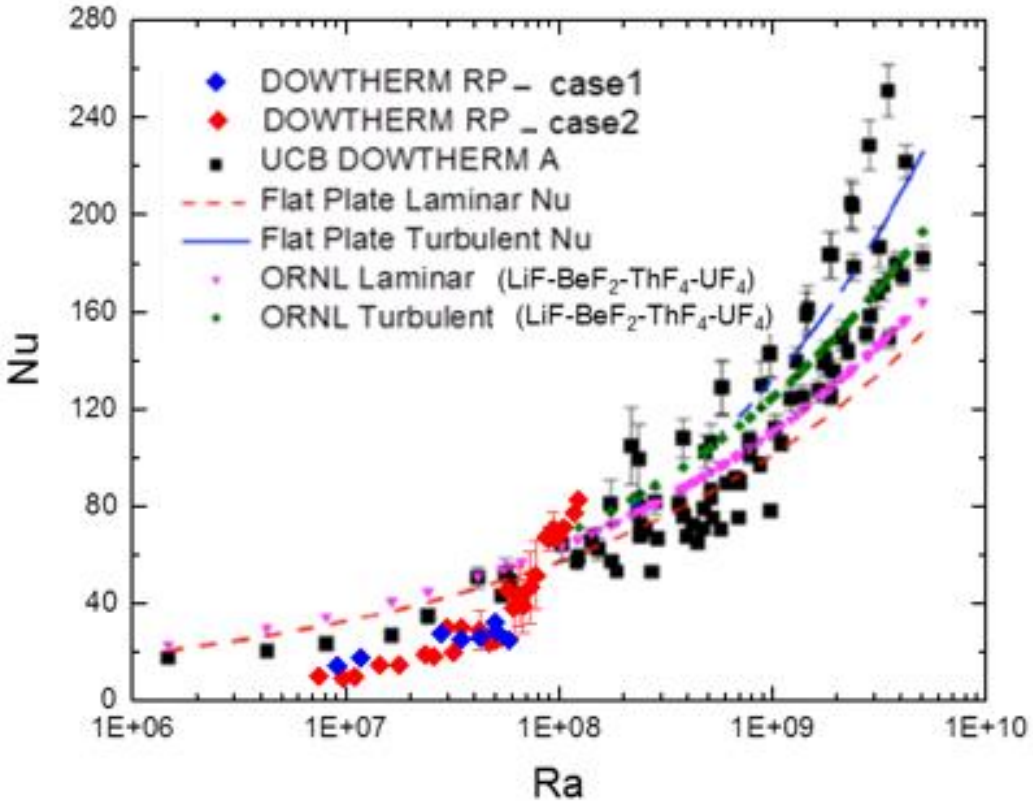

Fig. 3-10. Comparison between experimental correlation and experimental data of natural convection with molten salts and its simulants[38]
(case 1: ΔH=0.415 m, case 2: ΔH=1.415 m).

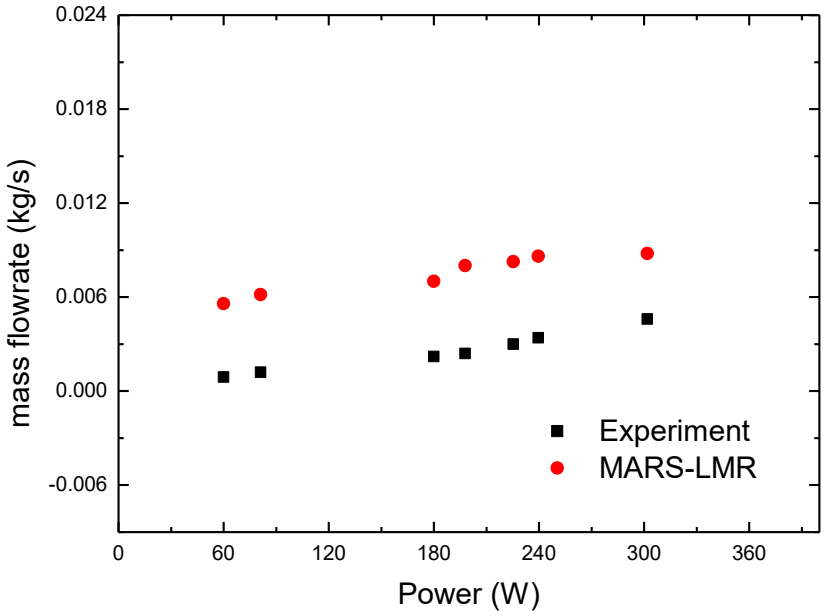

Fig. 3-11. Comparison of mass flow rate in natural circulation of ΔH=0.415 m.

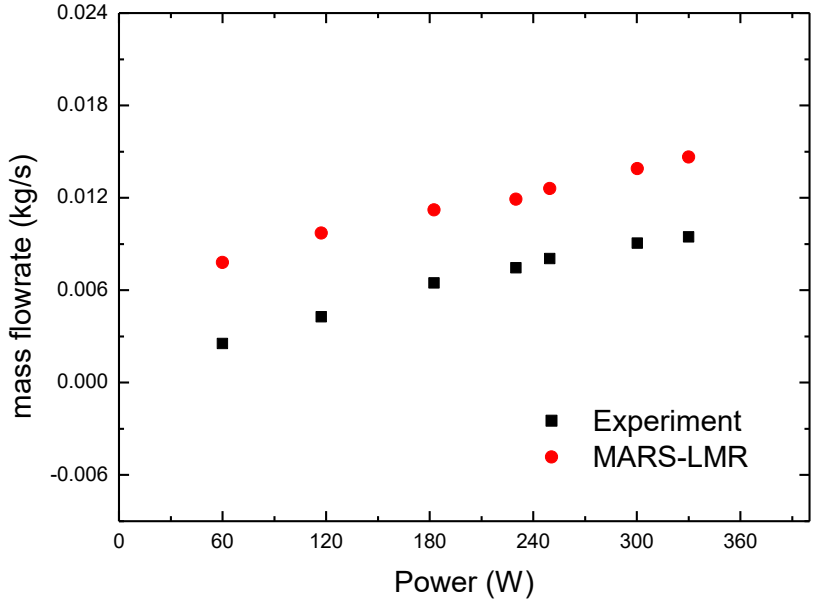

Fig. 3-12. Comparison of mass flow rate in natural circulation of ΔH=1.415 m.

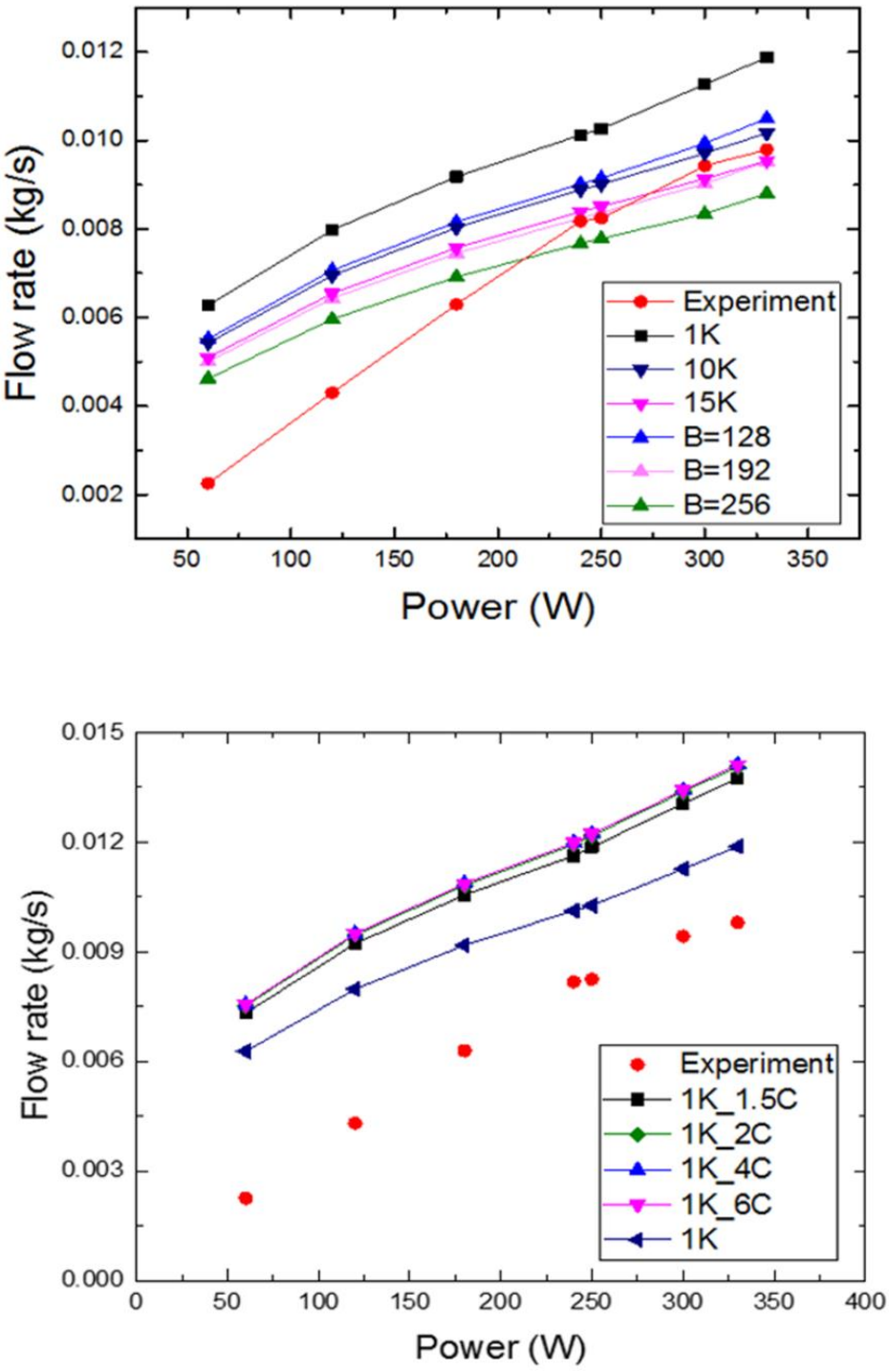

Fig. 3-13. Natural circulation mass flow rate following the change of loss coefficients.

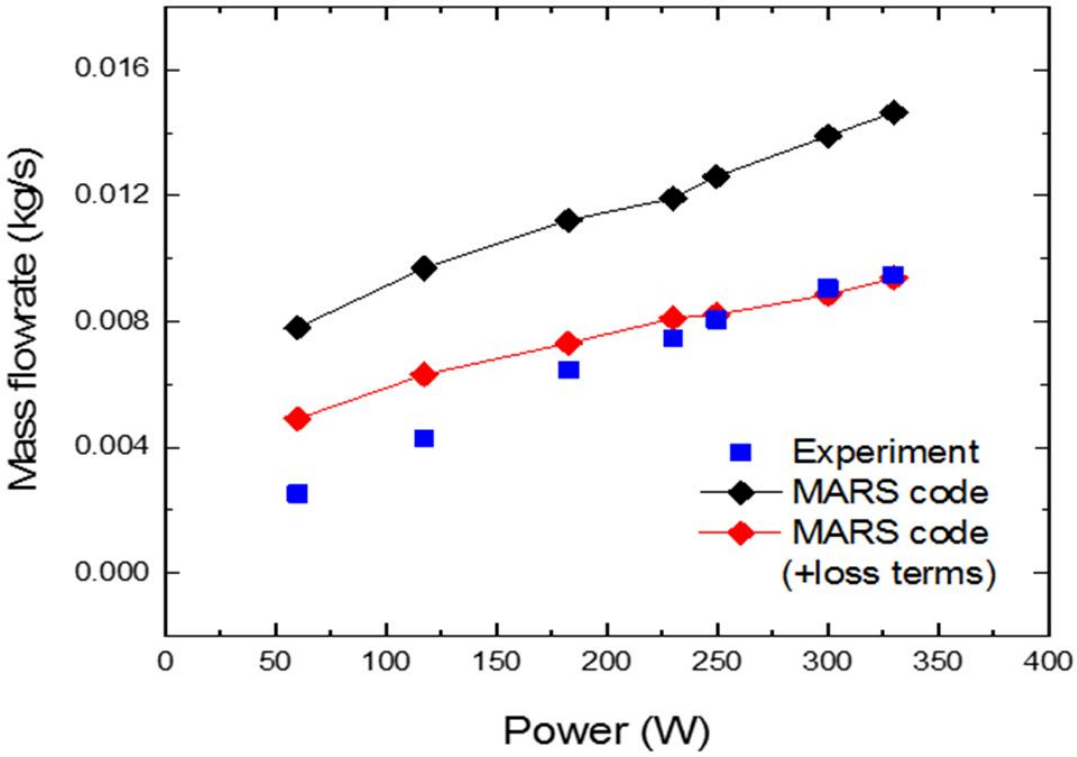

Fig. 3-14. Comparison of mass flow rate in natural circulation of ΔH=1.415 m.

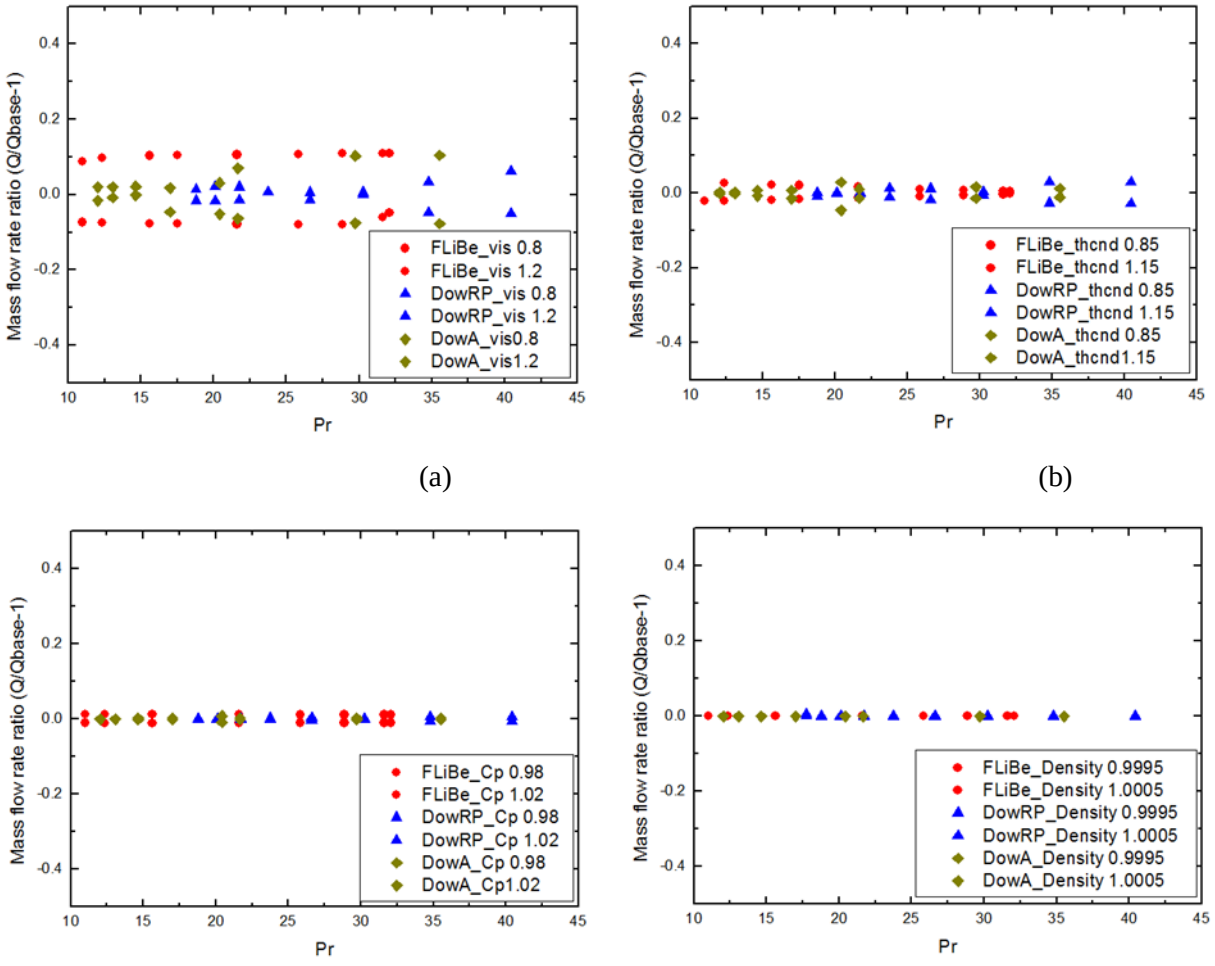

Fig. 3-15. Sensitivity of mass flow rate in natural circulation following each property uncertainty.

Table 3-8. Sensitivity effect of mass flow rate in natural circulation for FLiBe and its simulants.

Property uncertainty	Viscosity (Pa s)	Thermal conductivity (W/m K)	Heat capacity (J/kg K)	Density (kg/m^3)
	20 %	15 %	2 %	0.05 %
$LiF\text{-}BeF_2$ (FLiBe)	10.96 %	2.63 %	1.17 %	0.001 %
DOWTHERM RP	6.30 %	3.07 %	0.49 %	0.048 %
DOWTHERM A	10.45 %	4.57 %	0.85 %	0.044 %

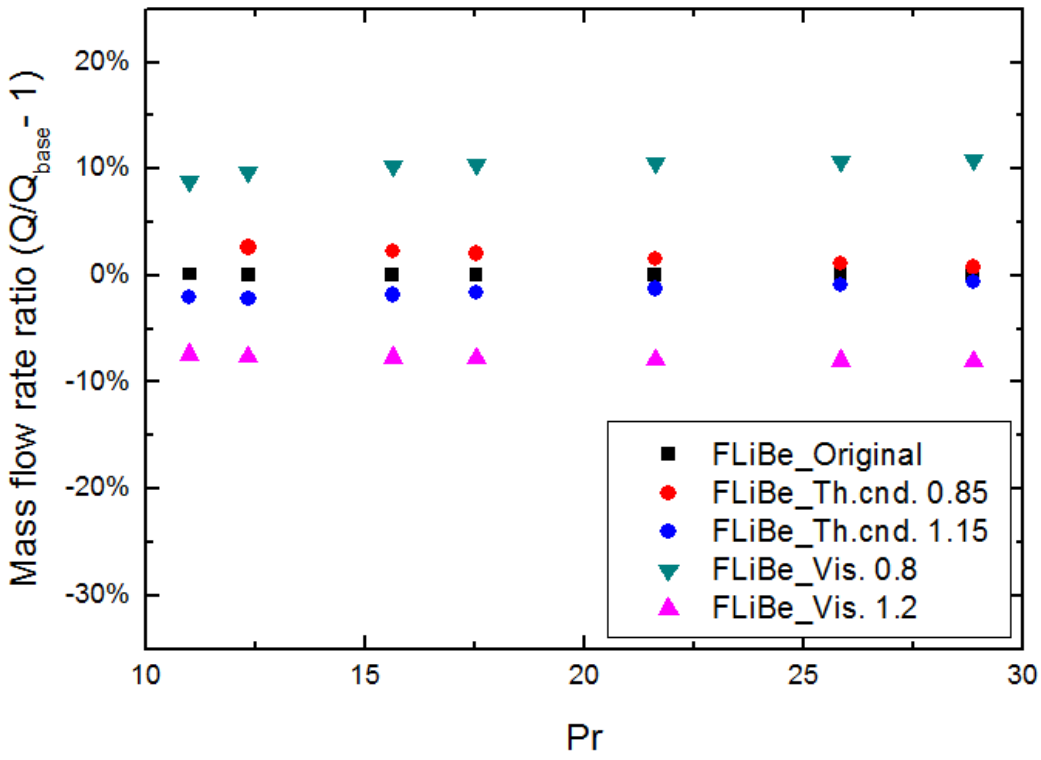

Fig. 3-16. Sensitivity of mass flow rate in natural circulation following each property uncertainty with power increasing (FLiBe).

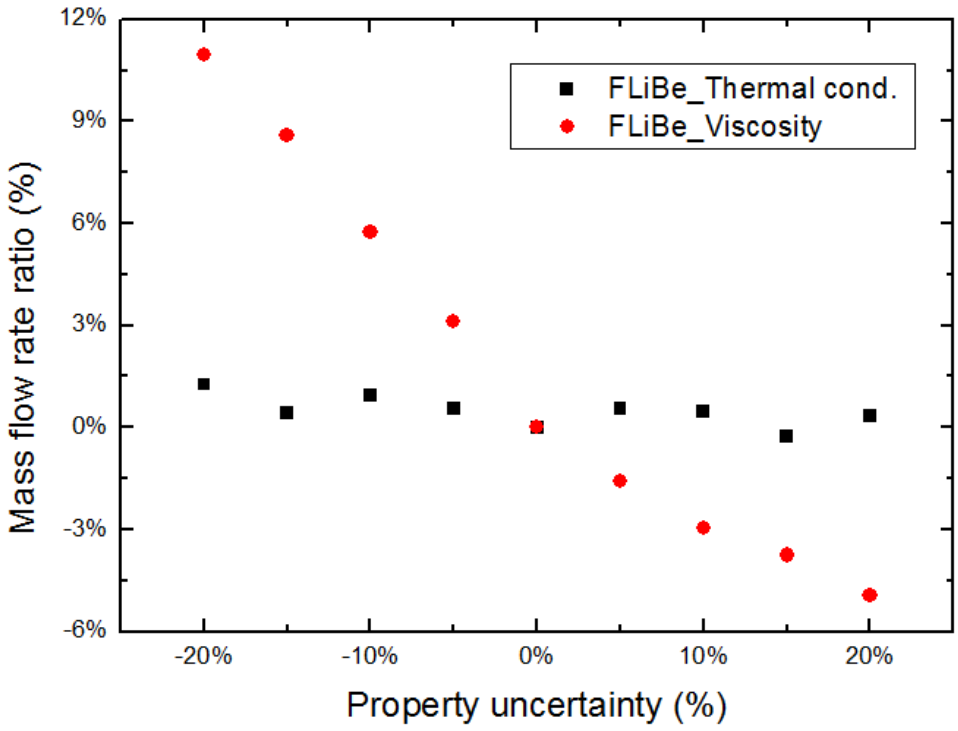

Fig. 3-17. Sensitivity of mass flow rate in natural circulation following random uncertainty of viscosity and thermal conductivity (FLiBe).

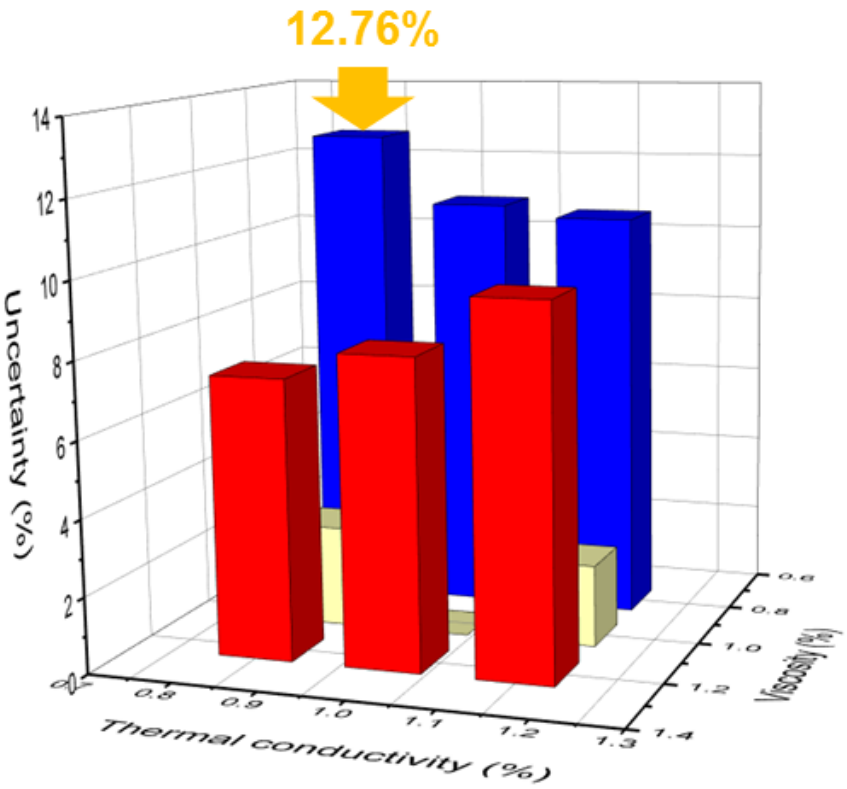

Fig. 3-18. Sensitivity effects of viscosity and thermal conductivity of FLiBe on mass flow rate in natural circulation.

Table 3-9. Sensitivity effects of viscosity and thermal conductivity of FLiBe on mass flow rate in natural circulation.

FLiBe	Vis. 0.8	Vis. 1.0	Vis. 1.2
Th. Cnd. 0.85	12.76 %	2.63 %	7.32 %
Th. Cnd. 1.0	10.96 %	0 %	8.04 %
Th. Cnd. 1.15	10.66 %	2.13 %	9.58 %

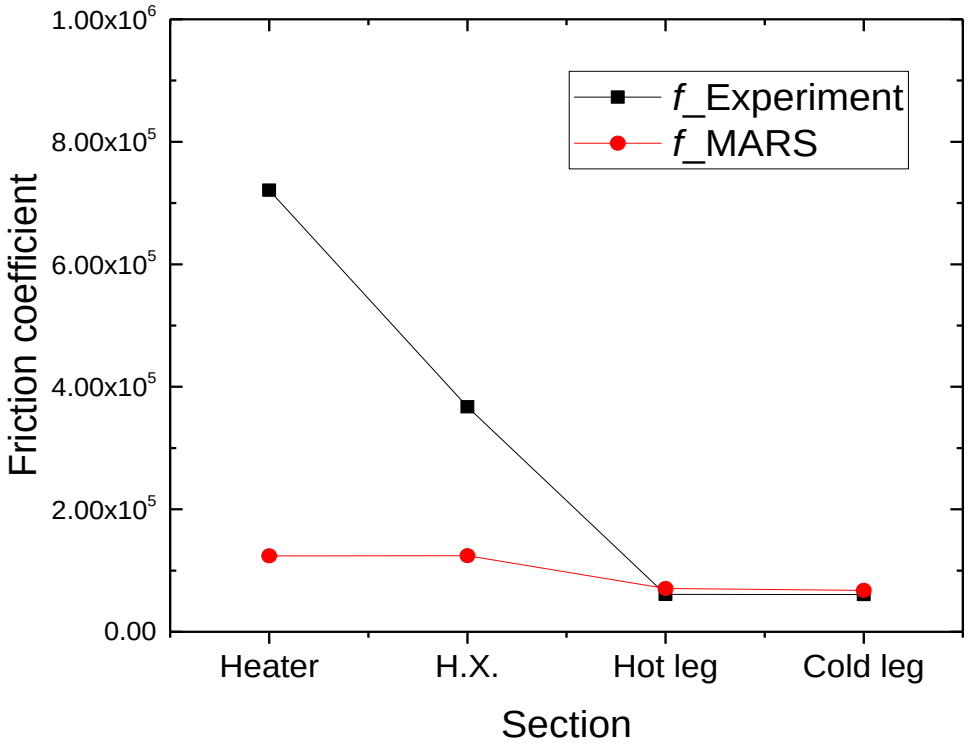

Fig. 3-19. Comparison of the friction coefficient between experimental data and MAR simulation of DOWTHERM RP in each section at 240 W.

Table 3-10. Comparison of the friction coefficient between experimental data and MAR simulation of DOWTHERM RP in each section.

	Power	Heater *f*	Heat exchanger *f*	Hot leg *f*	Cold leg *f*
Experiment	240 W	7.2088E5	3.6723E5	6.1216E4	6.0890E4
MARS		1.2406E5	1.2418E5	7.0635E4	6.7617E4
Experiment	300 W	4.5265E5	2.3002E5	3.8399E4	3.8179E4
MARS		0.9971E5	0.9977E5	5.6699E4	5.4384E4

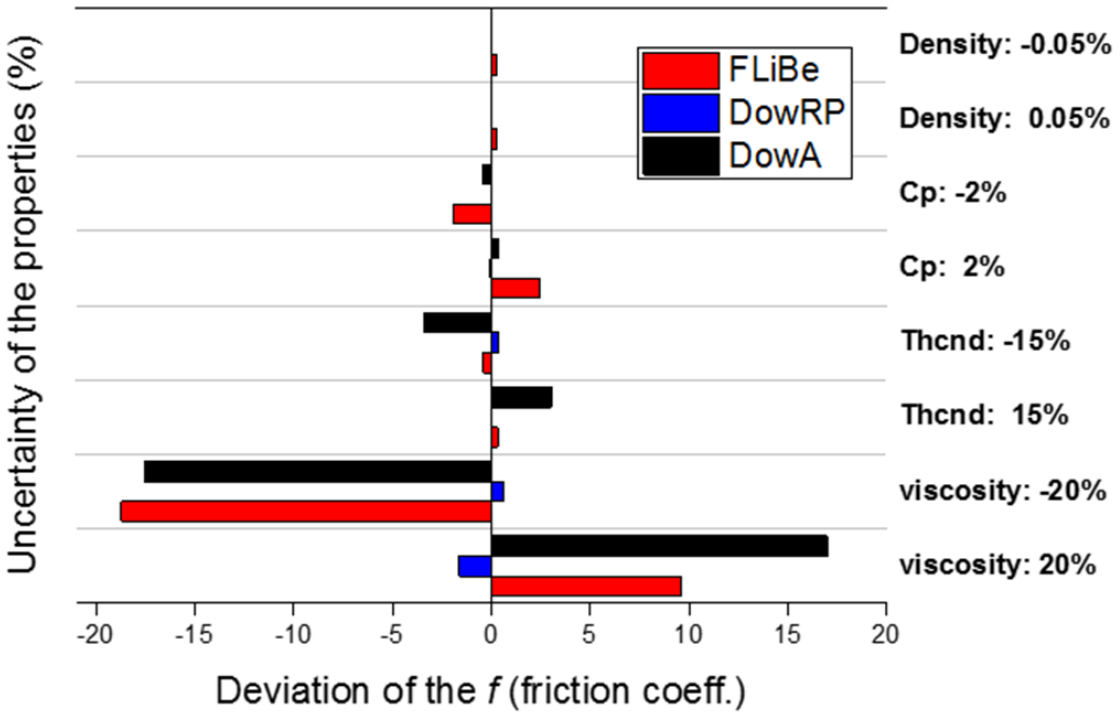

Fig. 3-20. Sensitivity effect of the thermophysical properties on friction coefficients.

Table 3-11. Sensitivity of the friction coefficients in heater section on the Pr range of 30.

Property uncertainty		Viscosity (Pa-s)	Thermal conductivity (W/m-K)	Heat capacity (J/kg-K)	Density (kg/m^3)
		20 %	15 %	2 %	0.05 %
Sensitivity of friction coefficient	$LiF\text{-}BeF_2$ (FLiBe)	18.72 %	0.42 %	2.44 %	0.29 %
	DOWTHERM RP	1.64 %	0.39 %	0.05 %	0.04 %
	DOWTHERM A	17.55 %	3.37 %	0.40 %	0.03 %

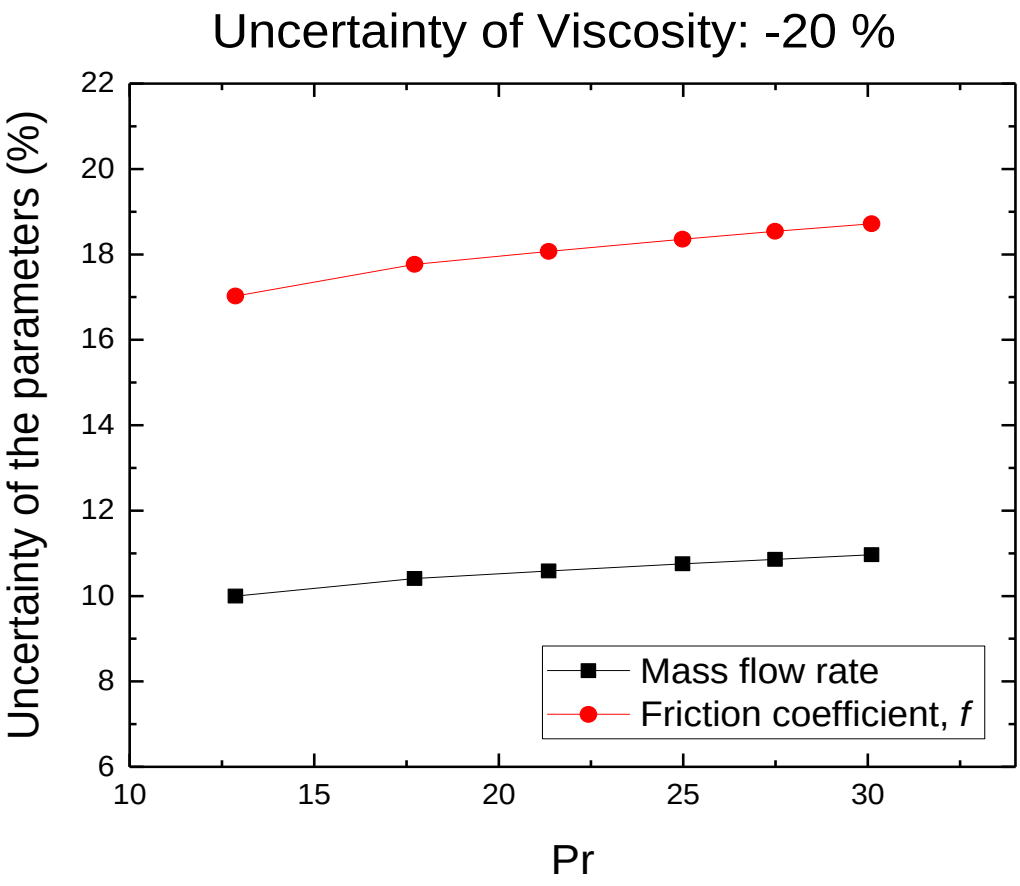

Fig. 3-21. Sensitivity effect of the viscosity on the mass flow rate and the friction coefficient.

IV. Performance for Flow Characteristics of High-Pr Natural Circulation

4.1 Introduction

DOWTHERM RP natural circulation is one of the high-Pr heat transfer. In the previous part, the heat transfer capability of high-Pr natural circulation using DOWTHERM RP. Because high-Pr fluid has different characteristics in terms of the boundary layers and distributions of temperature and velocity, the observation of the flow characteristics of DOWTHERM RP by PIV visualizing technique and CFD simulation can contribute to the study of the high-Pr heat transfer. Also, it can give the information to judge the similarity and realize the limitation in aspect of flow characteristics because the target molten salt, FLiBe, and its simulant oil, DOWTHERM RP, have different values of each thermo-physical property.

In the previous section, the quantitative experimental data of temperature and mass flow rate were discussed and the experimental correlation was developed. In this section, the visualized flow pattern and distribution of the high-Pr DOWTHERM RP natural circulation was treated. Because the similarity is satisfied only by matching the dimensionless numbers and the scaling law theoretically between FLiBe and simulant oil, the comparison of the flow pattern can give the reliable judgement of the feasibility of the similarity technique between the molten salt and simulant oil. Also, as DOWTHERM RP was used as a simulant oil of FLiBe molten salts, it also has high Pr range in the operating temperature of liquid phase. Thus, the study can be one of the beginning step of the understanding the flow characteristics of high-Pr molten salts, especially for the natural circulation. The observation of the flow region was conducted by the experiment and the CFD simulation. In the experiment, PIV visualization was used to observe the natural circulation of DOWTHERM RP in the experimental loop near the heating section. For the more detail observation, CFD simulation with the same condition of natural circulation was also conducted.

Theoretically, natural convection is driven by the buoyancy forces which is induced by the density differences of the working fluids occurring from the local temperature gradients. In a flat plate or in a pipe with enough developed length, the buoyancy forces are affected by the flow laminarization near the wall largely. In the previous study of T. Aicher and H. Martin (1997), the laminarization of the flow in natural convection was investigated following the buoyancy effect[39]. As the fluid near the wall becomes hotter, the velocity difference between the boundary layer velocity and the average velocity decreases by the decrease of the shear stress between the bulk flow and the perimeter. The phenomenon leads the flow to the laminarization. As shown in Figure 4-1 (c), the turbulence can reappear in case of the strong buoyancy. This flow development is more important to the high-Pr fluid due to the high viscosity. It is because the velocity boundary layer is developed to be thicker than the thermal boundary

layer when a fluid has high-Pr with the criteria of 1 as seen in Figure 4-2. In actual, the effect of Pr is considered when the complex natural circulation is approximated theoretically for analysis.

The boundary layer theory which is induced from the approximated governing equations proves the correlation between the boundary layers and Pr. The Pr of the exact or approximated value influences on the ratio of the velocity and thermal boundary layer thickness[8]. One of the relationship is shown in Equation (41). This correlation can be more approximated for $0.6 \leq Pr \leq 50$ as a form of the Equation (42). This correlation can also be utilized as one of the approximation of the natural convection in terms of flow characteristics due to the boundary layer development. Therefore, the observation of the flow characteristics developed by the convective boundary layers in natural circulation is expected to have meaningful relationship with Pr.

$$\frac{\delta_t}{\delta} = \frac{1}{1.025Pr^{1/3}\left[1-(\delta_t^2/14\delta^2)\right]^{1/3}} \simeq \frac{1}{1.025Pr^{1/3}} \tag{41}$$

On the range of $0.6 \leq Pr \leq 50$,

$$\frac{\delta}{\delta_t} \cong Pr^{1/3} \tag{42}$$

4.2 PIV Visualization of DOWTHERM RP Natural Circulation

In the experimental facility of natural circulation with ΔH=1.415 m, visualizing section was installed in the upper part of the heating section for the identification of the natural circulation and observation of the flow behavior firstly, as shown in Figure 4-3. Because the heating was started from the low power range, the identification of the natural circulation was needed at first. Visualizing section was utilized to the confirmation with the turbine flowmeter. In the process, interesting flow pattern was observed which has iterative vortices flow and laminar flow around the boundary layer as shown in Figure 4-4. For the detail observation, the Particle Image Velocimetry (PIV) technique was used for visualization. PIV visualization focused on the flow characteristics of the high-Pr heat transfer oil natural circulation. Experimental equipment was shown in Figure 4-5. Nd-YAG double-cavity laser was set in the vertical direction of the charge-coupled device (CCD) camera. By the laser beam to the test section, the cross-sectional velocity field was observed. PIV tracer particles, silver-coated glass hollow spheres with a mean diameter of 20 μm, were mixed with DOWTHERM RP. It visualized the DOWTHERM RP natural circulation by the reaction with the laser. Based on the reaction, CCD camera traced the movement of the tracer particles which shows the DOWTHERM RP flow behavior.

4.3 CFD Simulation of High-Pr Natural Circulation

Though the PIV visualization was conducted directly, the experiment has some limitation as a flow patter analysis. One reason is the local flow field. Because the visualized section is only the narrow part, each local flow distribution cannot be observed in the real experiment. Also, the horizontal cross section cannot be observed. Another reason is the limit of temperature considering material and power. The visualizing section is the separated part which is composed of Teflon and quartz material. Thus, as power increase, the temperature limit of single-phase DOWTHERM RP and other solid materials must be considered. The last reason is the possibility of the distortion. Simple detection or PIV visualization in the real experimental facility include the distortion caused by the materials. A quartz pipe was used as the visualizing section and the tracer particles are mixed with DOWTHERM RP. From that reasons, the CFD simulation in which more detail analysis can be conducted was performed using ANSYS-CFX commercial CFD code. The simplified model of the experimental loop of DOWTHERM RP natural circulation was designed for the CFD simulation. The same dimensions of the geometry of the experimental natural circulation loop were applied without the drain part which is located on the bottom part of the right section of the loop. The boundary conditions in CFD simulations were based on the experimental conditions. Each power was applied in the form of the heat flux on the outer surface of the pipe. In the cooling section, constant temperature of 10°C was applied to the outer surface of the cooling part.

In the stage of the meshing, the dense grids near the wall with fine inflation in the boundary layers were formed over the whole section to evaluate the correlation between the boundary layer development and Pr more detail. Together with the meshing, the mesh convergence study was conducted for the mesh optimization. Basically, the sweep mesh with the inflation of the first-layer height was set. The conditions of the first-layer height and the number of the axial grids were changed in the comparison. As seen in Figure 4-6, the comparison of the mesh convergence was performed at the constant power of 300 W according to the change of the total number of the nodes and elements by the changing conditions: 517,774 to 2,246,420. Figure 4-6 and Table 4-1 show the results of the major parameters following each condition. The temperature and velocity distribution of the radial cross-section of the heating section were converged when the total number of nodes exceeded about 2,000,000. The overall mesh convergence study showed that the results for the temperature and velocity converged well, within a deviation of 0.4 %. From the mesh convergence study, the 2,246,420 cells mesh was utilized in this CFD analysis with the minimum and maximum orthogonal qualities of 0.627 and 0.999 all over the region. Figure 4-7 shows the meshing of the natural circulation model in CFD simulation.

In the stage of the setting of the simulation conditions, initial and boundary conditions and the thermophysical properties of the working fluid, DOWTHERM RP, was set. Most conditions were based

on the experimental facility of the natural circulation. For the real-time observation of the temperature and velocity change, several monitoring points were also set. The location was considered as the center of the inlet and outlet of the heating and cooling sections. For the additional observation of the radial distribution, the locally positions of the upper heating section with several points in a radial direction were also applied. In terms of material, the thermophysical properties of DOWTHERM RP were not included in the basic code. Thus, those values are inserted based on the experimental data from the reference data sheet[9]. Table 4-2 shows the references data of DOWTHERM RP at 110 °C.

CFD simulation of DOWTHERM RP natural circulation was conducted with several purposes of investigation. First is the basic investigation of the high-Pr natural circulation on the developing heating section. It was compared with the PIV visualization based on the assumption of the flow characteristics. Second is the analysis of the flow characteristics in terms of the relation with Pr near the wall. In this part, the theoretical boundary layer theory was considered. Third part is the effect of the values of thermophyiscal properties and the types of heat sources. It was induced from the change of those condition according to the application of molten salts such as coolant or fuel.

4.4 Results and Discussion

In the experiment of PIV visualization, the filming was conducted at the three stage of the power, 100, 200, 300 W. The target section of the observation was the upper part of the heating section as seen in Figure 4-5. The average velocity distribution and the instantaneous velocity of the cross-section along the centerline were obtained and compared among the three cases. From the observation of the cross-section, the upstream flow by the indirect heating was observed. Figure 4-8 shows the average velocity of DOWTHERM RP in the steady state of each power. The difference of each case was the thickness of the velocity boundary layer near the wall in which the thinner layers were formed as the power increased. From the video clip of the DOWTHERM RP natural circulation, the unusual and distinctive flow pattern was appeared as expected from the simple detection in the normal experiment. The flow characteristics can be supposed in the instantaneous velocity profile as seen in Figure 4-9. Basically, 300 W flow had thinner boundary layer and higher velocity distribution over all, compared to the 100 W case. Both cases also appear asymmetric with large zigzag-shape velocity distribution which can be considered the supposed flow pattern. Furthermore, in the stream line which is shown in the small cut in Figure 4-9, some local vortices near the boundary layer were also observed which can support the assumption.

From the PIV visualization, the local flow pattern in the upper part of the heating section was observed. To compensate the limitation of the PIV visualization and analyze the flow characteristics more detail, the CFD simulation was conducted. The wider power range up to 600 W was applied in this simulation.

Figure 4-10 shows the velocity distribution of the CFD simulation at power of 100 W and 600 W. On the upper part of the heating section, the helical upflow was observed as seen in the extended figure in Figure 4-10. For more investigation, the radial distribution of the velocity was observed. As shown in Figure 4-11, the concentration of the center-flow can be observed to be changed as the flow developed in the axial direction. This results agreed well with the PIV visualization. In addition to the flow characteristics, the velocity development near the wall also showed the clear gradient in a radial direction. Because the velocity gradient could not be observed in PIV visualization due to the limit of the reflection, the analysis of the velocity near the wall in terms of Pr change was conducted in this simulation reflecting the boundary layer concepts.

For the analysis of the velocity near the wall, the radial velocity development on the heating and cooling sections were observed. Before the analysis, the comparison of the velocity on the upper heating section among the three methods, PIV visualization, CFD simulation and MARS simulation, was conducted. As seen in Figure 4-12, 5 points in a radial direction were used in CFD simulation. From the comparison, it was identified that the major flow is developed on the boundary sections and the center had relatively lower or negligible flow as seen in Table 4-3. This results tell the importance of the CFD simulation due to the measurement limit in real experiment.

From the simple comparison of the velocity distribution in Table 4-3, the main development of both temperature and velocity is supposed to appear around the boundary sections. Thus, more analysis for the radial distribution of both parameters was also performed. Figure 4-13 to 4-15 shows the radial distribution of temperature and velocity. Figure 4-13 shows that as power increases with decrease of Pr, the gradient of the temperature near the wall increases on the outlet of the heating and cooling sections. In addition, the main value of temperature which was formed in core region increases as power increase. However, velocity distribution showed the clear difference. Differently from temperature distribution, velocity had almost constant value in core region on the heating section as seen in Figure 4-14. Instead, as Pr decreases, the velocity distribution in core region became more normalized. To investigate the velocity development on the heating section, velocity with increasing height on the upper part of the heating section was compared. As seen in Figure 4-15, the velocity showed that it developed actively on both boundary and core region as Pr increases. This can be translated that the thickness of the mainly developing velocity in a radial direction becomes to be thicker as Pr increases. To compare this observation related to Pr, some conditions are assumed.

- Velocity of free stream flow is assumed to have average value of the DOWTHERM RP velocity along the centerline of the whole loop
- Boundary layer thickness is simplified to calculate as the distance from the wall to the location where 99 % of free stream flow developed

- DOWTHERM RP properties are inserted as the correlation of fitting except the specific heat capacity (constant value of T_{avg})

Based on the conditions, the modified concept of the temperature and velocity boundary layer thickness was calculated from the CFD simulation results. Using the approximated correlation between Pr and the boundary layer thicknesses in reference 8, the ratio of the calculated thicknesses was compared with Pr. Figure 4-16 and Table 4-4 show the comparison of the quantitative distribution values. The results show similar value on higher power range but the gap between the ratio of the boundary layer thicknesses and Pr exists as power decreases. Several reasons can cause the gap. The first is the Pr range of the CFD simulation that is from 40 to 135 which is partially over the application range of the approximated correlation of the reference. The second is free stream velocity and the parameters which are calculated covering a wide range so that some error can occurs. The last is the simplified method of the calculation for boundary layer which can result in the considerable uncertainty of the measurement. In addition, the correlations between the boundary layer thicknesses and Pr have diverse value of index according to the approximation method. Reflecting these conditions, the adequate correlation between them can be developed and it will be utilized for the investigation of the high-Pr flow characteristics.

As a supplement of the CFD simulation, the investigation of the effect of the thermophyiscal properties and the types of heat sources was performed. As the importance of the thermophysical properties was identified in high-Pr natural circulation in the previous section of MARS simulation, the simulation results between the constant properties and the temperature-dependent properties were compared. With the change of the thermophysical properties, the heat source condition is also changed according to the application of molten salts in nuclear area, such as coolants or fuels. Especially, the internal heat source is important in case of the molten fuels or the integrated systems with coolants and fuels. Thus, simple comparison of the natural circulation between the locally-external and locally-internal heat sources was also conducted. For this study, the properties of DOWTHERM RP was inserted with two types. One is the constant values at bulk temperature and the other is temperature-dependent properties that are composed of the polynomial or exponential correlations. Heat source was set as a form of heat flux in case of the locally-external heat and as a form of a volumetric heat source in case of the locally-internal heat.

Figure 4-17 to 4-21 shows the comparison of the natural circulation following the different property and heat source conditions. In the aspect of the property difference, the temperature distribution showed that the overall distribution was formed similarly between the two conditions but the condition of the constant property had lower temperature and the thermal stratification in a vertical direction on the upper horizontal parts. In case of the velocity distribution, the overall distribution had similar range of

velocity between the two conditions. However, more clear difference of the velocity was observed in case of the temperature-dependent property condition. From this comparison, the importance of the thermophysical property input can be identified to investigate the temperature and velocity gradients. On the other hand, the difference of heat source condition affected the formation of the different distribution for both temperature and velocity. The bulk velocity also showed higher value in case of the internal heat source. However, the bulk temperature was similar between the two types of heat sources. This results can be translated that the heat transfer ability with different flow characteristics appears according to the type of heat source which is important in safety concept.

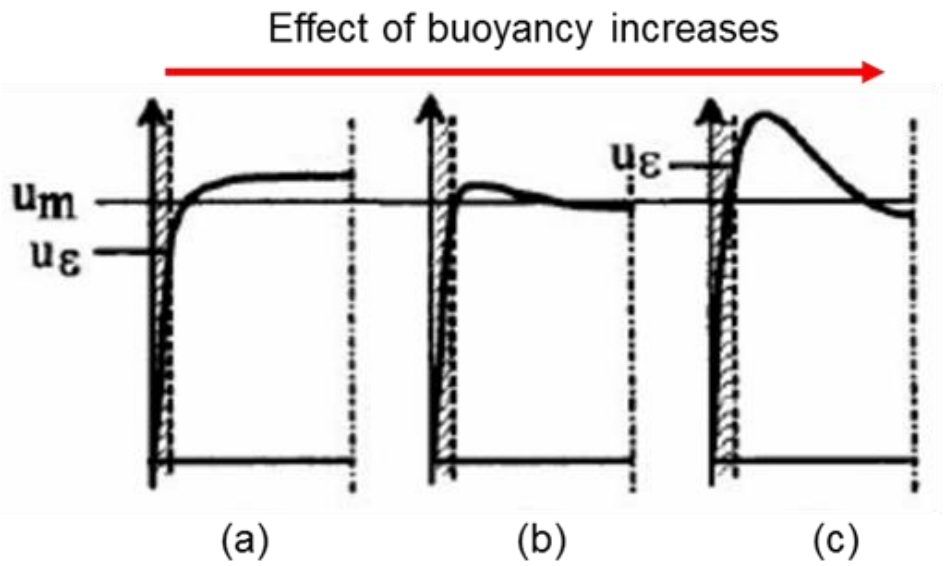

Fig. 4-1. Natural convection near the wall by the buoyancy effect (a) no buoyancy, (b) medium buoyancy, (c) strong buoyancy[39].

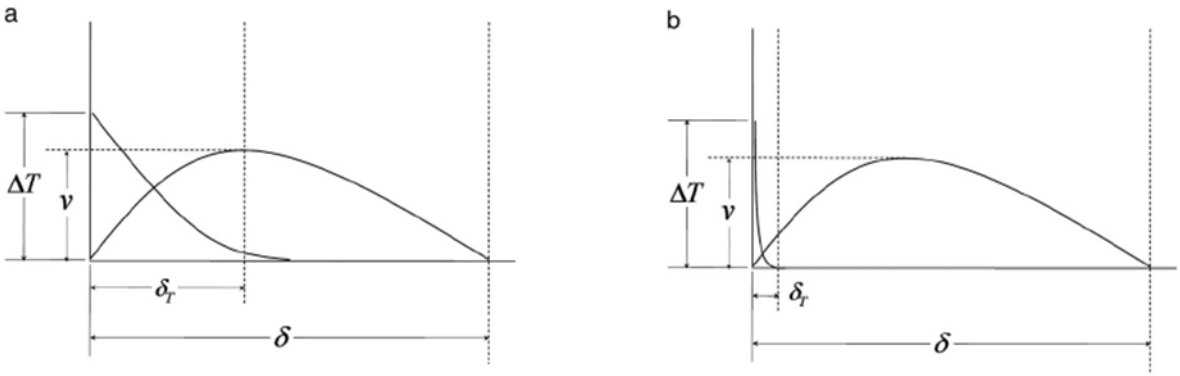

Fig. 4-2. Thickness of the boundary layers near the vertical heating surface.

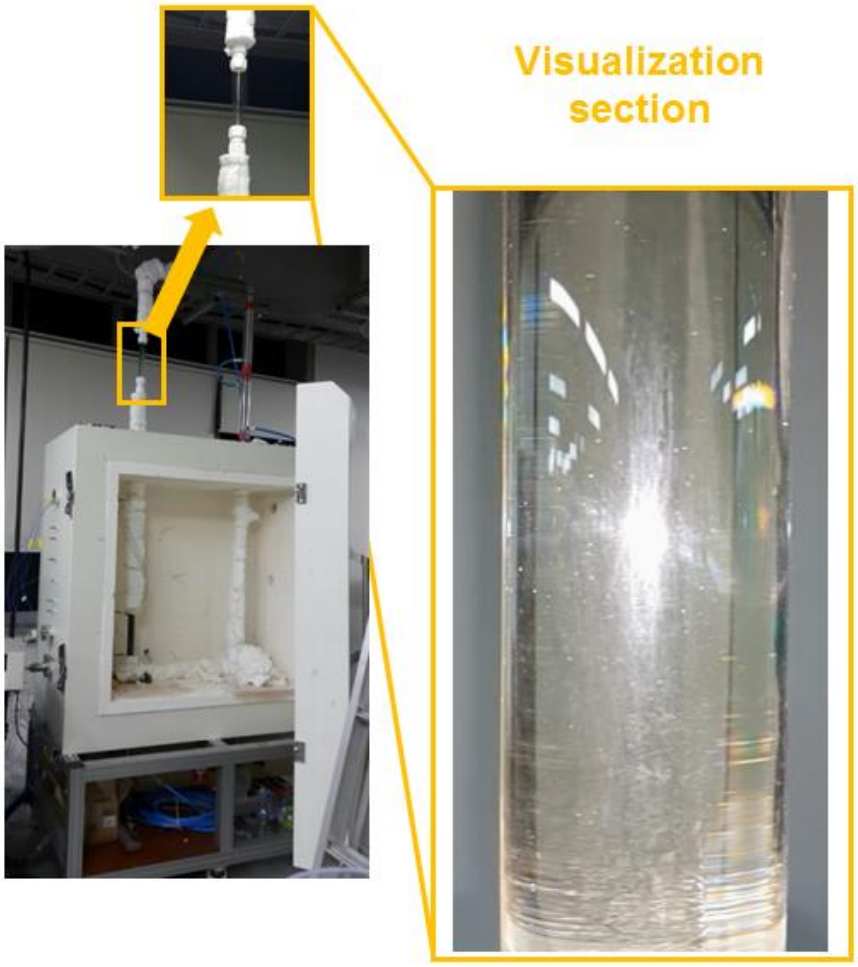

Fig. 4-3. Visualization section of natural circulation loop.

Fig. 4-4. Flow of DOWTHERM RP in visualizing section at 300 W.

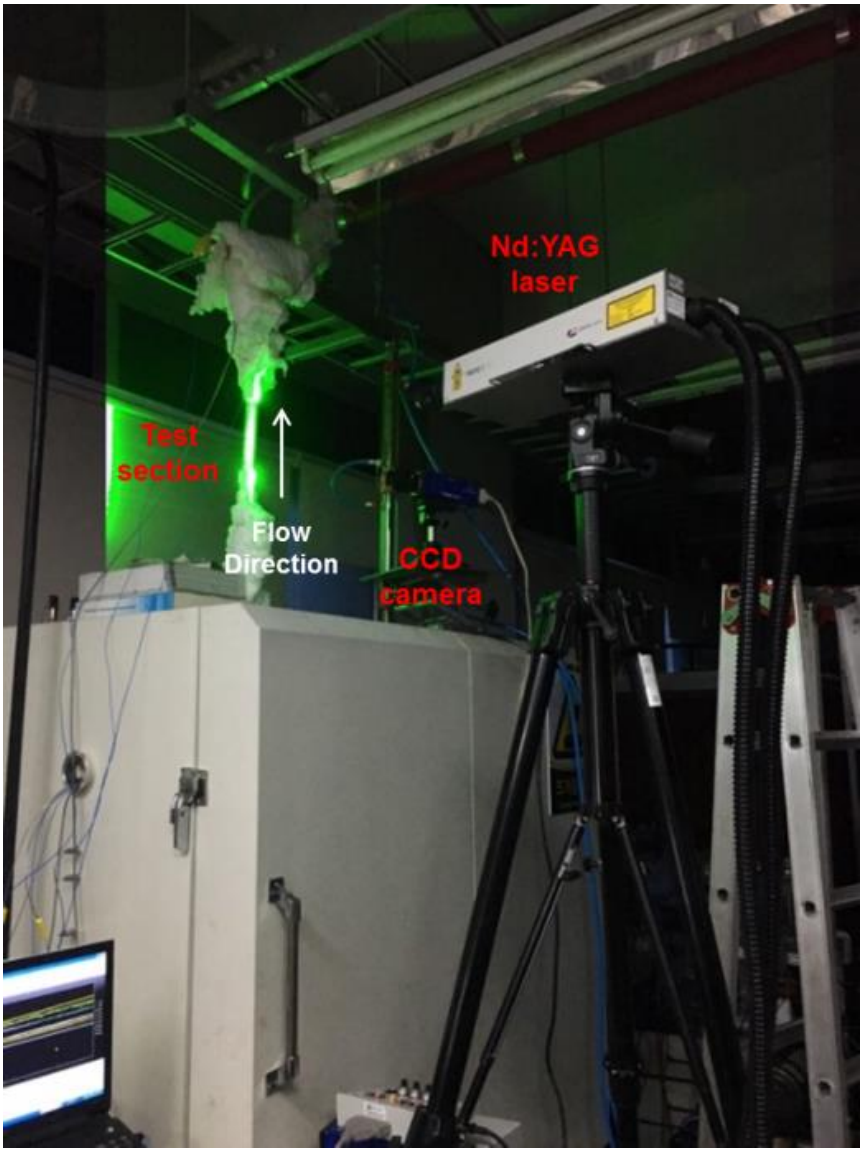

Fig. 4-5. Facilities of PIV technique.

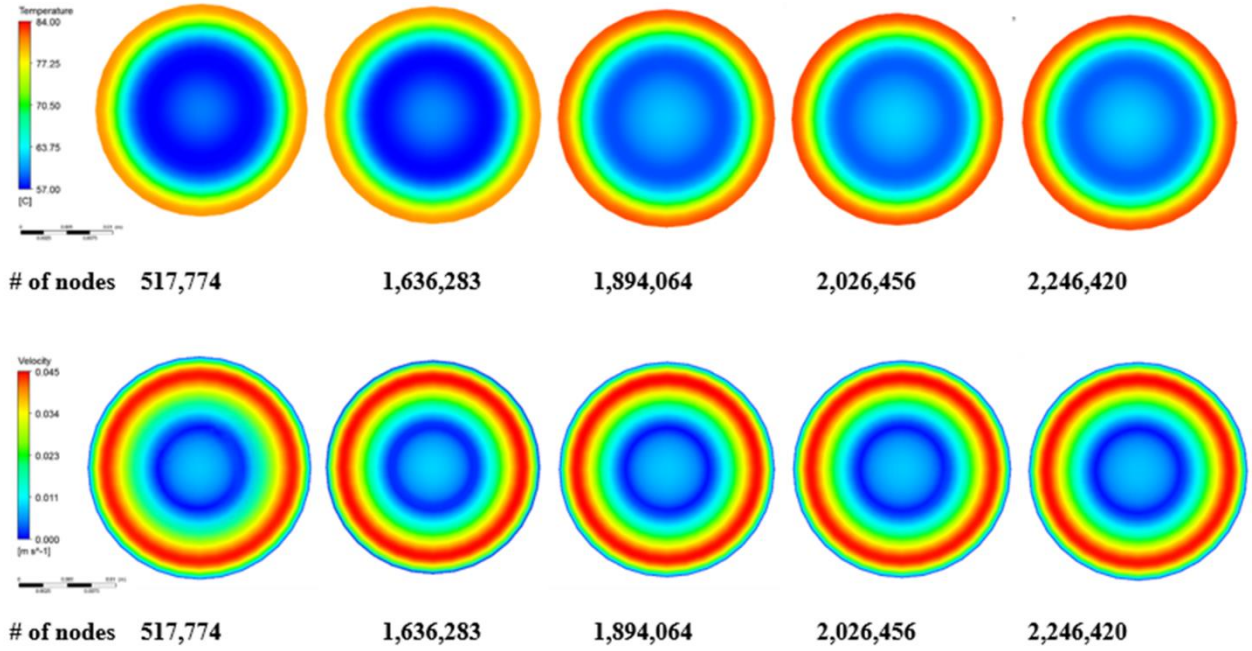

Fig. 4-6. Mesh convergence for temperature (upper) and velocity (lower) distribution on the cross-section of the upper vertical part of the heating section.

Table 4-1. Main parameters in comparison of the mesh convergence at 300 W.

Number of nods	517,774	1,636,283	1,894,064	2,026,456	2,246,420
Bulk temperature (˚C)	56.28	59.28	60.96	61.27	61.42
Bulk velocity (m/s)	0.018	0.021	0.021	0.021	0.021

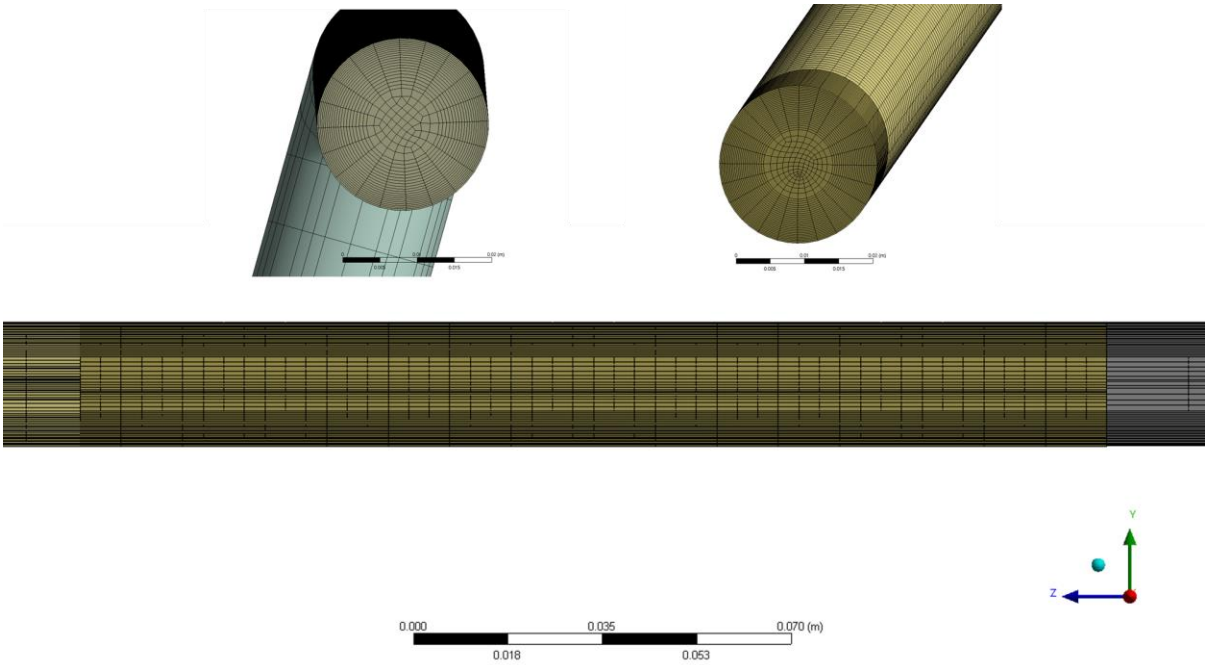

Fig. 4-7. Meshing of natural circulation loop in CFD simulation.

Table 4-2. Reference thermophysical properties of DOWTHERM RP (110 ˚C)[23].

	Molar Mass (g/mol)	Density (kg/m^3)	Heat Capacity (J/kg-K)	Viscosity (Pa-s)	Thermal Conductivity (W/m-K)	Thermal Expansion Coefficient (1/K)
DOWTHERM RP (Diaryl alkyl)	236.4	965.9	1888	0.00232	0.1197	0.000733

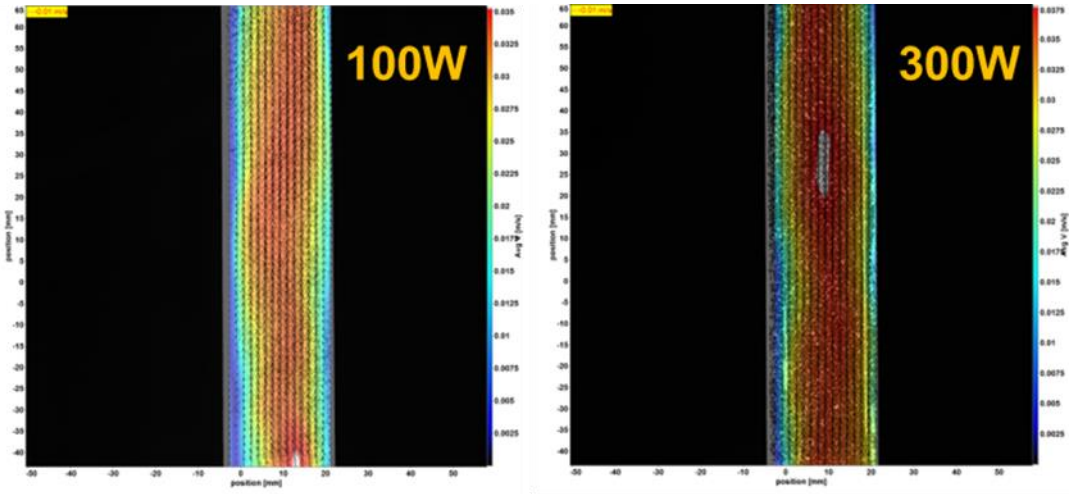

Fig. 4-8. Average velocity profile of DOWTHERM RP natural circulation (left: 100 W, right: 300 W).

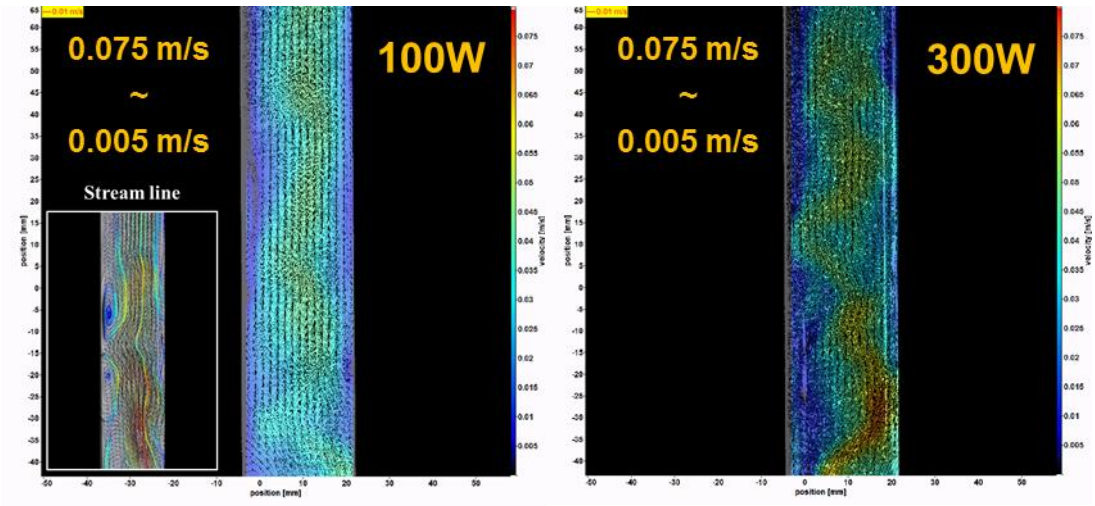

Fig. 4-9. Instantaneous velocity profile of DOWTHERM RP natural circulation (left: 100 W, right: 300 W).

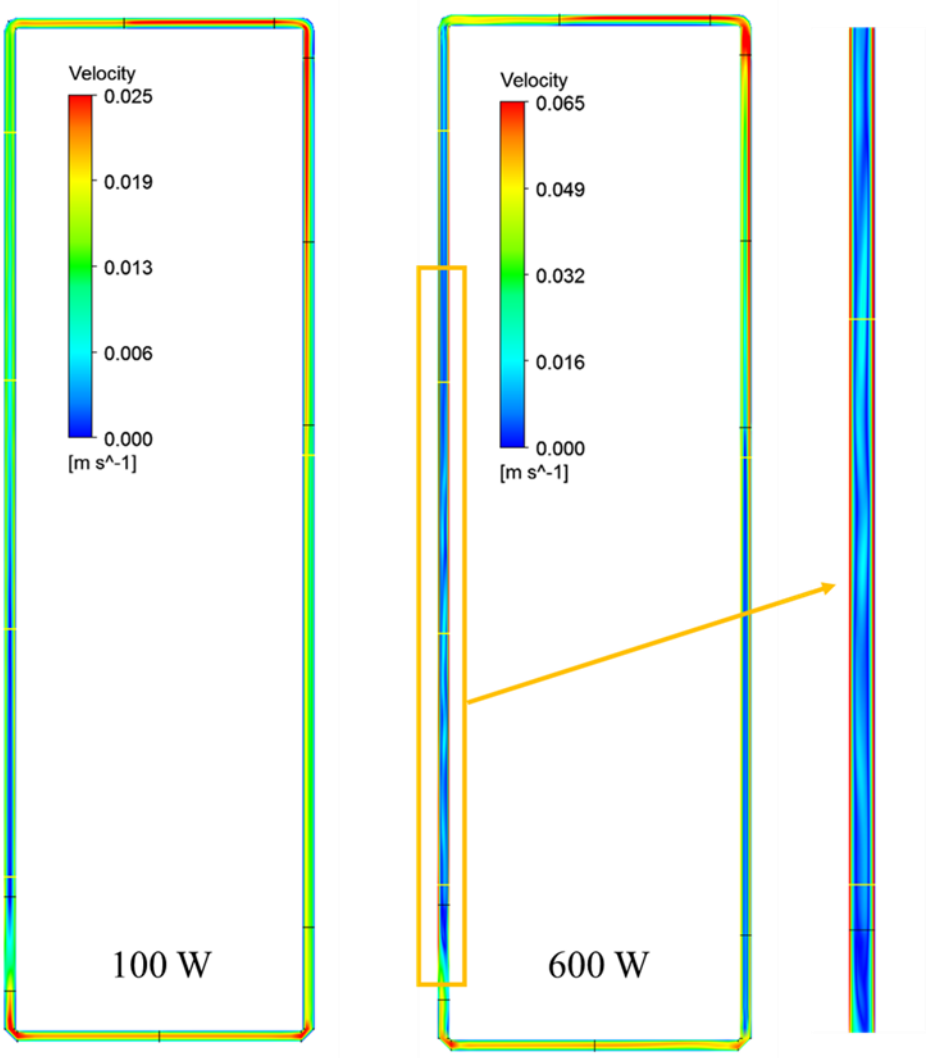

Fig. 4-10. Velocity distribution of DOWTHERM RP natural circulation.

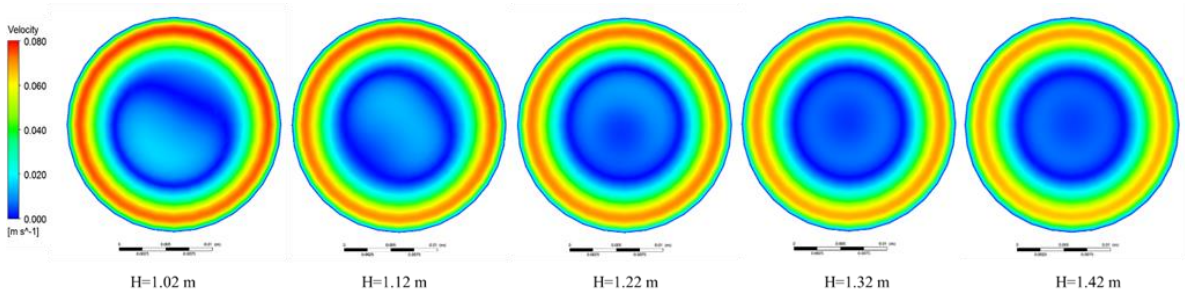

Fig. 4-11. Velocity distribution on the horizontal cross-section of the upper heating section of DOWTHERM RP natural circulation
(vertical height increases with the interval of 0.1 m).

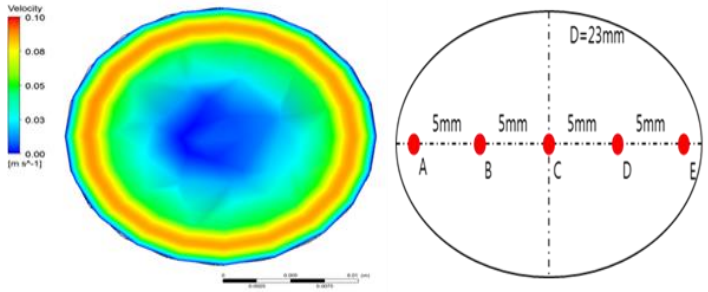

Fig. 4-12. Observation points on the cross section in the radial direction (CFD simulation).

Table 4-3. Comparison of velocity on the upper part of heating section.

		A	B	C	D	E
300 W	PIV (m/s)	0.02-0.07				
	CFD (m/s)	0.069	0.0205	0.009	0.0256	0.069
	MARS (m/s)	0.032				

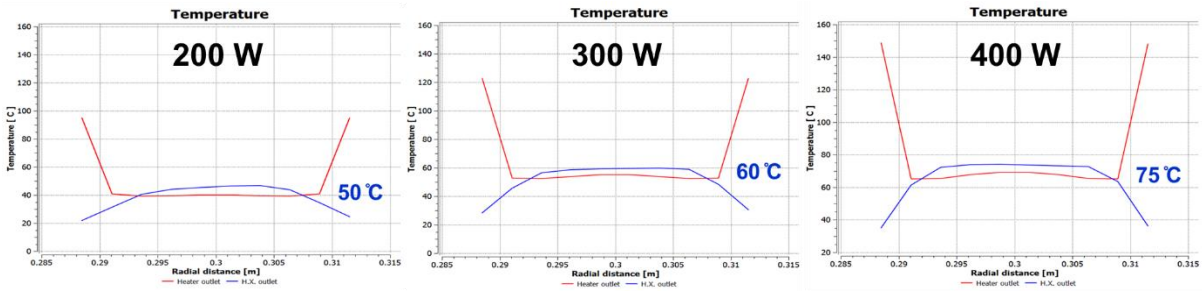

Fig. 4-13. Comparison of the heater and H.X. outlet temperature profile in a radial direction in DOWTHERM RP natural circulation.

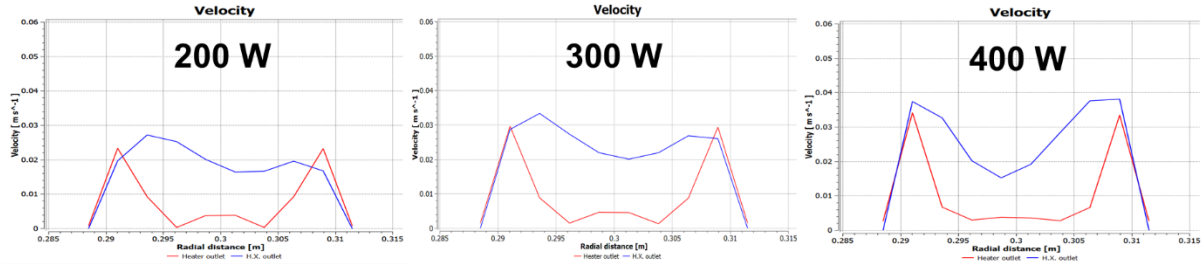

Fig. 4-14. Comparison of the heater and H.X. outlet velocity profile in a radial direction In DOWTHERM RP natural circulation.

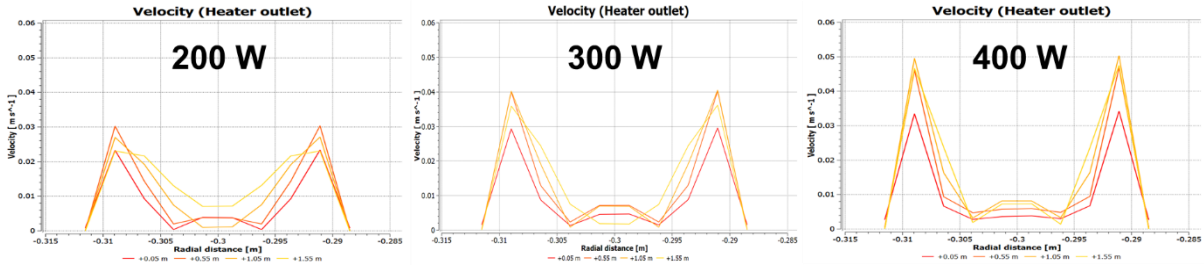

Fig. 4-15. Comparison of the heater outlet velocity profile in a radial direction in DOWTHERM RP natural circulation.

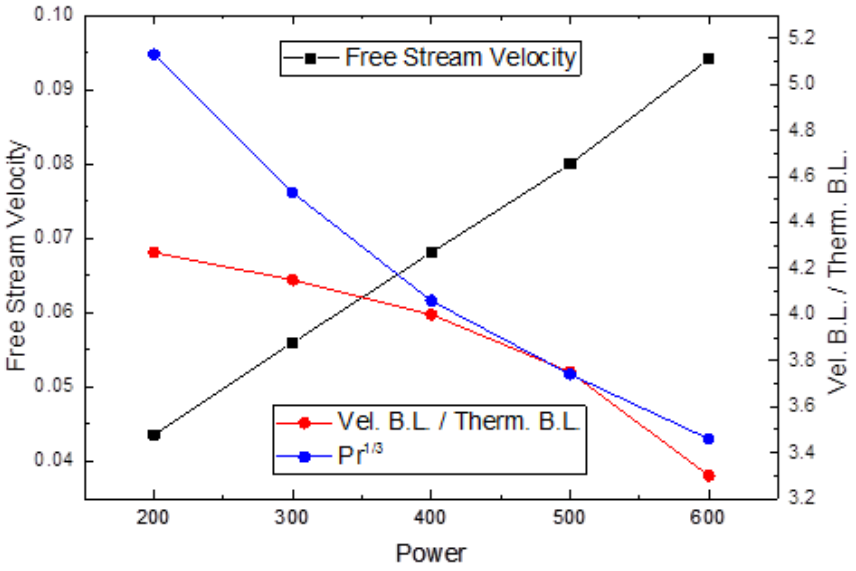

Fig. 4-16. Comparison between boundary layer thickness and Pr in CFD simulation results.

Table 4-4. Comparison between boundary layer thickness and Pr in CFD simulation results.

Power (w)	Free Stream Velocity (m/s)	Ratio of Velocity B.L. per Thermal B.L. (Thickness)	$Pr^{1/3}$	1.025* $Pr^{1/3}$
200	0.0436	4.27	5.13	5.26
300	0.0560	4.	4.53	4.65
400	0.0681	4.00	4.06	4.17
500	0.0800	3.75	3.74	3.83
600	0.0941	3.30	3.46	3.54

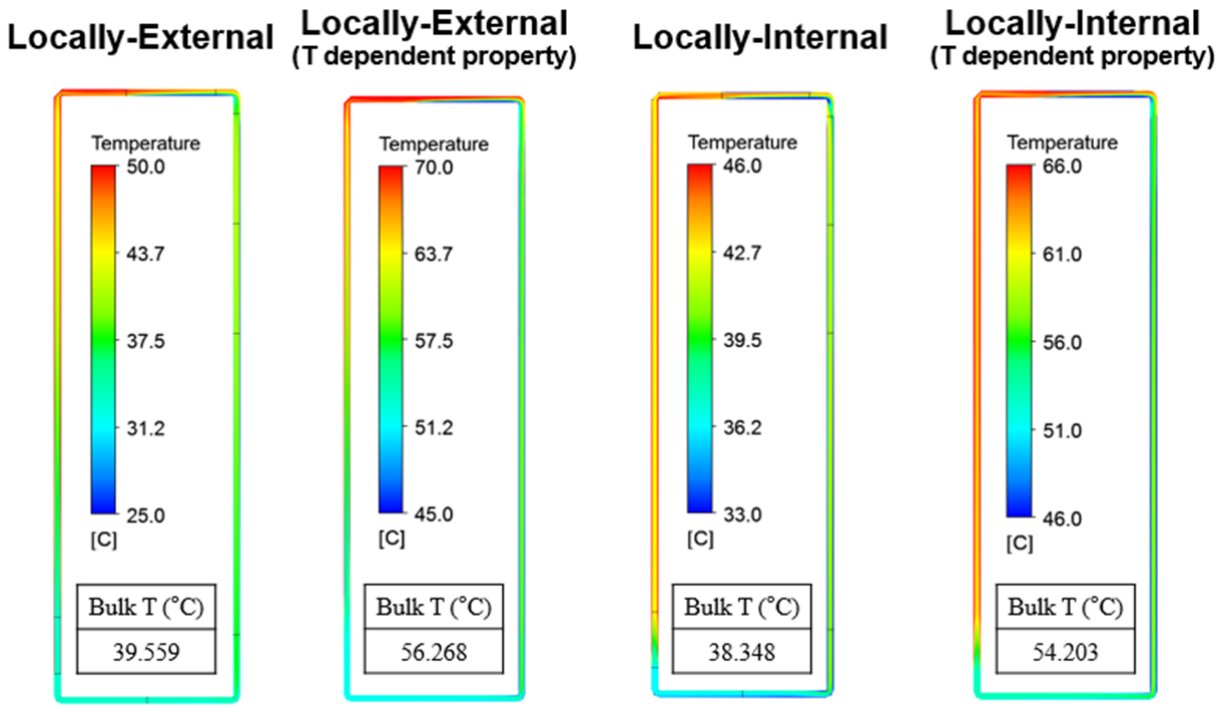

Fig. 4-17. Temperature distribution of DOWTHERM RP natural circulation at 300 W.

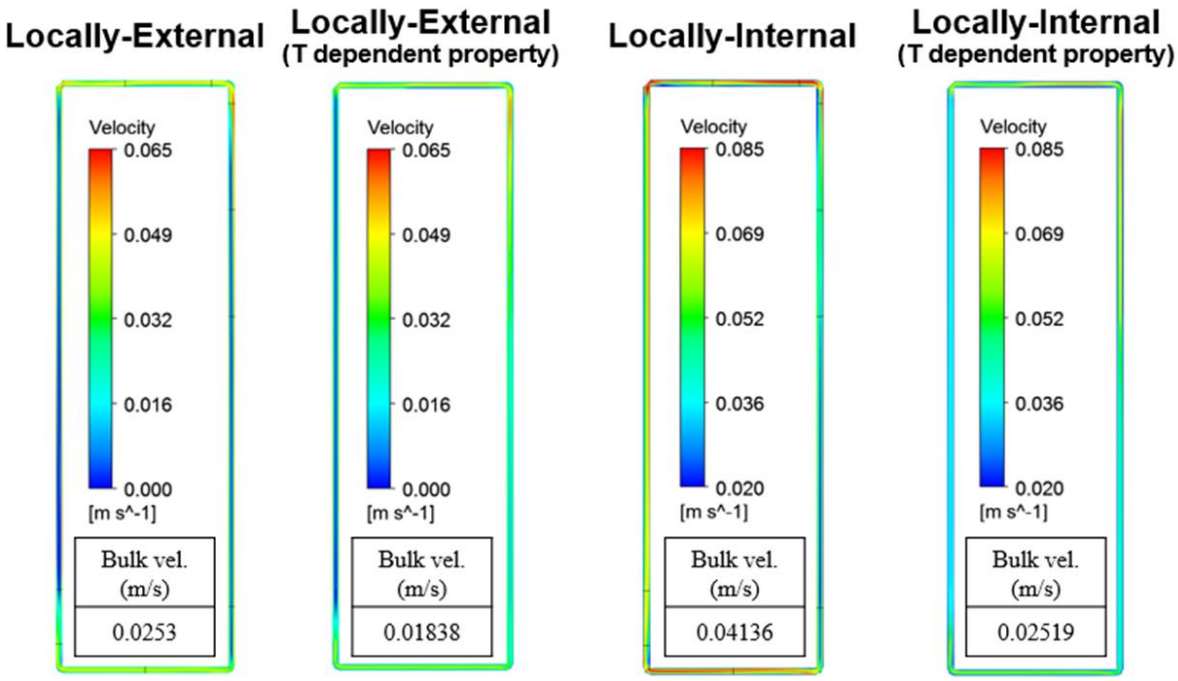

Fig. 4-18. Velocity distribution of DOWTHERM RP natural circulation at 300 W.

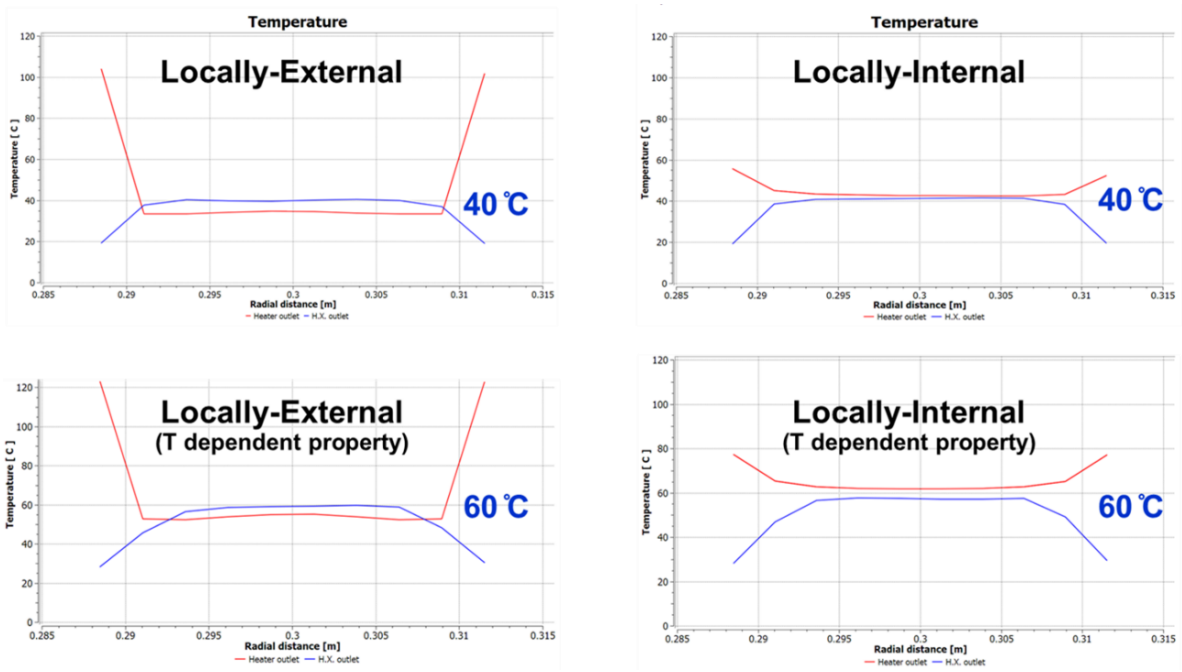

Fig. 4-19. Heater and H.X. outlet temperature profile in a radial direction In DOWTHERM RP natural circulation at 300W.

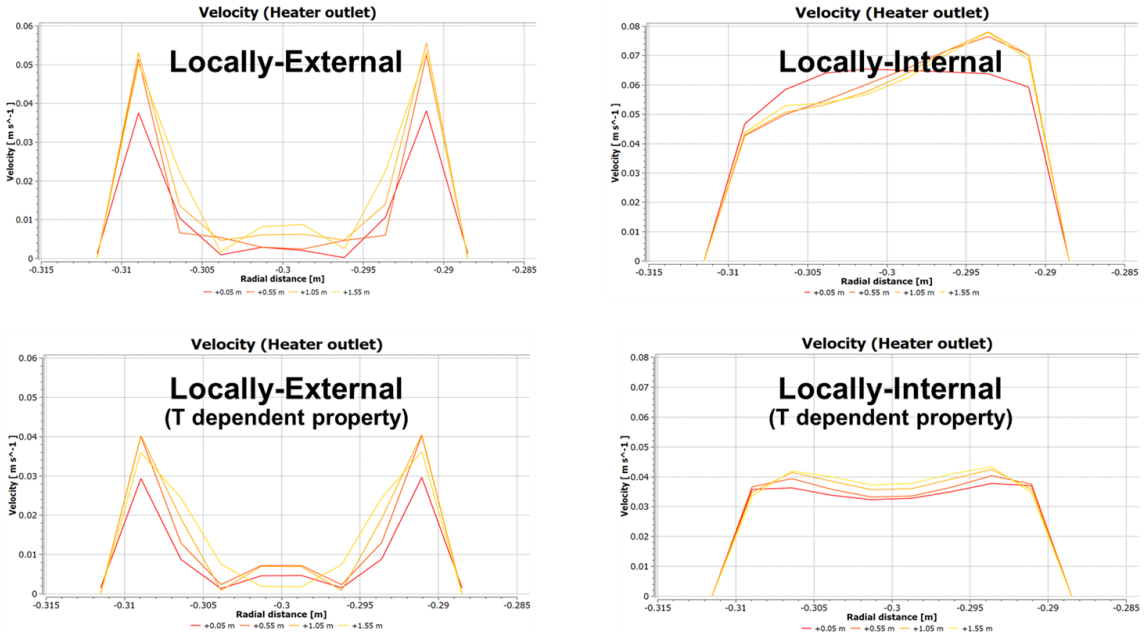

Fig. 4-20. Heater outlet velocity profile in a radial direction
In DOWTHERM RP natural circulation at 300W.

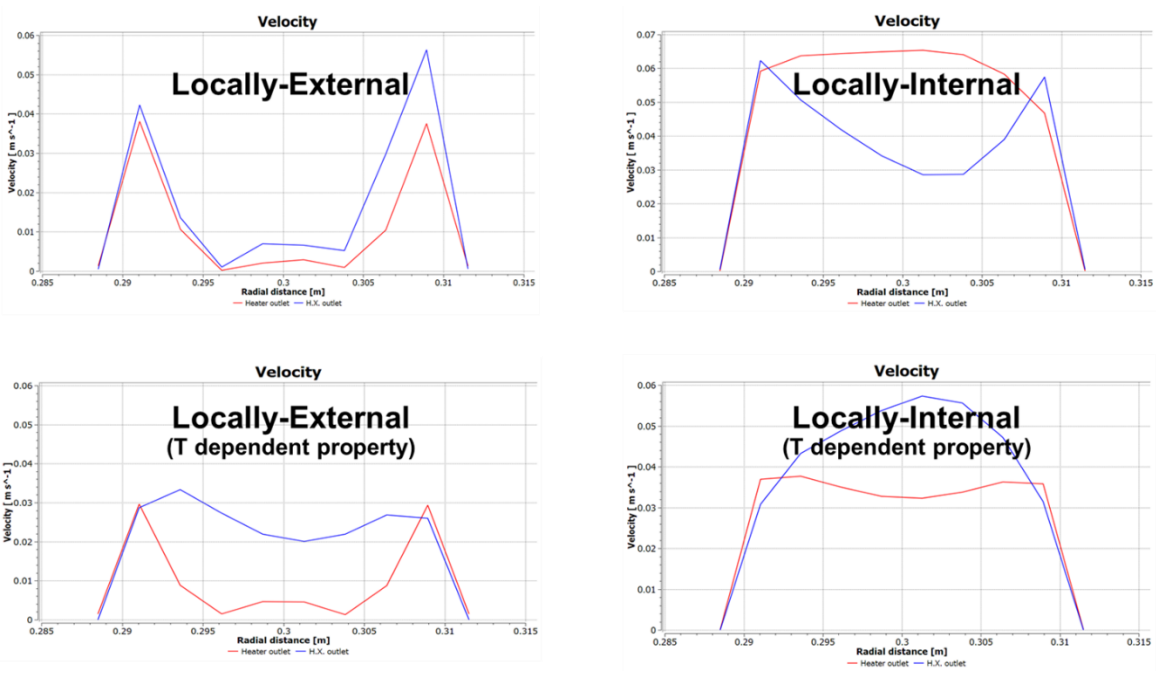

Fig. 4-21. Heater and H.X. outlet velocity profile in a radial direction
In DOWTHERM RP natural circulation at 300W.

V. Conclusions

For the development of the similarity technique on the molten salt heat transfer area, the feasibility of new simulant, DOWTHERM RP, was evaluated in this thesis. The evaluation was focused on the large two aspects of the high-Pr natural circulation, the heat transfer capability and the flow characteristics. Based on the theoretical characteristics of 'high-Pr' and 'natural circulation', the experimental and numerical performance were conducted. For the similarity application, the theoretical similarity of natural circulation was applied between the prototypic and the simulating fluids and systems, firstly. From the comparison of Pr and Gr, the theoretical feasibility of a simulant, DOWTHERM RP, was identified and the detail condition of the similarity experiment was set.

With the concept of similarity, the heat transfer ability of DOWTHERM RP was evaluated through the natural circulation experiment in the first part. Temperature and mass flow rate on the major locations were obtained from the two types of DOWTHERM RP natural circulation with different height difference (ΔH). From the experimental data, the experimental correlation of natural circulation was developed and the adequacy of molten salt simulant was assessed by comparing with the reference data of molten salts natural convection. For the extended application of the simulant to numerical analysis and the validation of the experiment, the simulation using the thermal-hydraulic safety analysis code, MARS-LMR was also conducted. Before the simulation, the thermophysical properties of the simulants, DOWTHERM RP and DOWTHERM A, was implemented in MARS-LMR code. Using the implemented properties, natural circulation of DOWTHERM RP and FLiBe was conducted. Using the simulation results, the loss terms were investigated and the effect of each thermophysical property was evaluated through the sensitivity study.

In the second part, the flow characteristics in the natural circulation development was observed using the PIV visualization and the CFD simulation. The motivation of this study started from the confirmation of natural circulation in low power with low-mass flow rate. From the visualizing section which was for the confirmation, the irregular and rotating flow pattern was observed. The supposition of the flow patterns observed with the naked eye and the normal video camera was analyzed with PIV visualization and the CFD simulation. The investigation put emphasis on the 'Pr' and 'boundary layer' which was induced from the theoretical boundary layer theory. In the experiment of PIV visualization, the supposed flow patterns were identified with the instantaneous velocity field and the direct observation. However, the PIV application had some limitation of the observation. To supplement those limitation, CFD simulation was conducted. From the CFD analysis, the fundamental distribution of the temperature and velocity were observed including the thermal stratification. The assumed helical upflow was also observed on the upper part of the heating section. Especially, the radial distribution of temperature and velocity in each section can be observed in CFD simulation. Using the advantages of

the CFD simulation, the correlation between Pr and boundary layer development was also analyzed.

On the overall process of this study, the aspect of similarity of molten salts was also considered. Especially, the effect of the change of thermophysical properties and the types of heat source which are critical to the direct molten salt application in nuclear fields was evaluated using the simulant, DOWTHERM RP. Using the numerical methods, MARS code and CFD code, the variation of the major parameters in natural circulation such as mass flow rate, temperature, and velocity was investigated, too. From that, significant difference according to the conditions of the two variation was identified.

In this thesis, the study on the evaluation of new simulant of FLiBe molten salt in the basic natural circulation was conducted. Adding to the typical investigation of natural circulation with similarity application, the novel observation was also performed through the visualization and analysis of the high-Pr natural circulation. This multimodal approach can contribute to the development of both similarity technique and high-Pr natural circulation.

REFERENCES

1. Alvin M.; Weinberg; The status and Technology of Molten-Salt Reactors-A Review of Molten-Salt Reactor Work at the ORNL, *Nuclear Technology*, **1970**, 8, 2.

2. David LeBlanc; Molten salt reactors: A new beginning for an old idea, *Nuclear Engineering and Design*, **2010**, 240, 1644-1656.

3. O. Benes; R.J.M. Konings; Thermodynamic evaluation of the NaCl-$MgCl_2$-UCl_3-$PuCl_3$ system, *Journal of Nuclear Materials*, **2008**, 375, 202-208.

4. Natural circulation in water cooled nuclear power plants, IAEA-TECDOC-1474, IAEA, November, **2005**.

5. Charalampos "Harry" Andreades et al.; Technical Description of the "Mark 1" Pebble-Bed Fluoride-Salt-Cooled High-Temperature Reactor (PB-FHR) Power Plant, UCBTH-14-002, University of California, Berkeley, September, **2014**.

6. Manohar S. Sohal; Matthias A. Ebner; Piyush Sabharwall; Phil Sharpe; Engineering database of liquid salt thermophysical and thermochemical properties, INL/EXT-10-18297, INL, March, **2010**.

7. Coulson. J.M.; Richardson, J. F.; Chemical Engineering, *Elsevier*, **1999**

8. Sadik Kakac; Ramesh K. Shah; Win Aung; Handbook of Single-Phase Convective Heat Transfer, *Wiley Wiley & Sons*, **1987**

9. Charles Forsberg; Lin-Wen Hu; Per Peterson; Kumar Sridharan; Fluoride-Salt-Cooled High-Temperature Reactor (FHR) for Power and Process Heat, Final Project Report, MIT-ANP-TR-157, MIT, December, **2014**.

10. Peterson P et al.; FHR code benchmarking white paper; integrated research project-2, workshop 1. Fluoride-Salt-Cooled, High-Temperature Reactor Code Benchmarking White Paper, UCBTH-15-001, University of California, Berkeley, March, **2015**.

11. Eirik Eide Pettersen; Coupled multi-physics simulations of the Molten Salt Fast Reactor using coarse-mesh thermal-hydraulics and spatial neutronics, Master thesis, The University of Paris-Saclay, Villigen, September, **2016**.

12. A. Griveau; F. Fardin; H. Zhao; P.F. Peterson; Transient Thermal Response of the PB-AHTR to Loss of Forced Cooling, *Proceedings of the Global 2007*, **2007**, September 9-13, Boise.

13. S. R. Greene et al.; Pre-Conceptual Design of a Fluoride-Salt-Cooled Small Modular Advanced High-Temperature Reactor (SmAHTR), ORNL/TM-2010/199, ORNL, December, **2010**.

14. MSR Review_Feasibility of Developing a Pilot Scale Molten Salt Reactor in the UK, Energy Process Developments Ltd., July, **2015**.

15. Seaborg Wasteburner_Molten Salt Reactor, SEAB-WP-2015-001, Seaborg Technologies, March, **2015**.

16. Natural circulation in water cooled nuclear power plants, IAEA-TECDOC-1474, IAEA, November, **2005**.

17. B.S. Massery; Mechanics of Fluids, *D Van Nostrand Co.* **1968**

18. Pijush K. Kundu; Ira M. Cohen; David R Dowling Ph.D.; Fluid Mechanics 5th Edition, *Elsevier*, **1987**

19. Zweibaum N et al.; Role and status of scaled experiments in the development of fluoride-salt-cooled, high-temperature reactors, *Proceedings of the International Congress on Advances in Nuclear Power Plants 2015*, **2015**, May 3-6, Nice.

20. Jeffrey E. Bickel et al.; Design, Fabrication and Startup Testing in the Compact Integral Effects Test (CIET 1.0) Facility in Support of Fluoride-Salt-Cooled, High-Temperature Reactor Technology, UCBTH-14-009, University of California, Berkeley, December, **2014**.

21. Philippe M. Bardet; Per F. Peterson; Options for scaled experiments for high temperature liquid salt and helium fluid mechanics and convective heat transfer, *Thermal Hydraulics*, **2008**, 163, 344-357.

22. Lv Q.; Scaling analysis for the Direct Reactor Auxiliary Cooling System for AHTRs, Master thesis, The Ohio State University, Columbus, **2012**.

23. DOWTHERM RP Heat Transfer Fluid, *DOW Chemical Company*

24. DOWTHERM A Heat Transfer Fluid, *DOW Chemical Company*

25. DOWTHERM SR-1 Heat Transfer Fluid, *DOW Chemical Company*

26. Joshua Richard et al.; Implementation of Liquid Salt Working Fluids into TRACE, *Proceedings of the International Congress on Advances in Nuclear Power Plants 2014*, **2014**, April 6-9, Charlotte.

27. Richard L. Moore; Implementation of DOWTHERM A properties into RELAP5-3D/ATHENA, INL/EXT-10-18651, INL, April, **2010**.

28. Incropera; Frank P.; DeWitt; David P.; Fundamentals of Heat and Mass Transfer 4th Edition, *Wiley*, **2000**

29. E.N. Sieder; G.E. Tate; Heat transfer and pressure drop of liquids in tubes, *Industrial and Engineering Chemistry*, **1936**, 28, 1429-1435.

30. V. Gnielinski; New equations for heat and mass transfer in turbulent pipe and channel flow, *International Journal of Chemical Engineering*, **1976**, 16, 359-367.

31. Cooke J.W.; Cox B.; Forced Convection Heat Transfer Measurements with a Molten Fluoride Salt Mixture Flowing in a Smooth Tube, ORNL-TM-4079, ORNL, March, **1973**.

32. MARS code manual, KAERI/TR-3872/2009, KAERI, December, **2009**.

33. Sarah Kang; In Cheol Bang; Numerical Analyses of a single-phase natural convection system for Molten Flibe using MARS-FLIBE code, *Proceedings of the Korean Nuclear Society Autumn*

meeting, **2014**, October 30-31, Pyeongchang.

34. Benchmarking of thermal-hydraulic loop models for lead-alloy-cooled advanced nuclear energy systems (Phase I: Isothermal forced convection case), NEA/NSC/WPFC/DOC(2012)17, OECD, June, **2012**.

35. Flow of Fluids, Technical Paper No. 410, ISBN 1-40052-712-0, *Crane Co.*, **2009**

36. R. R. Romatoski et al.; Thermophysical Property Sensitivity Study of LiF-BeF_2 and NaF-ZrF_4 Coolants on Thermal Hydraulic Licensing Limits for a Fluoride Salt-cooled High Temperature Test Reactor, *Proceedings of the International Congress on Advances in Nuclear Power Plants 2015*, **2015**, May 3-6, Nice.

37. Nicolas Zweibaum; Raluca O. Scarlat; Per F. Peterson; Verification and Validation of a Single-Phase Natural Circulation Loop Model in RELAP5-3D, *Proceedings of the 2013 RELAP5 International Users Group Seminar*, **2013**, September 12-13, Idaho Falls.

38. Gyeong-Uk Kang; Bum-Jin Chung; Hyoung-Jin Kim; Natural convection heat transfer on a vertical cylinder submerged in fluids having high Prandtl number, *International Journal of Heat and Mass Transfer*, **2014**, 79, 4-1.

39. Aicher; H. Martin; New correlations for mixed turbulent natural and forced convection heat transfer in vertical tubes, *International Journal of Heat and Mass Transfer*, **1997**, 40, 3617-3626.

Acknowledgement

2년이라는 길지도 짧지도 않은 시간의 석사과정을 거치며, 학부 과정에서 겪어보지 못한 경험과 배움을 얻을 수 있었습니다. 이 과정에서 제 스스로의 삶의 목적 및 방향에 대해서도 많이 생각할 수 있었고, 무엇보다 주변의 많은 사람들과의 소통 및 관계를 되돌아 보며 감사할 수 있었습니다.

우선, 학부 과정의 원자력 대학생 및 인턴 과정부터 석사과정까지 꾸준히 성장할 기회를 주시고 많은 조언과 함께 지도해주신 방인철 교수님께 감사의 마음을 전하고 싶습니다. 걱정과 염려 속에서도 따끔한 충고와 가르침으로 석사과정까지 이끌어주셔서 정말 감사합니다. 또한, 연구자로서의 적극적인 생각과 행동을 보여주시고 함께 성장할 수 있게 도와주신 덕분에 후회되지 않고 발전할 수 있는 2년의 석사과정을 보낼 수 있었습니다.

바쁘신 중에도 석사 학위 디펜스와 논문에 대해 부족한 부분을 가르쳐주시고 평가해주신 유춘상 교수님과 최성열 교수님께도 정말 감사합니다. 졸업 준비 과정에서 교수님들의 조언과 가르침을 통해 학위 주제에 대해 좀 더 다양하게 생각해보고 발전시킬 수 있었습니다.

또, 연구원 인턴을 통해, 연구자으로서의 조언과 학생인 저의 진로 및 개인적 고민 상담을 듣고 아낌없이 많은 이야기를 해주시며 가르쳐주셨던 이동원 박사님, 윤재성 박사님, 김석권 박사님, 이어확 박사님, 진형곤 박사님께도 감사 드립니다. 짧은 기간이었지만 연구원 생활을 통해 개인적인 진로와 흥미에 대해 많이 생각하고 방향을 정할 수 있었습니다.

또한, 밤낮으로 같이 연구실 생활을 하며, 가족보다 더 많은 시간을 함께 보낸 연구실 선후배, 동기 분들께도 고마운 마음을 전하고 싶습니다. 연구실 선배로서 힘들게 익히고 얻은 경험과 지식을 아낌없이 가르쳐주셨던 강사라 박사님, 연구나 생활에서 어려움이 있을 때 항상 신경 써주시고 도와주신 박성대 박사님 모두 감사합니다. 랩장으로서, 또한 연구실 최고 선배로서 연구실 많은 일을 도맡아 하지만 후배들까지 신경 써주시는 서한선배와 경모선배도 항상 고맙습니다. 함께 과제를 맡아나가며 실험과 세세한 연구방향까지 신경 쓰며 항상 도와주는 석빈선배, 랩원들에게 항상 잘 베풀고 도와주는 인국선배, 연구실 분위기를 잘 이끌어주는 성보선배 덕분에 랩에 더 잘 적응할 수 있었습니다. 가장 기본적인 것부터 많이 가르쳐주신 영신선배, 연구실에서 오래 머무는 덕분에 일적으로, 사적으로 많이 도움 받고 의지했던 허효선배와 민호오빠 모두 고맙습니다. 연구원 인턴부터 같이 지내며 함께 연구실 동기로 지내온 규민이와 1년밖에 안됐지만 동갑이라 많이 친해진 수민이도 제가 연구실 생활을 더 즐겁게 할 수 있게 도와줘서 정말 고맙습니다. 서로 다른 선후배들이 함께 있어 재미있는 일도, 힘든 일도 많았지만, 2년 동안 좋은 사람들과 많은 추억을 쌓은 것 같아 모두에게 정말 감사합니다.

연구실만큼이나 긴 시간을 함께 보내며, 대학원 과정까지 함께 겪어온 친구들, 나경이, 주현이, 항상 힘이 되는 친구들, 주영이, 부산 패밀리들, 예진이, 소윤이, 이 외의 친구들 모두 고맙습니다. 또, 학부 및 대학원 과정에서 즐겁게 학교 생활을 할 수 있었던 같은 원자력과 선배 및 동기들 모두 고맙습니다. 학부 때부터 선배지만 친구처럼 원자력과에 흥미를 붙일 수 있게 도와준 유동한 박사님, 병진선배, 주앙선배, 관윤선배, 욱제선배, 미진언니, 같이 학부를 지내온 동기들, 소정이, 재민오빠, 형준, 준우, 정일, 경훈이, 대학원 동기인 희재까지 모두 고맙습니다.

마지막으로, 모두 떨어져 바쁘게 지내지만 항상 의지하고 도와주는 가족들, 엄마, 아빠, 언니, 동생, 친척들 및 민수오빠 모두 감사합니다. 앞으로는 좀 더 가족들에게 신경 쓸 수 있는 좋은 딸, 동생, 누나가 되도록 노력하겠습니다.

아직 고민도 많고 꿈도 많은 나이지만, 석사 과정을 통해 그 과정을 한 단계 더 좁혀 나아갈 수 있었던 2년이라 의미 있었습니다. 학부를 졸업할 때는 석사가 연장선이라 잘 느끼지 못했는데, 석사 졸업이 되니 성인이 되어 처음 한 가지의 목표를 마무리하는 느낌이 들어 시원섭섭한 것 같습니다. 모두가 그렇듯, 이 다음의 선택과 목표가 정해지고 계속 나아가는 가운데 2년의 석사과정 경험과 추억이 나아가는 힘이 될 수 있길 바라며 마무리하겠습니다.

2017년 1월

신 유 경